

UNIVERSITÉ DU QUÉBEC À MONTRÉAL

IMPACT DU DÉBOISEMENT ET DE LA MISE EN EAU DE RÉSERVOIRS SUR  
LE CYCLE DE LA MATIÈRE ORGANIQUE ET SA PHOTODÉGRADATION  
DANS LES PLANS D'EAU DE LA RÉGION BORÉALE QUÉBÉCOISE

THÈSE  
PRÉSENTÉE  
COMME EXIGENCE PARTIELLE  
DU DOCTORAT EN SCIENCES DE L'ENVIRONNEMENT

PAR  
JEAN-BAPTISTE PLOUHINEC

NOVEMBRE 2012

UNIVERSITÉ DU QUÉBEC À MONTRÉAL  
Service des bibliothèques

Avertissement

La diffusion de cette thèse se fait dans le respect des droits de son auteur, qui a signé le formulaire *Autorisation de reproduire et de diffuser un travail de recherche de cycles supérieurs* (SDU-522 – Rév.01-2006). Cette autorisation stipule que «conformément à l'article 11 du Règlement no 8 des études de cycles supérieurs, [l'auteur] concède à l'Université du Québec à Montréal une licence non exclusive d'utilisation et de publication de la totalité ou d'une partie importante de [son] travail de recherche pour des fins pédagogiques et non commerciales. Plus précisément, [l'auteur] autorise l'Université du Québec à Montréal à reproduire, diffuser, prêter, distribuer ou vendre des copies de [son] travail de recherche à des fins non commerciales sur quelque support que ce soit, y compris l'Internet. Cette licence et cette autorisation n'entraînent pas une renonciation de [la] part [de l'auteur] à [ses] droits moraux ni à [ses] droits de propriété intellectuelle. Sauf entente contraire, [l'auteur] conserve la liberté de diffuser et de commercialiser ou non ce travail dont [il] possède un exemplaire.»

## REMERCIEMENTS

Je tiens tout d'abord à remercier mon directeur Marc Lucotte de m'avoir permis d'entreprendre cette aventure extraordinaire. Un grand merci pour avoir donné la chance au jeune matheux que j'étais alors de contribuer à la recherche en sciences de l'environnement. Mes premiers pas dans le monde réel étaient mal assurés et après tout ce chemin parcouru, je te suis extrêmement reconnaissant. Merci également pour le temps que tu as consacré aux lectures et relectures de cette thèse et qui en ont grandement amélioré la qualité.

Je tiens également à remercier mon codirecteur Yves Gélinas pour l'énergie que tu as mise à corriger ce travail, pour la patience dont tu as su faire preuve quand mes idées n'étaient plus claires et finalement pour l'encadrement de cette thèse en général, merci Yves.

Je souhaite également remercier chacun et chacune des personnes qui ont participé aux nombreuses campagnes d'échantillonnages, Myriam, Marianne, Adam, Marilou et Sophie. Merci également à Dragosh et Bianca pour les sacrés coups de main sur le terrain. À Jean-François et Jean-Sébastien également pour avoir mis la main à la pâte au cours des campagnes d'automne. Pour les analyses en laboratoire, merci à Isabelle et Sophie, et à Serge pour les analyses statistiques et SIG.

Merci à Jean-Pierre Blanchet de m'avoir fait confiance pour le cours de dynamique des systèmes dans lequel je me suis particulièrement régalé. Superviser la partie modélisation dans le cadre du cours de dynamique a été un pur plaisir.

Merci au FQRNT pour le soutien financier de fin de thèse qui m'a permis de découvrir le Vermont, à Breck Bowden pour avoir accepté de me prendre sous sa direction.

Aux différentes générations d'étudiants de Marc également, qui auront croisé ma route. Merci à Matt pour son aide précieuse dans les discussions de lignine et au plaisir d'avoir pris quelques bières ensemble. À Irina, pour sa bonne humeur et les petits coups de folie quand le travail commençait à devenir trop pesant. À Cynthia pour ces moments d'échange tellement agréables. À Sky et JS pour les partys et les discussions que l'on a pu avoir ensemble. Finalement, à Roman, qui m'a bien manqué une fois sa thèse complétée, tu as été un appui important tout au long de ce travail.

Aux étudiants du Géotop également, à Quentin pour ces virées agréables à San Francisco à Sandrine et Olivia pour les différentes soirées, discussions cafés ou vins chauds. À Bass pour sa gentillesse et ses explications sur les datations au plomb. À René pour avoir participé aux réunions des ligneux.

Finalement, un grand merci à Émilie et Nico, ça a été un plaisir incroyable de faire ces sorties dans les montagnes des Adirondacks. De voyager jusqu'à Chicoutimi pour la soutenance de Nico, de profiter des belles balades là-bas, vivement que vous reveniez ici ! À Laurence et Dim, les Belges fêtards, aux petites sorties en kayaks et aux soirées bien arrosées. À JS et Gaïdig, pour ces moments de folie à l'appart, on s'est vraiment régalé quand on était tous les quatre ici, c'était que du bonheur ! Estelle et Chip, vous avez été un soutien incroyable tout au long de cette aventure, merci pour toutes ces soirées, ces jeux, ces sorties en raquette, ces week-ends en chalet, merci d'avoir été présent dans les moments de joie et dans les autres. Finalement à Jona et Ben, à toutes ces aventures extraordinaires, l'achat d'une voiture bidon, à nos soirées BBQ, à toutes ces soirées à ne faire que profiter, quelques multitudes de bons moments, merci d'être là, c'est tellement formidable de pouvoir compter sur les amis !

Un immense merci à ma belle, Jenny, tu as été un ange dans cette dernière ligne droite vers le dépôt de thèse, merci pour ton soutien dans les moments difficiles, pour tes encouragements. Pour tous ces moments magiques que l'on a passés ensemble, merci ma belle.

À mes parents, frères et sœurs, merci pour tous ces super moments, à faire de la marche, partir au ski, à faire de la plongée. Merci d'être passé me voir ici, de m'avoir encouragé tout au long de ces études ... qui finalement se terminent un jour.

## TABLE DES MATIÈRES

LISTE DES FIGURES .....	vii
LISTE DES TABLEAUX.....	xi
RÉSUMÉ .....	xvii
INTRODUCTION.....	1
0.1 Mise en Contexte .....	1
0.2 Objectifs de la thèse .....	2
0.3 Chapitre I.....	3
0.4 Chapitre II.....	3
0.5 Chapitre III .....	4
0.6 L'analyse des composés de la lignine.....	4
0.7 Les méthodes d'échantillonnage de la matière organique .....	5
0.8 Les méthodes d'évaluation de production et d'émissions de CO <sub>2</sub> .....	6
0.9 Importance des travaux .....	6
CHAPITRE I	
PHOTODÉGRADATION DE LA MATIÈRE ORGANIQUE DISSOUE DANS LES EAUX DE SURFACES ET DIFFUSION DU CO <sub>2</sub> VERS L'ATMOSPHÈRE POUR LES PLANS D'EAU PERTURBÉS ET VIERGES EN RÉGION BORÉALE QUÉBÉCOISE (CANADA)	
1.1 Introduction .....	16
1.2 Methods.....	17
1.2.1 Research sites.....	17
1.2.2 Sampling method for a thin layer of surface water and analysis by gas chromatography.....	18
1.2.3 The measurement of CO <sub>2</sub> produced by photochemical mineralization using quartz cell irradiation.....	20

1.2.4	Calculation of the theoretical amount of CO <sub>2</sub> produced by photochemical mineralization:.....	21
1.2.5	Chemical analyses .....	25
1.3	Results .....	26
1.3.1	Physical and Chemical Parameters.....	26
1.3.2	Photochemical parameters .....	26
1.3.3	Amounts of CO <sub>2</sub> produced by photochemical mineralization .....	28
1.4	Discussion.....	28
1.5	Conclusion.....	34
CHAPITRE II		
CONTRIBUTION DE LA PHOTODÉGRADATION DE LA MATIÈRE ORGANIQUE TERRIGÈNE À L'HÉTÉROTROPHIE DES ÉCOSYSTÈMES AQUATIQUES EN RÉGION BORÉALE QUÉBÉCOISE (CANADA).....		
2.1	Introduction .....	57
2.2	Methods.....	58
2.2.1	Sampling sites .....	58
2.2.2	Measurements of the total diffusive fluxes of CO <sub>2</sub> from the water surface to the atmosphere using the thin boundary layer method .....	59
2.2.3	Measurements of CO <sub>2</sub> from photochemical mineralization, bacterial respiration, and CO <sub>2</sub> uptake by photosynthesis.....	61
2.2.4	Theoretical model for the daily production of CO <sub>2</sub> by photochemical mineralization, integrated over the entire water column .....	62
2.2.5	Empirical model of CO <sub>2</sub> diffusive fluxes.....	65
2.2.6	Evaluation of the dissolved and particulate organic matter terrigenous fractions .....	67
2.3	Results .....	68
2.3.1	Diffusive fluxes of CO <sub>2</sub> .....	68
2.3.2	Daily production of CO <sub>2</sub> by photochemical mineralization integrated over the water column .....	68
2.3.3	CO <sub>2</sub> uptake by photosynthesis .....	70
2.3.4	CO <sub>2</sub> production by bacterial respiration .....	71
2.3.5	Terrigenous organic matter in the water column .....	71
2.4	Discussion.....	72

2.4.1 CO <sub>2</sub> diffusive fluxes and $DIPM_{CO_2}$ .....	73
2.4.2 Relation between photochemical mineralization of DOM and bacterial respiration .....	75
2.4.3 Diffusive flux of CO <sub>2</sub> among various incubation experiments .....	76
2.5 Conclusion .....	77
CHAPITRE III	
3.2 Material and Methods .....	102
3.2.1 Sampling sites .....	102
3.2.2 Lignin Biomarkers .....	103
3.2.3 Data collection, processing and analysis .....	104
3.3 Results .....	105
3.4 Discussion .....	112
3.5 Conclusion .....	119
CONCLUSION GÉNÉRALE .....	155

## LISTE DES FIGURES

Figure	Page
Figure 1.1 Amount of CO <sub>2</sub> produced by photochemical mineralization across different aquatic environments .....	45
Figure 1.2a Relationship between amount of CO <sub>2</sub> produced by photochemical mineralization $PM_{CO_2}(0)$ and DOC concentrations.....	46
Figure 1.2b Relationship between amount of CO <sub>2</sub> produced by photochemical mineralization $PM_{CO_2}(0)$ and $pm(0 - .04)$ .....	47
Figure 1.3 Relationship between the theoretical amount of CO <sub>2</sub> produced by photochemical mineralization integrated over the top four centimeters $pm(0 - .04)$ and the standardized amount of CO <sub>2</sub> produced by photochemical mineralization integrated over in the top four centimeters $pm(0 - .04)$ .....	48
Figure 1.4 Relationship between the standardized amount of CO <sub>2</sub> produced by photochemical mineralization in the top four centimeters $\overline{PM}_{CO_2}(0)$ and DOC concentrations in the surface of the bodies of water ( <i>DOC</i> ).....	49
Figure 1.5 Relationship between the daily quantity of photodegraded DOM $PM_{CO_2}(0)/DOC$ and Fe concentrations.....	50
Figure 1.6 Relationship between the standardized amount of CO <sub>2</sub> produced by photochemical mineralization in the top four centimeters $\overline{PM}_{CO_2}(0)$ and the total diffusive fluxes of CO <sub>2</sub> ( $f_{CO_2}$ ).....	51
Figure 2.1 Quantum yield ( $\phi_\lambda$ ) across different aquatic environments.....	89
Figure 2.2 Photochemical mineralization over the entire water column across different aquatic environments .....	90
Figure 2.3 The daily flux of CO <sub>2</sub> comes from the mineralization of dissolved organic matter standardized for average photon flux value over the water column ( $DIPM_{CO_2}$ ) according to the environmental conditions in spring and summer season .....	91

Figure 2.4 Relationship between the daily flux of CO <sub>2</sub> comes from the mineralization of dissolved organic matter standardized for average photon flux value over the water column ( $\overline{DIPM}_{CO_2}$ ) and the absorption coefficient of CDOM at 360nm ( $a_{360}$ ).....	92
Figure 2.5 Relationship between the daily flux of CO <sub>2</sub> comes from the mineralization of dissolved organic matter over the water column ( $DIPM_{CO_2}$ ) and total diffusive fluxes of CO <sub>2</sub> ( $f_{CO_2}$ ).....	93
Figure 2.6 Relationship between the total diffusive fluxes of CO <sub>2</sub> ( $f_{CO_2}$ ) and the theoretical diffusive fluxes of CO <sub>2</sub> ( $f^*_{CO_2}$ ).....	94
Figure 3.1 Map of the sampled sites on the Cabonga reservoir .....	136
Figure 3.2 Map of the sampled sites on the Decelles reservoir.....	137
Figure 3.3 Map of the watershed of the Ottawa River ( <a href="http://fr.academic.ru">http:// fr.academic.ru</a> ).....	138
Figure 3.4 S / V ratio versus C / V ratio in sediments.....	139
Figure 3.5 S / V ratio versus C / V ratio in the particulate fraction.....	140
Figure 3.6 S / V ratio versus C / V ratio in the dissolved fraction .....	141
Figure 3.7 The various phenolic compounds constituting of the lignin biomarkers, according to the dissolved fraction, the particulate fraction and the sedimentary matter for every environmental conditions.....	142
Figure 3.8a The lignin biomarkers values of $\lambda_8$ measured according to various environmental conditions (LNAL, LAL, RNAL, RAL) in the dissolved and the particulate fraction and in the sedimentary matter.....	143
Figure 3.8b The lignin biomarkers values of $\Sigma_8$ measured according to various environmental conditions (LNAL, LAL, RNAL, RAL) in the dissolved and the particulate fraction and in the sedimentary matter.....	143
Figure 3.8c The lignin biomarkers values of the S/V ratio, measured according to various environmental conditions (LNAL, LAL, RNAL, RAL) in the dissolved and the particulate fraction and in the sedimentary matter.....	144
Figure 3.8d The lignin biomarkers values of the C/V ratio, measured according to various environmental conditions (LNAL, LAL, RNAL, RAL) in the dissolved and the particulate fraction and in the sedimentary matter.....	144
Figure 3.8e The lignin biomarkers values of $\Sigma_C$ measured according to various environmental conditions (LNAL, LAL, RNAL, RAL) in the dissolved and	

- the particulate fraction and in the sedimentary matter
- Figure 3.8f The lignin biomarkers values of  $\Sigma_P$  measured according to various environmental conditions (LNAL, LAL, RNAL, RAL) in the dissolved and the particulate fraction and in the sedimentary matter.....145
- Figure 3.8g The lignin biomarkers values of  $\Sigma_V$  measured according to various environmental conditions (LNAL, LAL, RNAL, RAL) in the dissolved and the particulate fraction and in the sedimentary matter.....146
- Figure 3.8h The lignin biomarkers values of  $\Sigma_S$  measured according to various environmental conditions (LNAL, LAL, RNAL, RAL) in the dissolved and the particulate fraction and in the sedimentary matter.....146
- Figure 3.8i The lignin biomarkers values of the P/(V+S) ratio, measured according to various environmental conditions (LNAL, LAL, RNAL, RAL) in the dissolved and the particulate fraction and in the sedimentary matter.....147
- Figure 3.8j The lignin biomarkers values of the 3,5 Bd/V ratio, measured according to various environmental conditions (LNAL, LAL, RNAL, RAL) in the dissolved and the particulate fraction and in the sedimentary matter.....147
- Figure 3.8k The lignin biomarkers values of the (Ac/Ad)<sub>v</sub> ratio, measured according to various environmental conditions (LNAL, LAL, RNAL, RAL) in the dissolved and the particulate fraction and in the sedimentary matter.....148
- Figure 3.8l The lignin biomarkers values of the (Ac/Ad)<sub>s</sub> ratio, measured according to various environmental conditions (LNAL, LAL, RNAL, RAL) in the dissolved and the particulate fraction and in the sedimentary matter.....148
- Figure 3.9  $\lambda_8$  values measured in the dissolved fraction in relation with  $\lambda_8$  measured for the particulate fraction .....149
- Figure 3.11a  $\lambda_{DOC}$  values obtained in the dissolved fraction in relationship with the CO<sub>2</sub> production deriving from the photochemical mineralization .....151
- Figure 3.11b  $\lambda_{DOC}$  values obtained in the dissolved fraction according to the environmental conditions .....151
- Figure 3.12a  $\lambda_{Vol}$  values obtained in the dissolved fraction in relationship with the CO<sub>2</sub> production deriving from the photochemical mineralization .....152
- Figure 3.12b  $\lambda_{Vol}$  values obtained in the dissolved fraction according to the environmental conditions .....152
- Figure 3.13a  $\lambda_{POC}$  values obtained in the dissolved fraction in relationship with the CO<sub>2</sub> production deriving from the photochemical mineralization .....153

- Figure 3.13b  $\lambda_{\text{POC}}$  values obtained in the dissolved fraction according to the environmental conditions .....153
- Figure 3.14a Values of the C/V ratio measured in the sedimentary matter in relationship with the total diffusive fluxes of  $\text{CO}_2$  ( $f_{\text{CO}_2}$ ).....154
- Figure 3.14b Values of the C/V ratio measured in the sedimentary matter in relationship with the daily production of  $\text{CO}_2$  from photochemical mineralization over the entire water column ( $\text{DIPM}_{\text{CO}_2}$ ) .....154

## LISTE DES TABLEAUX

Tableau	Page
Table 1.1 Average values of the main physical and chemical parameters .....	42
Table 1.2 The photochemical mineralization depending on different wavelengths....	43
Table 2.1 $C/N$ ratios according to the environmental scenarios for soil and the POC, DOC, or SED material .....	85
Table 2.2 Terrigenous fraction for POC, DOC and SED material.....	86
Table 2.3 CO <sub>2</sub> production and CO <sub>2</sub> fluxes according to photochemical mineralization (DIPM <sub>CO2</sub> ), bacterial respiration (DIBR <sub>CO2</sub> ), and consumption by photosynthesis (DIPH <sub>CO2</sub> ) .....	87
Tableau 3.1 Summary of data obtained through the GIS (forest cover, watershed morphometry, lakes volume).....	127
Tableau 3.2 Main characteristics of the Cabonga reservoir sampled sites .....	128
Tableau 3.3 Main characteristics of the Decelles reservoir sampled sites.....	129
Tableau 3.4 Sedimentation rates (Ouellet, 2010) and sedimentary characteristics of the sampled cores.....	130
Tableau 3.5 Mean $C/N$ atomic ratio for each environmental conditions evaluated for the organic horizon of soils ( $C/N_{hor}$ ), for the inorganic horizon of soils ( $C/N_{in}$ ), and for each fraction POC, DOC and SED .....	131

## LISTE DES ACRONYMES

DOM	Matière organique dissoute
CDOM	Matière organique dissoute colorée
DOC	Carbone organique dissous
TBL	Couche mince de surface
LAL	Ensemble des lacs à l'étude perturbés par récolte forestière
LNAL	Ensemble des lacs à l'étude non perturbés par récolte forestière
RAL	Ensemble des sites d'un réservoir perturbés par récolte forestière
RAL	Ensemble des sites d'un réservoir non perturbés par récolte forestière

## LISTE DES SYMBOLES

$a_{CDOM,\lambda}$	Coefficient d'absorption spectral du DOM
$BR_{CO_2}(0)$	Mesure de la production de $CO_2$ par respiration bactérienne en surface
$DIPM_{CO_2}$	Flux quotidien de $CO_2$ provenant de la minéralisation du DOM sur l'ensemble de la colonne d'eau
$DIBR_{CO_2}$	Flux quotidien de $CO_2$ provenant de la respiration bactérienne sur l'ensemble de la colonne d'eau
$DIPH_{CO_2}$	Flux négatif quotidien de $CO_2$ provenant de la fixation du carbone par photosynthèse sur l'ensemble de la colonne d'eau
$f_{CO_2}$	Flux diffusifs totaux de $CO_2$
$f_{CO_2}^*$	Flux diffusifs de $CO_2$ mesurés pour l'épilimnion et évalués à partir de $DIPM_{CO_2}$ , $DIBR_{CO_2}$ et $DIPH_{CO_2}$
$[Fe]$	Concentration en fer dissous
$f_{terr}$	Fraction terrigène de la matière organique

$k_{CO_2}$	Vélocité de piston
$K_{d,I,\lambda}$	Coefficient d'atténuation descendante de l'irradiance spectrale
$pCO_{2atm}$	Pression atmosphérique partielle
$PH_{CO_2}(0)$	Mesure de la fixation de $CO_2$ par photosynthèse en surface
$PM_{CO_2}(0)$	Mesure de la production de $CO_2$ par photodégradation de la DOM en surface
$pm(0 - .04)$	Estimation de la production de $CO_2$ par photodégradation de la DOM intégrée sur les quatre premiers centimètres
$pm_z$	Estimation de la production de $CO_2$ par photodégradation de la DOM à la profondeur z
$\overline{pm}_z$	Taux de photodégradation de la DOM à la profondeur z standardisé selon $\overline{Q}_{d,v,0+,\lambda}$
$Q_{d,v,0+,\lambda}$	Vecteur descendant de la densité de flux de photons en surface
$\overline{Q}_{d,v,0+,\lambda}$	Moyenne du vecteur descendant de la densité de flux de photons en surface pour l'ensemble des échantillons
$Sc_{CO_2}$	Nombre de Schmidt

$T_{\omega}^{\circ}$	Température de l'eau en surface
$Z_{1\%, \lambda}$	Profondeur de la zone photique
$\lambda_8$	Indicateur de quantité relative de matière organique terrigène (MOT) pour 100mg CO estimé pour différentes fractions du carbone organique
$\lambda_{vol}$	Indicateur de quantité de matière organique (MOT) terrigène estimé pour pour la fraction dissoute du carbone organique présent dans l'épilimnion
$\lambda_{DOC}$	Indicateur de quantité relative de matière organique terrigène (MOT) pour 100mg CO estimé pour la fraction dissoute de l'épilimnion
$\lambda_{POC}$	Indicateur de quantité relative de matière organique terrigène (MOT) pour 100mg CO estimé pour la fraction particulaire de l'épilimnion
$\phi_{\lambda}$	Rendement quantique de la photodégradation à $\lambda$

- $\Sigma_8$             Indicateur de quantité relative à de matière organique terrigène pour 10 g d'échantillons estimé pour différentes fractions du carbone organique
- $\Sigma_C$             Composés de la famille des Cinnamyles (acide férulique et acide p-coumarique)
- $\Sigma_p$             Composés de la famille des p-hydroxyphénols (p-hydroxybenzaldéhyde, p-hydroxyacétophénone et acide p-hydroxybenzoïque).
- $\Sigma_S$             Composés de la famille des Syringyles (syringaldéhyde, acétosyringone et acide syringique)
- $\Sigma_V$             Composés de la famille des Vanillyles (vanilline, acétovanillone, et acide vanillique)
- 
- 3,5 - *Bd*        Acide 3,5 dihydroxybenzoïque

## RÉSUMÉ

Le présent projet de recherche a pour objet l'étude des changements opérés sur les apports en matière organique terrigène dans les milieux aquatiques (réservoirs hydroélectriques, lacs naturels) tant au niveau de sa quantité que de sa réactivité, ceci lors du déboisement d'une partie de leurs bassins versants. Nous souhaitons caractériser le devenir de la matière organique terrigène en milieux aquatiques, en matière d'émissions de gaz à effets de serre. Nous évaluons la quantité de  $\text{CO}_2$  produite par photodégradation pour les systèmes aquatiques naturels et perturbés en fonction du coefficient d'absorption spectral du milieu étudié ( $a_{CDOM,\lambda}$ ). La photoréactivité de la matière organique dissoute présente dans la colonne d'eau est évaluée pour deux situations environnementales : l'une considère la perturbation des bassins versants par récolte forestière, l'autre porte sur l'opposition entre lacs naturels et réservoirs hydroélectriques. L'observation de la photoréactivité des composés de taille inférieure à  $0,2 \mu\text{m}$  sous conditions naturelles permet de mettre en évidence une forte variabilité de cette réactivité selon les situations, de la production de  $\text{CO}_2$  issue de la dégradation photochimique. Dans un second temps, nous avons souhaité comprendre l'origine des processus hétérotrophes observés dans des lacs et réservoirs de la forêt boréale québécoise. Les émissions atmosphériques dérivées de cette production pour chaque plan d'eau, conduisent à l'estimation d'un flux de  $\text{CO}_2$  total qui peut être comparé aux flux diffusifs totaux de  $\text{CO}_2$  obtenus suite à l'échantillonnage de la couche mince de surface (méthode TBL). Nous avons mesuré la quantité de  $\text{CO}_2$  produite quotidiennement, pour l'ensemble de la colonne d'eau par photodégradation de la matière organique dissoute ( $DIPM_{\text{CO}_2}$ ). Les flux de  $\text{CO}_2$  provenant de la respiration bactérienne ( $DIBR_{\text{CO}_2}$ ) tout comme les flux de fixation de  $\text{CO}_2$  par photosynthèse ( $DIPH_{\text{CO}_2}$ ), ont également été caractérisés. Finalement, nous avons cherché à vérifier si les variations observées dans les processus d'émissions selon les flux diffusifs totaux pouvaient être expliquées en fonction du niveau de perturbation de nos systèmes.

Mots Clés : Cycle du carbone, Lacs, Réservoirs hydroélectriques, Biomarqueurs de la lignine, Photodégradation, Gaz à effet de serre.

## INTRODUCTION

### 0.1 Mise en Contexte

Les activités anthropiques comme la coupe forestière ou la création de réservoirs hydroélectriques conduisent à des changements transitoires et permanents des processus biogéochimiques au niveau du cycle du carbone aquatique. La fraction organique des sols constitue le plus grand réservoir de carbone organique terrestre (Kern and Johnson 1993) et se trouve être une importante source de carbone organique pour les lacs et les réservoirs hydroélectriques (Houel et al. 2006; Thurman 1985). Les liens entre l'apport en matière organique terrigène et les émissions de gaz à effet de serre (GES) sont relativement peu étudiés, ce que cette étude propose d'approfondir afin de comprendre également dans quelle mesure les milieux aquatiques agissent comme sources ou puits de carbone. La variation de l'apport et la composition moléculaire de la matière organique ont des effets notoires sur les processus biogéochimiques des milieux lacustres (Meyers and Ishiwatari 1993). Plus récemment, des recherches ont été faites concernant le transport de la matière organique terrigène, de même que sa quantification et sa réactivité, en fonction de la physiographie du bassin versant (D'arcy and Carignan 1997). Des modèles sur le transport de la matière organique terrigène (MOT) du bassin versant vers le milieu aquatique ont d'ores et déjà été élaborés (Dillon and Molot 1997). L'impact du couvert végétal (Quideau et al. 2001) ou du déboisement (Farella et al. 2001) sur la dynamique de la matière organique commence en partie à être caractérisé. Les biomarqueurs ligneux constituent des outils précieux permettant d'étudier la dynamique de la MOT, une approche également préconisée lorsqu'on analyse les sédiments et les carottes de sols (Houel et al. 2006). Ces biomarqueurs moléculaires

sont utilisés pour suivre le devenir de la MOT en milieux aquatiques. Puisque les produits de l'oxydation de la lignine se dégradent lentement, il est possible de suivre l'état diagénétique de cette matière (Louchouart et al. 1999). Les processus de dégradation pédogénétique des composés ligneux commencent à être suffisamment documentés (Weissenberger 2007), tout comme les altérations que subissent les composés phénolés par dégradation bactérienne (Moran and Hodson 1994) ou photochimique (Louchouart et al. 2000; Opsahl and Benner 1995), ce qui devrait permettre une caractérisation fine de la signature ligneuse de la MOT parvenant aux milieux aquatiques. Des travaux récents portant sur les processus de dégradation aquatiques bactériens en plus de ceux concernant la minéralisation de la matière organique (Soumis et al. 2007) mettent à jour les interactions entre ces processus et les émissions de GES et permettent enfin de quantifier les flux de carbone. Il semble ainsi possible de suivre le cycle de dégradation de la MOT à l'échelle d'un bassin versant et de déterminer l'importance relative que son apport revêt, suite à des perturbations anthropiques, sur le plan des émissions de GES (principalement CO<sub>2</sub> et CH<sub>4</sub>).

## 0.2 Objectifs de la thèse

Le présent projet de recherche a pour objet l'étude des changements opérés sur les apports en MOT dans les milieux aquatiques (réservoirs hydroélectriques, lacs naturels) tant au niveau de sa quantité que de sa réactivité, ceci lors du déboisement d'une partie de leurs bassins versants. Elle cherche également à circonscrire précisément les liens existant entre ce déboisement et les émissions de GES. À cette fin, nous proposons une évaluation saisonnière de l'apport en matière organique terrigène au sein des systèmes aquatiques sélectionnés. Nous voulons ultimement caractériser le devenir de la MOT en milieux aquatiques, en matière d'émissions de GES, sous différents scénarios.

### 0.3 Chapitre I

Ce chapitre évalue la quantité de CO<sub>2</sub> produite par photodégradation pour les systèmes aquatiques naturels et perturbés en fonction du coefficient d'absorption spectral du milieu étudié ( $a_{CDOM,\lambda}$ ). La photoréactivité de la matière organique dissoute présente dans la colonne d'eau est évaluée pour deux situations environnementales : l'une considère la perturbation des bassins versants par récolte forestière, l'autre porte sur l'opposition entre lacs naturels et réservoirs hydroélectriques. L'observation de la photoréactivité des composés de taille inférieure à 0,2 µm sous conditions naturelles permet de mettre en évidence une forte variabilité de cette réactivité selon les situations, de la production de CO<sub>2</sub> issue de la dégradation photochimique.

### 0.4 Chapitre II

L'objet de ce chapitre est de comprendre l'origine des processus hétérotrophes observés dans des lacs et réservoirs de la forêt boréale québécoise. La quantification du CO<sub>2</sub> produit dans la colonne d'eau est obtenue grâce à un système d'incubation/irradiation. Les émissions atmosphériques dérivées de cette production pour chaque plan d'eau, conduisent à l'estimation d'un flux de CO<sub>2</sub> total qui peut être comparé aux flux diffusifs totaux obtenus suite à l'échantillonnage de la couche mince de surface (méthode TBL). La méthode d'incubation est ainsi validée et il a été possible de mesurer l'importance relative des processus hétérotrophes. Nous avons, de plus, mesuré la quantité de CO<sub>2</sub> produite quotidiennement, pour l'ensemble de la colonne d'eau par photodégradation de la matière organique dissoute ( $DIPM_{CO_2}$ ). Les flux de CO<sub>2</sub> provenant de la respiration bactérienne ( $DIBR_{CO_2}$ ) tout comme les flux de fixation de CO<sub>2</sub> par photosynthèse ( $DIPH_{CO_2}$ ), sont également caractérisés dans ce chapitre.

### 0.5 Chapitre III

Ce chapitre porte sur le cycle du carbone aquatique des lacs et des vieux réservoirs hydroélectriques. Nous avons cherché à caractériser l'origine de la matière organique afin de vérifier si les variations observées dans les processus d'émissions selon les flux diffusifs totaux pouvaient être expliquées en fonction du niveau de perturbation de nos systèmes. Afin de valider cette hypothèse, il a été nécessaire de caractériser finement le cycle du matériel organique terrigène (MOT). Cette caractérisation est basée sur une analyse des composés terrigènes présents dans la colonne d'eau sous leur forme dissoute (COD) ou particulaire (COP), mais également dans les sédiments (SED).

### 0.6 L'analyse des composés de la lignine

Les biomarqueurs moléculaires spécifiques de la matière organique ligneuse terrigène sont obtenus selon la méthode développée par Gofni et Montgomery (2000) utilisant l'oxyde de cuivre (CuO). Cette oxydation permet de mesurer 14 composés phénoliques dérivés de la lignine et regroupés en quatre familles principales : les cinnamiles (C ; acide férulique et acide p-coumarique), les syringiles (S ; syringaldéhyde, acétosyringone et acide syringique), les vanillyles (V ; vanilline, acétovanillone, et acide vanillique), les p-hydroxyphénols (P ; p-hydroxybenzaldéhyde, p-hydroxyacétophénone et acide p-hydroxybenzoïque) ainsi que l'acide 3,5 dihydroxybenzoïque (3,5 Bd). Une combinaison judicieuse de ces composés phénolés permet de construire les six indicateurs suivants : (i) lambda qui est une représentation de la contribution relative du matériel terrigène dans la matière organique ( $\lambda_8$  est la somme des C, S et V normalisée pour 100 mg de CO), (ii) sigma qui est également un indicateur relatif de la fraction terrigène ( $\Sigma_8$  est la somme normalisée pour 10 g d'échantillon des C, S, et V) (iii) le rapport C/V qui est utilisé pour différencier les sources de MOT boisées et non boisées (Hedges and Mann 1979), (iv) le rapport S/V qui permet de différencier les angiospermes des

gymnospermes (Teisserenc et al. 2010), (v) le rapport  $P/(V+S)$  qui est un indicateur diagénétique, c'est-à-dire un indicateur de l'état de dégradation de la lignine (Dittmar and Lara 2001), et (vi) le rapport  $3,5Bd/V$ , indicateur de maturation dans les sols, qui permet également de différencier les horizons organiques et inorganiques des sols boréaux (Houel et al. 2006).

#### 0.7 Les méthodes d'échantillonnage de la matière organique

Afin de recueillir, concentrer et analyser les biomarqueurs ligneux servant à l'établissement des signatures particulières à chaque processus d'introduction de la MOT en milieux aquatiques, nous nous proposons d'adopter un protocole rigoureusement évalué (Houel et al. 2006; Ouellet et al. 2009; Teisserenc et al. 2010). Ainsi, l'eau échantillonnée est d'abord filtrée à  $210 \mu\text{m}$  avant d'utiliser la filtration tangentielle pour recueillir les fractions de matière organique comprises entre  $210 \mu\text{m}$  et  $0,45 \mu\text{m}$ . La portion dissoute de la matière organique (c'est-à-dire la fraction des tailles inférieures à  $0,45 \mu\text{m}$ ) est ensuite déminéralisée à l'aide d'une résine échangeur de cations (Chelex-200) puis concentrée par osmose inverse. Bien que les biomarqueurs ligneux soient relativement peu susceptibles de se dégrader en milieux aquatiques (Weissenberger, comm. pers.) et soient davantage affectés par l'activité fongique sur les bassins versants (Moran and Hodson 1994) la signature aquatique sera évaluée dans les différentes fractions, dissoutes, particulaires et sédimentaires afin de fournir une discussion sur les variations des signatures ligneuses ainsi obtenues.

Afin d'obtenir les signatures aquatiques, nous avons procédé à la collecte des échantillons dans la colonne d'eau selon un prélèvement de 250 L d'eau filtrée à  $70 \mu\text{m}$  dans l'épilimnion. Ces échantillons ont été concentrés par osmose inverse sur le site d'échantillonnage puis lyophilisés lors du retour en laboratoire. Une analyse des biomarqueurs ligneux a été faite sur chacun de ces échantillons. Cette analyse nous a permis de déterminer « la signature aquatique », c'est-à-dire la quantité relative des

composés phénoliques analysés dans les échantillons de notre plan d'eau. Chaque échantillon d'eau recueilli sur le bassin versant a été lyophilisé puis analysé au Carlo Erba (NA-1500) pour déterminer le rapport atomique du carbone sur l'azote (C/N), (indicateur des proportions respectives de matériel organique autochtone ou allochtone). Le pourcentage de carbone est également obtenu afin de suivre la méthode d'oxydation de la matière organique par l'oxyde de cuivre. Les échantillons sont ensuite extraits, dérivatisés puis analysés par chromatographie en phase gazeuse (Varian 3800) couplée à la spectrométrie de masse (Varian Saturn 2000).

#### 0.8 Les méthodes d'évaluation de production et d'émissions de CO<sub>2</sub>

Nous avons finalement évalué les taux de minéralisation biotique et abiotique selon un protocole déjà bien rodé (Soumis et al. 2007). Des cellules transparentes faites de quartz et des cellules obscures sont remplies d'eau prélevée sur les sites d'échantillonnages. Suite à une incubation/irradiation de ces échantillons pendant 24 h, le contenu de ces cellules est analysé à l'aide d'un chromatographe en phase gazeuse (GC Varian 3800) afin de mesurer leur concentration en CO<sub>2</sub>. Trois phénomènes sont analysés à l'aide de cette méthode : (i) le taux de production de CO<sub>2</sub> imputable à la photodégradation (ii) la respiration bactérienne en présence ou absence de lumière, et (iii) un bilan de la respiration planctonique pour la fraction de taille  $\leq 210 \mu\text{m}$ . La quantité totale de CO<sub>2</sub> émise vers l'atmosphère est quant à elle évaluée à partir de la concentration en CO<sub>2</sub> mesurée dans la couche mince de surface (Duchemin et al. 1998).

#### 0.9 Importance des travaux

La dynamique de la matière organique entre les écosystèmes terrestres et aquatiques de la zone boréale n'est pas précisément connue. L'impact de la déforestation sur les apports en MOT et la réactivité de cette dernière dans les milieux aquatiques reste peu documenté malgré l'importance que revêt la recherche dans ce domaine. De nombreuses études permettent par ailleurs de lier l'apport en mercure et en nutriments

à la quantité de MOT transitant vers les écosystèmes aquatiques (Mierle and Ingram 1991; Porvari et al. 2003; Scherbatskoy et al. 1998). Compte tenu, aujourd'hui, de l'importance que présente une compréhension fine du cycle du carbone à l'échelle planétaire, il apparaît nécessaire de caractériser, comme le propose cette thèse, les différents processus de dégradation de la matière organique présente dans la colonne d'eau. Finalement, cette recherche devrait permettre de mieux saisir le rôle que pourrait jouer le carbone organique terrigène dans les processus d'émissions totales de CO<sub>2</sub> des milieux aquatiques vers l'atmosphère.

## Références

- D'arcy, P., and R. Carignan. 1997. Influence of catchment topography on water chemistry in southeastern Québec Shield lakes. *Can J Fish Aquat Sci* **54**: 2215-2227.
- Dillon, P. J., and L. A. Molot. 1997. Dissolved organic and inorganic carbon mass balances in central Ontario lakes. *Biogeochemistry* **36**: 29-42.
- Dittmar, T., and R. J. Lara. 2001. Molecular evidence for lignin degradation in sulfate-reducing mangrove sediments (Amazonia, Brazil). *Geochimica et Cosmochimica Acta* **65**: 1417-1428.
- Duchemin, E., M. Lucotte, and R. Canuel. 1998. Comparison of Static Chamber and Thin Boundary Layer Equation Methods for Measuring Greenhouse Gas Emissions from Large Water Bodies. *Environmental Science & Technology* **33**: 350-357.
- Farella, N., M. Lucotte, P. Louchouart, and M. Roulet. 2001. Deforestation modifying terrestrial organic transport in the Rio Tapajos, Brazilian Amazon. *Organic Geochemistry* **32**: 1443-1458.
- Goñi, M. A., and S. Montgomery. 2000. Alkaline CuO Oxidation with a Microwave Digestion System: Lignin Analyses of Geochemical Samples. *Analytical Chemistry* **72**: 3116-3121.
- Hedges, J. I., and D. C. Mann. 1979. The characterization of plant tissues by their lignin oxidation products. *Geochimica et Cosmochimica Acta* **43**: 1803-1807.
- Houel, S., P. Louchouart, M. Lucotte, R. Canuel, and B. Ghaleb. 2006. Translocation of Soil Organic Matter Following Reservoir Impoundment in Boreal Systems: Implications for In situ Productivity. *Limnology and Oceanography* **51**: 1497-1513.
- Kern, J. S., and M. G. Johnson. 1993. Conservation Tillage Impacts on National Soil and Atmospheric Carbon Levels. *Soil Sci. Soc. Am. J.* **57**: 200-210.
- Louchouart, P., M. Lucotte, and N. Farella. 1999. Historical and geographical variations of sources and transport of terrigenous organic matter within a large-scale coastal environment. *Organic Geochemistry* **30**: 675-699.
- Louchouart, P., S. Opsahl, and R. Benner. 2000. Isolation and Quantification of Dissolved Lignin from Natural Waters Using Solid-Phase Extraction and GC/MS. *Analytical Chemistry* **72**: 2780-2787.

- Meyers, P. A., and R. Ishiwatari. 1993. Lacustrine organic geochemistry—an overview of indicators of organic matter sources and diagenesis in lake sediments. *Organic Geochemistry* **20**: 867-900.
- Mierle, G., and R. Ingram. 1991. The role of humic substances in the mobilization of mercury from watersheds. *Water, Air, & Soil Pollution* **56**: 349-357.
- Moran, M. A., and R. E. Hodson. 1994. Dissolved Humic Substances of Vascular Plant Origin in a Coastal Marine Environment. *Limnology and Oceanography* **39**: 762-771.
- Opsahl, S., and R. Benner. 1995. Early diagenesis of vascular plant tissues: Lignin and cutin decomposition and biogeochemical implications. *Geochimica et Cosmochimica Acta* **59**: 4889-4904.
- Ouellet, J.-F., M. Lucotte, R. Teisserenc, S. Paquet, and R. Canuel. 2009. Lignin biomarkers as tracers of mercury sources in lakes water column. *Biogeochemistry* **94**: 123-140.
- Porvari, P., M. Verta, J. Munthe, and M. Haapanen. 2003. Forestry Practices Increase Mercury and Methyl Mercury Output from Boreal Forest Catchments. *Environmental Science & Technology* **37**: 2389-2393.
- Quideau, S. A., O. A. Chadwick, A. Benesi, R. C. Graham, and M. A. Anderson. 2001. A direct link between forest vegetation type and soil organic matter composition. *Geoderma* **104**: 41-60.
- Scherbatskoy, T., J. Shanley, and G. Keeler. 1998. Factors Controlling Mercury Transport in an Upland Forested Catchment. *Water, Air, & Soil Pollution* **105**: 427-438.
- Soumis, N., M. Lucotte, C. Larose, F. Veillette, and R. Canuel. 2007. Photomineralization in a boreal hydroelectric reservoir: a comparison with natural aquatic ecosystems. *Biogeochemistry* **86**: 123-135.
- Teisserenc, R., M. Lucotte, S. Houel, and J. Carreau. 2010. Integrated transfers of terrigenous organic matter to lakes at their watershed level: A combined biomarker and GIS analysis. *Geochimica et Cosmochimica Acta* **74**: 6375-6386.
- Thurman, E. M. 1985. *Organic geochemistry of natural waters*. M. Nijhoff, Distributors for the U.S. and Canada, Kluwer Academic.

Weissenberger, S. 2007. Émissions de gaz à effet de serre et cycle du carbone de réservoirs hydroélectriques du moyen Nord québécois. Université du Québec à Montréal.

## CHAPITRE I

PHOTODÉGRADATION DE LA MATIÈRE ORGANIQUE DISSOUE DANS  
LES EAUX DE SURFACES ET DIFFUSION DU CO<sub>2</sub> VERS L'ATMOSPÈRE  
POUR LES PLANS D'EAU PERTURBÉS ET VIERGES EN RÉGION BORÉALE  
QUÉBÉCOISE (CANADA)

DISSOLVED ORGANIC MATTER PHOTODEGRADATION IN SURFACE  
WATERS AND CO<sub>2</sub> ATMOSPHERIC DIFFUSION IN PRISTINE AND  
PERTURBED WATERBODIES OF THE BOREAL REGION IN QUÉBEC  
(CANADA)

Jean-Baptiste Plouhinec<sup>1</sup>, Marc Lucotte<sup>1</sup>, Alexandre Ouellet<sup>2</sup> and Yves  
Gélinas<sup>2</sup>

<sup>1</sup>GEOTOP and Institute of Environmental Sciences, UQAM, C.P. 8888, Succursale  
Centre-Ville, Montréal, Québec, Canada, H3C-3P8

<sup>2</sup>GEOTOP and Department of Chemistry and Biochemistry, Concordia University,  
7141 Sherbrooke Street West, Montréal, Québec, Canada, H4B-1R6

Corresponding author:  
Jean-Baptiste PLOUHINEC  
Université du Québec à Montréal  
GEOTOP-UQAM-McGill  
CP 8888 Succ. Centre-Ville,  
Montréal, Québec, Canada  
H3C 3P8

Phone number: 514-987-3000 #5662  
Fax: 514-987-3635  
Email: [plouhinec.jean-baptiste@uqam.ca](mailto:plouhinec.jean-baptiste@uqam.ca)

**Acknowledgments:**

We thank the Natural Science and Engineering Research Council of Canada (NSERC) and the *Fonds Québécois de la recherche sur la nature et les technologies* (FQRNT). The authors thank Nicolas Soumis (UQAM) for his precious advice on experimental protocols, as well as Sophie Chen from UQAM for her help in the laboratory. This study was funded through grants (M.L. and Y.G.) and scholarships (A.O. and J.B.P.) from BIOCAP-Canada and NSERC. This is GEOTOP contribution 2012-XXXX.

## Résumé

Cette étude présente différentes mesures de photodégradation de la matière organique dissoute (MOD) pour des plans d'eau qui ont été impactés, ou non, par la coupe forestière et qui sont situés en région boréale du Québec (Canada). Nous avons considéré l'impact de deux activités anthropiques sur le cycle du carbone aquatique, l'exploitation forestière massive sur le bassin versant de lacs ou sur le bassin de réservoirs mis en eau il y a plusieurs décennies. Pendant l'été, la production quotidienne de CO<sub>2</sub> par photodégradation entraîne des émissions de CO<sub>2</sub> vers l'atmosphère qui varient entre 0 et 32.4 μmol·L<sup>-1</sup>·d<sup>-1</sup>. La production quotidienne de CO<sub>2</sub> par minéralisation photochimique est très différente pour les lacs ou les réservoirs. Au printemps et durant l'été, la production moyenne de CO<sub>2</sub> a été évaluée à 5.45 ± 5.61 μmol·L<sup>-1</sup>·d<sup>-1</sup> pour les lacs, comparativement à 14.21 ± 8.77 μmol·L<sup>-1</sup>·d<sup>-1</sup> pour les réservoirs. Une comparaison similaire entre les écosystèmes touchés ou non par l'exploitation forestière, a également montré une variation importante de la photodégradation de la MOD dans les eaux de surface. Les plans d'eau naturels présentent des émissions de CO<sub>2</sub> par photodégradation de 4.52 ± 3.58 μmol·L<sup>-1</sup>·d<sup>-1</sup> alors que la MOD dans les lacs ou réservoirs affectés par l'exploitation forestière est beaucoup plus photodégradable dans les eaux de surface avec 18.47 ± 6.59 μmol·L<sup>-1</sup>·d<sup>-1</sup> de CO<sub>2</sub> produite quotidiennement par photodégradation. Pour représenter le rendement de la photodégradation de la MOD dans des conditions d'exposition contrôlées, nous avons créé l'indicateur  $\overline{PM}_{CO_2}(0)$  qui fournit une valeur normalisée selon la densité de flux de photons ce rendement. Cet indicateur est fortement corrélé aux flux diffusifs totaux de CO<sub>2</sub> ( $f_{CO_2}$ ). Enfin, la concentration en fer dissous  $[Fe]$ , est corrélée à l'indicateur de rendement de photodégradation de la MOD normalisée selon la concentration de carbone organique dissous (COD) dans l'eau de surface avec une valeur R<sup>2</sup> de 0.74. Cela suggère que la photodégradabilité de la MOD dans les eaux boréales de surface soit corrélée à la fraîcheur de la matière organique terrigène lessivé du bassin versants vers les cours d'eau.

Mots Clés: Photominéralisation, Récolte forestière, Réservoirs hydroélectriques boréaux, Rendement quantique, Cycle du carbone aquatique.

## Abstract

This study presents the differentiated photodegradation of dissolved organic matter (DOM) in pristine and human impacted water bodies located in the boreal forest domain of Quebec (Canada). We considered the impact of two human activities on the aquatic carbon cycle, recent massive logging on the watershed and large reservoirs impounded several decades ago. During summer, photodegradation entailed daily atmospheric CO<sub>2</sub> emissions that varied between 0 and 32.4 μmol·L<sup>-1</sup>·d<sup>-1</sup>. The daily production of CO<sub>2</sub> by photochemical mineralization was strikingly different between lakes and reservoirs. Average springtime and summertime CO<sub>2</sub> production was evaluated at 5.45 ± 5.61 μmol·L<sup>-1</sup>·d<sup>-1</sup> for lakes, compared to 14.21 ± 8.77 μmol·L<sup>-1</sup>·d<sup>-1</sup> for reservoirs. A similar comparison between ecosystems affected or not by logging, also showed contrasting results for DOM photodegradation in surface waters. Natural water bodies showed CO<sub>2</sub> emissions of 4.52 ± 3.58 μmol·L<sup>-1</sup>·d<sup>-1</sup> whereas DOM in lakes or reservoir affected by logging was much more photodegradable in surface waters, with daily production of CO<sub>2</sub> by photochemical mineralization of 18.47 ± 6.59 μmol·L<sup>-1</sup>·d<sup>-1</sup>. To represent the DOM photodegradation yield under controlled exposure conditions, we created the indicator  $\overline{PM}_{CO_2}(0)$  standardized for photon flux density. This indicator was highly correlated to total diffusive fluxes of CO<sub>2</sub> ( $f_{CO_2}$ ). Finally, the dissolved iron concentrations ( $[Fe]$ ) were correlated to the DOM photodegradation yield indicator normalized to dissolved organic carbon concentrations (DOC) with an  $r^2$  value of 0.74. This suggests that the DOM photodegradability in surface boreal waters is correlated to the freshness of terrigenous organic matter brought from the watersheds to the water bodies.

Keywords: Photochemical mineralization, forest harvesting, boreal hydroelectric reservoirs, quantum yield, aquatic carbon cycle.

## 1.1 Introduction

Carbon emissions from the world's freshwater resources represent a recently estimated annual flux of 0.75 PgC (Cole et al. 2007). Despite this estimate, much remains to be explored regarding the mechanisms of production and emission of CO<sub>2</sub> in aquatic ecosystems. Some categories of water bodies, such as hydroelectric reservoirs, have only been sparsely studied even though they account for more than 37% of the total global production of CO<sub>2</sub> from freshwater systems (Cole et al. 2007). Since the mid-1990s, new analytical approaches, such as static chambers or the thin boundary layer method, have been used to calculate the diffusive fluxes of CO<sub>2</sub> to the atmosphere thus allowing global quantification of emissions by aquatic systems (Cole et al. 1994). These analyses have also led to a number of studies on the comparison of the different measurement methods for quantifying these emissions, their accuracy and their costs in human resources (Soumis et al. 2008; Soumis et al. 2005), as well as on the degree to which sampling has been representative of the real fluxes between the water column and the atmosphere (Soumis et al. 2004).

Regardless of whether the type of site being studied is a hydroelectric reservoir or a natural lake, the three main processes of carbon emissions that make up the total diffusive fluxes of CO<sub>2</sub> are plankton respiration, bacterial respiration, and the degradation of carbon compounds by photochemical processes (Prairie 2008; Soumis et al. 2007). This article targets one of these processes, i.e. the photodegradation of dissolved organic matter (DOM) in the water column. Interest in this particular process stems from its relative importance in terms of total carbon emissions compared to the other processes (Soumis et al. 2007).

Photodegradation depends mainly upon the downward vector photon flux density in surface water layers for a given wavelength  $\lambda$  ( $Q_{d,v,0+,\lambda}$ ), the absorption coefficient of chromophoric dissolved organic matter (CDOM) at  $\lambda$  ( $a_{CDOM,\lambda}$ ), the downward attenuation coefficient of irradiance at  $\lambda$  ( $K_{d,l,\lambda}$ ) and the quantum yield for photodegradation at  $\lambda$  ( $\phi_\lambda$ ). Reports by Tranvik and Betilsson (2001) suggest that important fraction of CO<sub>2</sub> emissions from photodegradation can be attributed to terrigenous DOM. The main objective of this study was thus to test the latter hypothesis by examining sites with contrasting environmental conditions that affect dissolved organic carbon (DOC) concentrations, namely, recent logging activities in the lake watershed and the impoundment of large reservoirs. Our working hypothesis is that the contrast between these different environmental conditions should offer evidence that the variations in the quantity of terrigenous DOM has a substantial effect on the quantity of CO<sub>2</sub> produced by photodegradation.

## 1.2 Methods

### 1.2.1 Research sites

This study examined seven lakes located in Quebec, at the heart of the Forêt de l'Aigle conservation area, 30 km west of Maniwaki, as well as two large reservoirs impounded several decades ago, Decelles and Cabonga, located in the Vérendrye wildlife reserve. Each water body studied, Lakes Mary, Ellard, Jean, Claire, Brock, and Bouleau, as well as Cabonga and Decelles Reservoirs, were categorized according to four environmental conditions (see Table 1.1). These conditions are as follows: lakes affected by logging (LAL), lakes not affected by logging (LNAL), also defined as pristine lakes, Decelles, a reservoir affected by logging (RAL), and Cabonga, a reservoir that has not been affected by logging (RNAL). A water body

was deemed to be affected by logging if massive logging activity occurred over the past 10 years on the lake's watershed. All water bodies are situated on the Precambrian shield, in the boreal region, in a mixed forest ecozone. The surface area of each lake is relatively small, ranging from 0.280 km<sup>2</sup> for Lake Ellard to 1.879 km<sup>2</sup> for Lake Jean. It should be noted that small lakes with areas of 0.1 to 10 km<sup>2</sup> cover a surface equivalent to that of lakes with areas comprised between 10 and 100 km<sup>2</sup> (Downing et al. 2006). The Cabonga Reservoir was impounded in 1928 while the Decelles Reservoir was impounded in 1941 and expanded in 1949. This study therefore relates to lakes and old reservoirs considered stabilized, sampled in the spring, summer and fall seasons of 2006 and 2007.

#### 1.2.2 Sampling method for a thin layer of surface water and analysis by gas chromatography

Different methods have been developed for the measurement of the fluxes of CO<sub>2</sub> emitted to the atmosphere, most notably static chambers and a method developed by Cole et al. (Cole et al. 1994) that measures concentrations of gases present in dissolved form in a thin layer of surface water (the thin boundary layer method, or TBL). According to a recent study, the use of static chambers introduces an important bias into the calculation of diffusive fluxes through disturbance of concentration gradients in the water column (Prairie 2008). Using the static chamber method also demands a significant logistical effort given the size of the reservoirs, and thus we selected the TBL method. The objective of this robust method (Duchemin et al. 1998; Kelly et al. 1997; Weissenberger 2007) is to obtain the value for the diffusive fluxes of CO<sub>2</sub> based on four factors: the concentration of these two gases dissolved in water, wind speed, air temperature, and water temperature. These variables are then integrated in the version of Cole and Caraco's (1998) equation modified by Soumis et al. (2007). In order to account for limits in the applicability of this model, we

assumed that surface waters were well mixed and that transfer of CO<sub>2</sub> across the interface took place through molecular diffusion (Liss and Slater 1974; Macintyre and Melack 1995).

Diffusive CO<sub>2</sub> fluxes were calculated on 30-mL samples taken from the first two centimeters of the water column at each site. Four samples were collected each time in 60-mL syringes to ensure the samples representativity. Then, 30 mL of ultrapure N<sub>2</sub> were added to each syringe. The four syringes were agitated by shaking for one minute before discarding the liquid part of the 30-mL sample. Upon shaking, CO<sub>2</sub> will migrate towards N<sub>2</sub> according to the equations developed by Duchemin et al. (1995). They were analyzed on a Varian Star-3400 gas chromatograph (GC) fitted with a 1-mL sampling loop and a stainless steel Hayesep-Q column (200 mm long, 3 mm in diameter, 80/100 mesh), as in Soumis et al. (2005). Helium was used as the carrier gas at a flow rate of 30 mL·min<sup>-1</sup>. Quantification of the gases was done with a thermal conductivity detector (TCD).

The diffusive flux of CO<sub>2</sub> at the water-air interface is calculated according to Fick's first law:

$$f_{CO_2} = k_{CO_2} \cdot ([CO_2]_{surf} - pCO_{2atm} \cdot K_H)$$

where  $f_{CO_2}$  is the diffusive flux of carbon dioxide,  $k_{CO_2}$  the piston velocity,  $K_H$  Henry's constant adjusted according to temperature and  $pCO_{2atm}$  (the partial atmospheric pressure). The piston velocity is defined by the equation:

$$k_{CO_2} = k_{600} \cdot (600 / Sc_{CO_2})^{0.67}$$

where  $k_{600}$  represents the constant of piston velocity normalized for a Schmidt number ( $Sc_{CO_2}$ ) of 600. We used a value of the constant  $k_{600}$ , which is determined using the model developed by Cole et al. (1994), where  $U_{10}$  is the wind speed at 10 m

over the surface of the lake. The constant for piston velocity is thus obtained from the empirical equation:

$$k_{600} = 2.07 + (0.215 \cdot U_{10}^{1.7})$$

finally, the Schmidt number for carbon dioxide is calculated according to the equation of Wanninkhof (1992):

$$Sc_{CO_2} = 1911.1 - 118.11 \cdot T_w^\circ - 3.4527 \cdot (T_w^\circ)^2 - 0.04132 \cdot (T_w^\circ)^3$$

where  $T_w^\circ$  is the temperature at the surface of the water.

### 1.2.3 The measurement of CO<sub>2</sub> produced by photochemical mineralization using quartz cell irradiation

The following sampling procedure was used at each site irrespectively of the season. The CO<sub>2</sub> produced by photochemical mineralization was assessed from a volume of 10 L of water collected along the entire depth of the photic zone  $Z_{1\%,PAR}$ . This depth was determined with a PUV-2500/2510 radiometric probe upon arrival at a site. Water was collected using a peristaltic pump and filtered through a nylon filter with pores of 210 μm. In order to limit the study to the DOM photodegradation, each sample was then filtered through a 0.2-μm nylon filter (Pall®) to eliminate nearly all living organisms including bacteria (Soumis et al. 2007). Samples were then immediately brought to the field laboratory installed on the shore of the water body. Laboratory analyses include measurements of the dissolved CO<sub>2</sub> concentration and absorbance of CDOM at λ before irradiation.

In order to understand interactions between photodegradation and CO<sub>2</sub> production, we measured the downward vector photon flux density on surface and at λ

$(Q_{d,v,0+\lambda})$ , to which each sample was exposed over the course of irradiation. For this purpose, opaque and transparent quartz cells were used (200 mm long, 40 mm ID). The transmittance of quartz cells varied between 88% and 94% over the entire spectrum studied (205-700 nm). The cells were sealed at their extremities using Parafilm® and rubber stoppers. Once prepared, these opaque sterile (OS) cells and transparent sterile (TS) cells were returned to the locations where they were originally sampled and were exposed to natural irradiation just below the water surface (0.02 m depth). The next step is to evaluate the amount of CO<sub>2</sub> produced by photochemical mineralization just below the surface expressed as  $PM_{CO_2}(0) = TS_{CO_2}(0) - OS_{CO_2}(0)$ , where  $TS_{CO_2}(0)$  and  $OS_{CO_2}(0)$  represent the concentration of dissolved CO<sub>2</sub> ( $\mu\text{mol.L}^{-1}$ ) after 24h of incubation, for the TS and OS cells respectively.

#### 1.2.4 Calculation of the theoretical amount of CO<sub>2</sub> produced by photochemical mineralization:

The first step in the analysis was to measure the average absorbance of CDOM at  $\lambda$  ( $A_{CDOM,\lambda}$ ) at wavelengths of 305, 313, 320, 340, 380, 395, 400, 550, and 700 nm. The absorbance of filtered samples was measured using a Beijing Purkinge General Instrument TU-18005 UV-PAR spectrophotometer. The average absorption coefficient of CDOM at  $\lambda$  ( $a_{CDOM,\lambda}$ ) was then calculated based on measurements of spectral absorbance of CDOM before irradiation ( $A_{CDOM,\lambda}_{ini}$ ) and after irradiation ( $A_{CDOM,\lambda}_{end}$ ), to take into account the fact that the absorbance of samples can decrease with the DOM photodegradation (Lindell et al. 2000; Reche et al. 1999). The value ( $A_{CDOM,\lambda}$ ) is based on the mean values of absorbance

$A_{CDOM,\lambda} = \left( \left( A_{CDOM,\lambda} \right)_{ini} + \left( A_{CDOM,\lambda} \right)_{end} \right) / 2$ ; The average absorbance of CDOM at  $\lambda$  was then used to determine the average absorption coefficient of CDOM at  $\lambda$  ( $a_{CDOM,\lambda}$ ), using Equation 1 (Kirk, 1994). In this equation,  $l$  is the length of the optical path corresponding to the quartz cells of the spectrophotometer ( $l = 0.1$  m)

$$a_{CDOM,\lambda} = 2,303 \cdot A_{CDOM,\lambda} / l \quad (1.1)$$

As previously described, the PUV-2500/2510 radiometric probes were used to determine the spectrum of downward vector photon flux density ( $Q_{d,v,0+,\lambda}$ ) to which each sample was exposed over the course of irradiation. Downwelling spectral irradiance values ( $E_{d\lambda}$ ) (Soumis et al. 2007) were converted from  $\mu W \cdot cm^{-2} \cdot nm^{-1}$  to  $\mu E \cdot m^{-2} \cdot nm^{-1}$  to be consistent with  $pm_z$  units. For our purposes, it seemed necessary to construct homogenous classes of 1-nm wavelength intervals in order to evaluate the relative contribution of each interval to  $CO_2$  production by photochemical mineralization. The construction of these classes was based on a model that includes the spectrum of downward vector photon flux density ( $Q_{d,v,0+,\lambda}$ ) and the absorption coefficient of CDOM at  $\lambda$  ( $a_{CDOM,\lambda}$ ). As known,  $\ln(a_{CDOM,\lambda}) = -S \cdot (\lambda - 420) + \ln(a_{CDOM,420})$ , where  $S$  is the slope ( $nm^{-1}$ ),  $a_{CDOM,\lambda}$ , and  $a_{CDOM,420}$  are the absorption coefficients ( $m^{-1}$ ) at  $\lambda$  and 420 nm respectively (Vähätalo et al. 2000). For the modeling of the spectrum of downward vector photon flux density ( $Q_{d,v,0+,\lambda}$ ) as a function of  $\lambda$ , a first approximation was made by using a polynomial of degree 2 on the interval 305-365 nm. A second approximation was made using a logarithmic function for the rest of the spectrum (365-700 nm).

Solar declination ( $\delta$ ), was calculated for each sample:

$$\delta = 23.45 \cdot \sin\left(\frac{2\pi}{365}(284 + D)\right)$$

where  $D$  is the day of year calendar. Thus, we are able to calculate, for each bodies of water, the specular reflection from the surface of lakes

$$(R_{spe,\lambda}): R_{spe,\lambda} = 0.5 \left[ \frac{\sin^2(\theta - \theta_{w,\lambda})}{\sin^2(\theta + \theta_{w,\lambda})} + \frac{\tan^2(\theta - \theta_{w,\lambda})}{\tan^2(\theta + \theta_{w,\lambda})} \right]$$

where the zenith angle of radiation in air ( $\theta$ ) was calculated from the latitude ( $\varphi$ ), the solar declination ( $\delta$ ), and the solar hour (h):

$$\theta = \arccos((\sin(\varphi) \cdot \sin(\delta) + \cos(\varphi) * \cos(\delta) * \cos(h)))$$

The zenith angle of radiation in water at  $\lambda$  ( $\theta_{w,\lambda}$ ) is defined by:

$$\theta_{w,\lambda} = \arcsin(\sin(\theta)/n_\lambda)$$

where  $n_\lambda = 1,31279 + 15,762 \cdot \lambda^{-1} - 4382 \cdot \lambda^{-2} + 1,1455 \times 10^6 \cdot \lambda^{-3}$

Finally, the photon flux just below the surface ( $Q_{d,v,0-,\lambda}$ ) can be obtained from the equation:

$$Q_{d,v,0-,\lambda} = Q_{d,v,0+,\lambda} \times (1 - R_{spe,\lambda})$$

As mentioned at the beginning of this section, the purpose was to evaluate the  $CO_2$  produced by photochemical mineralization at the depth  $z$  ( $pm_z$ ).

We define a simplified attenuation coefficient of downward irradiance ( $K_{d,l,\lambda}$ ) as follows:

$$K_{d,l,\lambda} = a_{CDOM,\lambda} / \mu_\lambda$$

$$\text{with } \mu_\lambda = \cos(\theta_{w,\lambda})$$

This allowed us to determine the scalar photon flux density at depth  $z$  and at  $\lambda$ :

$$Q_{s,z,\lambda} = \mu_\lambda^{-1} \cdot Q_{d,v,0-\lambda} \cdot e^{-zK_{d,l,\lambda}}$$

The factor  $C_\phi$  is based on the theoretical  $pm_z$  developed by Vähätalo et al. (2000). The primary source for DOM photodegradation reactions is the absorption of solar radiation by CDOM (Mopper et al. 1991; Zafiriou et al. 1984). Thus, we can determine the rate of DOM photodegradation reactions at a depth  $z$  ( $pm_z$ ,  $\text{molC} \cdot \text{m}^{-3} \cdot \text{d}^{-1}$ ) as a product of three spectra modified from Miller (1998):

$$pm_z = \int_{\lambda_{\min}}^{\lambda_{\max}} \phi_\lambda Q_{s,z,\lambda} a_{CDOM,\lambda} d\lambda$$

Each term of this equation was previously described. The factors  $\lambda_{\min}$  and  $\lambda_{\max}$  represent the wavelengths at 300 nm and 700 nm respectively. As suggested by Vähätalo et al. (2000), the spectrum of apparent quantum yield for photodegradation  $\phi_\lambda$  (mol produced DIC/mol absorbed photons) related to natural DOM, decreases exponentially with increasing wavelength (Moore et al. 1993; Sikorski and Zika 1993; Vähätalo et al. 2000) and can be generalized to:

$$\phi_\lambda = c \times 10^{-d\lambda}$$

where  $c$  (dimensionless) and  $d$  ( $\text{nm}^{-1}$ ) are positive constants and  $\lambda$ , the wavelength in nanometers. As measured by Vähätalo et al. (2000), the constants  $c$  and  $d$  are fixed to 7.52 and 0.0122 throughout this article. We assigned the integrated value of  $pm_z$  over  $z \in ]0; 0.04]$  to  $pm(0-.04)$ . The transparent cells have internal radius of 2 centimeters. Thus,  $pm(0-.04)$ , the theoretical integrated value of DOM photodegradation over the

top four centimeters, can be directly compared to  $PM_{CO_2}(0)$  (in situ measurements).

Finally, we can define our factor  $C_\phi$ , as follows:

Firstly,

$$pm_z = c * \int_{\lambda \min}^{\lambda \max} 10^{-a\lambda} Q_{s,z,\lambda} a_{CDOM,\lambda} d\lambda$$

Thus, for d fixed to 0.0122, we define:

$$pm(0 - .04) = C_\phi \cdot PM_{CO_2}(0)$$

Thus, we obtain:

$$C_\phi = \frac{pm(0 - .04)}{PM_{CO_2}(0)}$$

### 1.2.5 Chemical analyses

DOC concentrations were measured using a high temperature catalytic combustion Shimadzu TOC-5000A analyzer. The samples were combusted in a column containing platinum-covered aluminum oxide beads maintained at a temperature of 680°C and the resulting CO<sub>2</sub> was then quantified by non dispersive infrared spectroscopy. The total concentration of iron in the samples was measured using a GBC-906AA atomic absorption spectrophotometer equipped with a graphite furnace. DOC and total iron concentrations were integrated over the entire photic zone.

## 1.3 Results

### 1.3.1 Physical and Chemical Parameters

The average DOC concentrations ranged from  $3.99 \pm 1.10 \text{ mg C}\cdot\text{L}^{-1}$  for lakes not affected by logging (LNAL), to  $7.75 \pm 1.38 \text{ mg C}\cdot\text{L}^{-1}$  for the Decelles Reservoir, where the watershed was affected by logging (RAL, Table 1.1). The Cabonga Reservoir, not affected by logging (RNAL), presented an average DOC concentration of  $5.13 \pm 1.30 \text{ mg C}\cdot\text{L}^{-1}$ , lower than the value for LALs ( $5.85 \pm 1.09 \text{ mg C}\cdot\text{L}^{-1}$ ). The average DOC concentration for both reservoirs ( $6.46 \pm 1.86 \text{ mg C}\cdot\text{L}^{-1}$ ) was greater than the average value for all lakes ( $4.61 \pm 1.40 \text{ mg C}\cdot\text{L}^{-1}$ ).

The pattern was the same for the total concentrations of Fe in the photic zone (Table 1.1). Variability in Fe concentrations across the four environmental scenarios was however much higher than for DOC ones, with values ranging from  $0.54 \pm 0.30 \mu\text{mol}\cdot\text{L}^{-1}$  for LNAL to  $2.73 \pm 0.8 \mu\text{mol}\cdot\text{L}^{-1}$  for RAL. Systems not affected by logging activities generally had lower Fe concentrations ( $0.54 \pm 0.30$  and  $0.98 \pm 0.63 \mu\text{mol}\cdot\text{L}^{-1}$  for LNAL and RNAL, respectively) compared to their logged counterparts. Finally, higher Fe concentrations were found in reservoirs ( $1.89 \pm 1.00 \mu\text{mol}\cdot\text{L}^{-1}$ ) than in lakes ( $1.05 \pm 0.83 \mu\text{mol}\cdot\text{L}^{-1}$ ). pH values followed an almost inverse pattern, with values ranging from  $6.39 \pm 0.20 \mu\text{mol}\cdot\text{L}^{-1}$  (RAL and LAL), to  $7.18 \pm 0.48 \mu\text{mol}\cdot\text{L}^{-1}$  for LNAL (Table 1.1).

### 1.3.2 Photochemical parameters

According to the weather conditions of incubations and the optical properties of the samples, the values of theoretical amount of  $\text{CO}_2$  produced by photochemical mineralization into the first four centimeters below the surface  $pm(0 - .04)$  varied between  $1.65 \mu\text{mol}\cdot\text{l}^{-1}$  and  $23.28 \mu\text{mol}\cdot\text{l}^{-1}$ . The total energy absorbed in TS cells varied between 0.18 kJ and 29.58 kJ for the samples incubated just below the

surface (0.02 m depth). Because we constructed intervals of 1 nm over which values of scalar photon flux density and theoretical amount of CO<sub>2</sub> produced by photochemical mineralization were integrated, it is possible to measure the relative contribution of each interval  $pm(0 - .04)$  from UV-B, UV-A and PAR radiations. The contributions of these three classes of wavelengths varied slightly in relation to whether the water body had been impacted by logging activities; there was however almost no difference between lakes and reservoirs (Table 1.2).

Noteworthy, UV-B radiations contributed from  $2.59 \pm 0.21\%$  to  $4.41 \pm 0.81\%$  of the total amount of CO<sub>2</sub> theoretically produced by photochemical mineralization in TS cells, which represent a proportionally similar contribution when compared to their relative weight in the spectrum range considered in this work (3.75%). Similarly, the contribution from UV-A radiations was much higher (between  $85.63 \pm 0.50\%$  et  $91.06 \pm 1.94\%$  of the total photodegradation) than their relative importance over the wavelength range of 300 to 700 nm. Only PAR were underrepresented in the total energy absorbed (between  $4.53 \pm 2.74\%$  and  $11.77 \pm 0.63\%$ ) compared to their relative weight over this range of  $\lambda$  (75%).

CDOM absorption coefficient values at  $\lambda$  ( $a_{CDOM,\lambda}$ ), always decreased exponentially as suggested by the logarithmic function  $a_{CDOM,\lambda} = a_{CDOM,420} \cdot \exp(-S \cdot (\lambda - 420))$ . Moreover, the absorption coefficient of any given wavelength was always strongly correlated to the average absorption coefficient of the entire spectrum (300-700 nm), with correlation coefficients of  $r^2=0.72$  to  $r^2=0.99$  ( $p<0.001$ ), as calculated by linear interpolation. The value of absorption coefficient specific to 365 nm provides the best individual representation of average absorption coefficient of the entire spectrum ( $r^2=0.99$ ,  $p<0.01$ ).

### 1.3.3 Amounts of CO<sub>2</sub> produced by photochemical mineralization

The amount of CO<sub>2</sub> produced by photochemical mineralization just below the surface ( $PM_{CO_2}(0)$ ) varies widely between water bodies. The average levels of production that we measured during spring and summer were higher in water bodies affected by logging. In the Decelles Reservoir (RAL), the average daily production reached  $20.51 \pm 7.72 \mu\text{mol CO}_2 \cdot \text{l}^{-1} \cdot \text{d}^{-1}$ , an average value comparable to that of LAL ( $19.29 \pm 9.13 \mu\text{mol CO}_2 \cdot \text{l}^{-1} \cdot \text{d}^{-1}$ ). Non-disturbed lakes and reservoirs produced less CO<sub>2</sub> by photochemical mineralization, with respective values of  $1.41 \pm 2.31 \mu\text{mol CO}_2 \cdot \text{l}^{-1} \cdot \text{d}^{-1}$  and  $7.71 \pm 2.62 \mu\text{mol CO}_2 \cdot \text{l}^{-1} \cdot \text{d}^{-1}$ . Nevertheless, when considering the entire range of values measured in the spring and summer, the  $C_\phi$  factor does not allow discrimination between the four types of water bodies with Kruskal Wallis test. Inversely, photodegradation yield at the surface ( $PM_{CO_2}(0)$ ), allows to distinguish the different systems, with Kruskal Wallis test (Figure 1.1,  $p < 0.001$ ;  $df=3$ ).

The average value of diffusive flux measured across all reservoirs was double that of the corresponding value for all lakes:  $30.94 \pm 23.34 \text{ mmol} \cdot \text{m}^{-2} \cdot \text{d}^{-1}$  and  $16.38 \pm 17.46 \text{ mmol} \cdot \text{m}^{-2} \cdot \text{d}^{-1}$  respectively. Variability according to logging in the watershed is even larger. The type of water body with the highest emissions was therefore the RAL ( $34.74 \pm 26.14 \text{ mmol} \cdot \text{m}^{-2} \cdot \text{d}^{-1}$ ), followed by the LAL ( $32.27 \pm 17.99 \text{ mmol} \cdot \text{m}^{-2} \cdot \text{d}^{-1}$ ), the RNAL ( $24.38 \pm 15.54 \text{ mmol} \cdot \text{m}^{-2} \cdot \text{d}^{-1}$ ) and finally the LNAL ( $9.69 \pm 12.11 \text{ mmol} \cdot \text{m}^{-2} \cdot \text{d}^{-1}$ ).

## 1.4 Discussion

Photochemical mineralization, i.e. the ultimate oxidation of DOM producing CO<sub>2</sub>, has been described as an important process in the degradation of terrigenous

DOM in the world's oceans (Miller and Zepp 1995). Some researchers have recently questioned whether the same conclusion applies to freshwater systems, and to what extent photodegradation depends on quantity and the photoreactive properties of DOM (Huttunen et al. 2003; Weissenberger 2007). The significant differences observed in the values of spectral absorbance between 300 to 700 nm among the four different environmental scenarios (Kruskal Wallis test  $p < 0.0001$  ;  $df=3$ ) may be attributed to larger quantities of terrigenous material present in reservoirs (as compared to lakes) or in water bodies affected by logging in the watershed (Tranvik and Bertilsson 2001). Moreover, Granéli et al. (1998) reported a linear relationship between DOC concentrations (varying from 2.9 to 41 mg C·L<sup>-1</sup>) and the DIC-production of CO<sub>2</sub> under controlled spectral irradiance value. Our results also show a linear relationship between these two variables (as illustrated in Figure 1.2a), though we suggest that the DOC concentrations in the water column seems to be correlated to the amount of CO<sub>2</sub> produced by photochemical mineralization into the top four centimeters of the water column ( $r^2=0.58$ ,  $p < 0.01$ ). A very interesting result concerns the strong relation between  $pm(0 - .04)$ , the theoretical amount of CO<sub>2</sub> produced by photochemical mineralization obtained according to the Vähätalo equations and the amount of CO<sub>2</sub> produced by photochemical mineralization,  $PM_{CO_2}(0)$  measured *in situ* as illustrated in Figure 1.2b ( $r^2=0.79$ ,  $p < 0.01$ ). As  $pm(0 - .04)$  comes from a mathematical construction supported by three main factors, the spectrum of apparent quantum yield for photodegradation ( $\phi_\lambda$ ), the spectrum of downward vector photon flux density ( $Q_{d,v,0+,\lambda}$ ) and the absorption coefficient of CDOM ( $a_{CDOM,\lambda}$ ), the fact that the slope  $\frac{\Delta(PM_{CO_2}(0))}{\Delta pm(0 - .04)}$  equal to 0.94 with parameters c and d fixed (obtained from the Swedish Valkea-Kotinen Lake) is remarkable. While DOC concentrations and  $pm(0 - .04)$  values are slightly different, both show strong degrees of correlation and both suggest a

similar relationship between the amount of  $\text{CO}_2$  produced by photochemical mineralization and the type of environmental scenario. Granéli et al. (1998) also suggested that there is no measurable amount of  $\text{CO}_2$  produced by photochemical mineralization in environments where DOC concentrations range between 2 and 3  $\text{mg C}\cdot\text{L}^{-1}$ . The same result was also apparent in our study, whereby the general tendency calculated indicates that a water body does not produce  $\text{CO}_2$  by photochemical mineralization when DOC concentrations are lower than 3.9  $\text{mg C}\cdot\text{L}^{-1}$  (Figure 1.2a). Linear modeling of this tendency in the LNAL scenario can however be inaccurate. While the DOC concentrations measured in these lakes are low ( $3.99 \pm 1.10 \text{ mg C}\cdot\text{L}^{-1}$ ), their production of  $\text{CO}_2$  by photochemical mineralization is not undetectable. This observation is tied to the fact that we are not able to measure DOC concentrations below which DOM is photorecalcitrant. Rather, it is possible that the reactivity of DOM is greater in freshly disturbed water bodies but noticeable more deeply in the water column (where the  $d$  parameter becomes important). Such interpretation of our results agrees with previous studies linking photoreactivity to the residence time of DOM in the water (Grzybowski 2000; Lindell et al. 2000; Waiser and Robarts 2004).

The four different environmental scenarii show significantly different amounts of  $\text{CO}_2$  produced by photochemical mineralization just below the surface ( $PM_{\text{CO}_2}(0)$ ) (Kruskal Wallis test,  $p < 0.001$ ;  $df=3$ ), as shown in Figure 1.1. We thus have tried to understand the origin of these variations to ascertain the solidity of the statistical test. As  $a_{\text{CDOM},\lambda}$  is strongly correlated to DOC concentration (by definition  $a_{\text{CDOM},\lambda}$  is the part of DOM able to absorb solar radiation), the amount of  $\text{CO}_2$  produced by photochemical mineralization at the surface level ( $PM_{\text{CO}_2}(0)$ ) (analyzed using the  $\text{CO}_2$  concentration method) is indirectly correlated to the absorption coefficient ( $a_{\text{CDOM},\lambda}$ ). In order to be able to affirm that the observed differences in measured amounts of  $\text{CO}_2$  produced by photochemical

mineralization can be linked to the different environmental scenarii, we first had to verify that variations in the photon flux density ( $Q_{d,v,0+, \lambda}$ ) had not substantially affected  $pm(0 - .04)$  values. We verified that the variations in photodegradation did not depend on daily differences in radiation intensity. For this purpose, we used the Vähätalo equations wherein  $pm(0 - .04)$  is defined. We merely change the photon flux value ( $Q_{d,v,0+, \lambda}$ ) that comes from the PUV-2500/2510 to the average photon flux value ( $\bar{Q}_{d,v,0+, \lambda}$ ), calculated as the average values of  $Q_{d,v,0+, \lambda}$  measured during summer and spring field campaigns. Thus,  $\overline{pm}(0 - .04)$  can be evaluated from

$$\overline{pm}_z = c * \int_{\lambda_{\min}}^{\lambda_{\max}} 10^{-a\lambda} \bar{Q}_{s,z,\lambda} a_{CDOM,\lambda} d\lambda, \text{ where } \bar{Q}_{s,z,\lambda} \text{ comes from } \bar{Q}_{d,v,0+, \lambda} \text{ as the average of}$$

the scalar photon flux density. A maximum total variation of 61.2% was obtained when comparing the values of absorbed spectral energy calculated for average and maximal values of exposure, while the quantity of energy absorbed ranged between 0.18 kJ and 29.58 kJ. Sunny conditions could therefore, in an extreme case, affect the total quantity of absorbed energy by 61.2% from the average value. Moreover, as can be seen in Figure 1.3, there is little difference between  $pm(0 - .04)$  and  $\overline{pm}(0 - .04)$  ( $r^2 = 0.8$ ,  $p < 0.01$ ). Thus, trends observed in Figure 1.1 do not depend upon the weather conditions. However, the linear regression obtained between  $pm(0 - .04)$  and  $\overline{pm}(0 - .04)$  does not go through 0 (intersection at 3.27) and the slope  $\frac{\Delta \overline{pm}(0 - .04)}{\Delta pm(0 - .04)}$  equal to 0.65, i.e. very different to 1 contrary to what was expected. By construction, the average value of the  $\frac{\overline{pm}(0 - .04)}{pm(0 - .04)}$  ratio equal to 1, thus, we have unfortunately sampled LNAL situation during cloudy conditions while RAL situation was sampled during sunny conditions. To be certain that we propose a photodegradation yield independent of the weather, we propose the following construction:

$\overline{pm}(0 - .04) = C_{\phi} \cdot \overline{PM}_{CO_2}(0)$ . As factor  $C_{\phi}$  is independent of the weather and that  $\overline{pm}(0 - .04)$  was standardized according to mean photon flux density, the value  $\overline{PM}_{CO_2}(0)$  corresponds exactly to photodegradation yield measured under controlled exposure conditions. In the context of this study and as other authors have also found (Osburn et al. 2001), the absorption coefficient of CDOM at  $\lambda$  ( $a_{CDOM,\lambda}$ ) was thus considered a preponderant factor in photodegradation yield during the spring and summer when exposure was the same as suggested by the relation between  $\overline{PM}_{CO_2}(0)$  and the DOC concentration (Figure 1.4). The reverse tendency was found when comparing values of total spectral energy absorbed with the minimal values of exposure, which were observed in the fall (diamond marks, Figure 1.4). It follows that the total average value of absorbed energy, can be 11.3 times more important than the minimal value obtained during the fall season.

The indicator of DOM photodegradation yield obtained over the top four centimeters of the water column and normalized to DOC,  $\overline{PM}_{CO_2}(0)/DOC$ , inspired from Granéli et al. (1998), seems relevant to our study. In addition, DOC concentrations always represent more than 10 times the photodegraded DOM quantity, which makes the indicator much more stable than  $C_{\phi}$  used alone but only representative of the photodegradability which take place in the top four centimeters. This stability comes from the fact that the value of  $\overline{PM}_{CO_2}(0)/DOC$  is much lower than 1.

The DOM photodegradability in the top four centimeters, analyzed using the indicator  $\overline{PM}_{CO_2}(0)/DOC$ , is strongly correlated to Fe concentrations ( $r^2=0.73$ ,  $p<0.001$ ) as shown in Figure 1.5. The daily photodegradation in surface water varies between 0 and 9.93% of the total quantity of material available in dissolved form, a range comparable but higher to that found by Granéli et al. (1996) for lakes

in Brazil and Sweden, with a  $\overline{PM}_{CO_2(0)}/DOC$  average value, after 6 hours of incubation, of 3.5%. While this value may seem extremely high compared to studies carried out over the entire water column (Soumis et al. 2007), it corresponds to photodegradation at the water surface where UV radiations are not attenuated and can therefore exert a maximal effect on photodegradation processes (Zepp and Cline 1977). Indeed, in average, the downward attenuation coefficients of irradiance at  $\lambda$  values ( $K_{d,I,\lambda}$ ), for all samples were 17.1 and 10.3  $m^{-1}$  for UV-B and UV-A radiations, respectively. These values correspond to photic zones of 26.9 and 44.0 cm, respectively, which translate into a much larger attenuation for PAR radiations (4.65 m). Therefore, while photodegradation yields at the surface are extremely high, the calculation of yields over the entire water column should produce results well below 1%, even in the summer (Vähätalo et al. 2000).

The relationship between the amount of DOC photochemically mineralized daily, as shown by the  $\overline{PM}_{CO_2(0)}/DOC$  ratio and the value of the Fe concentration ( $[Fe]$ ) can be established based on two complementary approaches. The first option is to consider ( $[Fe]$ ) of our samples both as an indicator of terrigenous DOM concentration and also as an indicator of the DOM photodegradability towards the absorption of electromagnetic radiations over the range 300 to 700 nm, which we assume here corresponds to the freshness of the material available for photodegradation (Duchemin et al. 1995; Huttunen et al. 2003; Weissenberger 2007). Upon exposure to radiations, molecules dissolved in water that are susceptible to photodegradation lose a part of their absorbance properties (Moran and Zepp 1997; Morris and Hargreaves 1997). DOM transferred from the watershed to the water system, which is greater in areas of recent logging (Carignan et al. 2000), would be fresher and thus more reactive. The higher DOM

photodegradability in hydroelectric reservoirs compared to lakes in the top four centimeters (Kruskal Wallis test,  $p < 0.003$ ;  $df=1$ ) could therefore be explained by a different photo-fenton yield of the dissolved organic carbon degradation between these two types of bodies of water (Figure 1.5). Moreover, the curve trend (Figure 1.5), which is assumed to be a logarithmic function, is typical of a catalytic reaction where  $[Fe]$  is the catalyst.

Finally, we have collected water sampled directly in the thin boundary layer to obtain total diffusive fluxes of  $CO_2$  emitted from the bodies of water toward the atmosphere. As shown in Figure 1.6, the standardized values of  $\overline{PM}_{CO_2}(0)$  are strongly correlated to total diffusive fluxes ( $f_{CO_2}$ ) ( $r^2=0.59$ ,  $p < 0.01$ ). This very interesting result seems to indicate that  $[Fe]$  and the photodegradation, which takes place in the top four centimeters of the water column are very good indicators of the diffusive fluxes emitted from the water bodies. Thus, if the parameter  $d$  is constant independently of our different environmental situation, contrary to what presented in Vähätalo et al. (2000), a limit value for each  $\lambda$  should exist, such as, under a value of scalar photon flux density,  $pm_\lambda$  could be zero. In other words, a Heaviside function could exist:

$$H_{0,S_i,\lambda} : \left\{ \forall i = 300 \leq 700; H_{0,S_i,\lambda} = 0, \forall pm_{\lambda,z} \leq S_{i,\lambda}; H_{0,S_i,\lambda} = 1, \forall pm_{\lambda,z} > S_{i,\lambda} \right\}$$

$$\text{whith } pm_z = \int_{\lambda \min}^{\lambda \max} H_{0,S_i,\lambda} \phi_\lambda Q_{s,z,\lambda} a_{CDOM,\lambda} d\lambda.$$

## 1.5 Conclusion

As Granéli et al. (1998) and Lindell et al. (2000) suggested, the amounts of  $CO_2$  produced by photochemical mineralization in surface waters is strongly

correlated to the DOC concentrations in the water column as well as values of spectral absorbance, whose measurement in our incubated water samples produced an  $r^2$  value of 0.79. This result can be explained, in large part, by the fact that the total photon flux density available for photodegradation is different between our scenarii. Because there is much less spectral exposure in the fall, photodegradation for this season is generally much lower than that observed for the spring and summer. In contrast, values of spectral absorbance are relatively stable from season to season.

In surface waters, photodegradation varied between the different environmental scenarii. Greater values were found in bodies of water from watersheds recently affected by logging activities (LAL:  $19.29 \pm 9.13 \mu\text{mol CO}_2\cdot\text{L}^{-1}\cdot\text{d}^{-1}$ ; and RAL:  $20.51 \pm 7.72 \mu\text{mol CO}_2\cdot\text{L}^{-1}\cdot\text{d}^{-1}$ ) compared to water bodies with a forested watershed (LNAL:  $1.41 \pm 2.30 \mu\text{mol CO}_2\cdot\text{L}^{-1}\cdot\text{d}^{-1}$ ; and RNAL:  $7.71 \pm 2.62 \mu\text{mol CO}_2\cdot\text{L}^{-1}\cdot\text{d}^{-1}$ ). This difference can mostly be attributed to the quantity of photodegradable material present in the systems, which was greater in reservoirs and in water bodies affected by recent logging.

The strong correlation that was observed between DOM photodegradation yields in surface waters and dissolved Fe concentrations could also be explained by the higher inputs of terrestrial material in the perturbed systems (Houel et al. 2006).

Higher dissolved Fe concentrations could lead to an increase in photodegradation yield due to photo-Fenton reactions, particularly since  $[Fe]$  is strongly correlated to  $\overline{PM}_{CO_2(0)}/DOC$  ( $r^2=0.74$ ,  $p<0.01$ ). The hypothesis of a tight coupling between bound  $[Fe]$  and photodegradation yield deserves further study. The significant variability of DOM photodegradability and total diffusive fluxes of  $\text{CO}_2$  between the different environmental scenarii is also paralleled by variations in amounts of  $\text{CO}_2$  produced by photochemical mineralization in surface waters. There are

therefore few possible explanations for these differences, and none can be excluded until they are studied further either through bulk spectroscopic ( $^{13}\text{C}$  NMR) or molecular (lignin oxidation products) approaches (Teisserenc et al. 2011). It should be noted that independently of the weather, the variation in photodegradation yield is due to differences in the freshness of DOM. Indeed,  $[Fe]$  and the total diffusive fluxes ( $f_{CO_2}$ ) are always positively correlated to the standardized values of  $\overline{PM}_{CO_2}(0)$ . Finally, if the hypothesis of the existence for a Heaviside function was confirmed, the photodegradability and the amounts of  $\text{CO}_2$  produced by photochemical mineralization could be closely quantitatively and qualitatively linked to inputs of terrestrial organic material.

## References:

- Carignan, R., P. D'arcy, and S. Lamontagne. 2000. Comparative impacts of fire and forest harvesting on water quality in Boreal Shield lakes. *Can J Fish Aquat Sci* **57**: 105-117.
- Cole, J. and others 2007. Plumbing the Global Carbon Cycle: Integrating Inland Waters into the Terrestrial Carbon Budget. *Ecosystems* **10**: 172-185.
- Cole, J. J., and N. F. Caraco. 1998. Atmospheric Exchange of Carbon Dioxide in a Low-Wind Oligotrophic Lake Measured by the Addition of SF<sub>6</sub>. *Limnology and Oceanography* **43**: 647-656.
- Cole, J. J., N. F. Caraco, G. W. Kling, and T. K. Kratz. 1994. Carbon Dioxide Supersaturation in the Surface Waters of Lakes. *Science* **265**: 1568-1570.
- Downing, J. A. and others 2006. The Global Abundance and Size Distribution of Lakes, Ponds, and Impoundments. *Limnology and Oceanography* **51**: 2388-2397.
- Duchemin, E., M. Lucotte, and R. Canuel. 1998. Comparison of Static Chamber and Thin Boundary Layer Equation Methods for Measuring Greenhouse Gas Emissions from Large Water Bodies. *Environmental Science & Technology* **33**: 350-357.
- Duchemin, E., M. Lucotte, R. Canuel, and A. Chamberland. 1995. Production of the greenhouse gases CH<sub>4</sub> and CO<sub>2</sub> by hydroelectric reservoirs of the boreal region. *Global Biogeochem. Cycles* **9**: 529-540.
- Granéli, W., M. Lindell, B. M. De Faria, and F. De Assis Esteves. 1998. Photoproduction of dissolved inorganic carbon in temperate and tropical lakes – dependence on wavelength band and dissolved organic carbon concentration. *Biogeochemistry* **43**: 175-195.
- Granéli, W., M. Lindell, and L. Tranvik. 1996. Photo-Oxidative Production of Dissolved Inorganic Carbon in Lakes of Different Humic Content. *Limnology and Oceanography* **41**: 698-706.
- Grzybowski, W. 2000. Effect of short-term sunlight irradiation on absorbance spectra of chromophoric organic matter dissolved in coastal and riverine water. *Chemosphere*.

- Houel, S., P. Louchouart, M. Lucotte, R. Canuel, and B. Ghaleb. 2006. Translocation of Soil Organic Matter Following Reservoir Impoundment in Boreal Systems: Implications for In situ Productivity. *Limnology and Oceanography* **51**: 1497-1513.
- Huttunen, J. T. and others 2003. Fluxes of methane, carbon dioxide and nitrous oxide in boreal lakes and potential anthropogenic effects on the aquatic greenhouse gas emissions. *Chemosphere* **52**: 609-621.
- Kelly, C. A. and others 1997. Increases in Fluxes of Greenhouse Gases and Methyl Mercury following Flooding of an Experimental Reservoir†. *Environmental Science & Technology* **31**: 1334-1344.
- Lindell, M. J., H. W. Granéli, and S. Bertilsson. 2000. Seasonal photoreactivity of dissolved organic matter from lakes with contrasting humic content. *Can J Fish Aquat Sci* **57**: 875-885.
- Liss, P. S., and P. G. Slater. 1974. Flux of Gases across the Air-Sea Interface. *Nature* **247**: 181-184.
- Macintyre, S., and J. M. Melack. 1995. Vertical and Horizontal Transport in Lakes: Linking Littoral, Benthic, and Pelagic Habitats. *Journal of the North American Benthological Society* **14**: 599-615.
- Miller, W. 1998. Effects of UV radiation on aquatic humus: Photochemical principles and experimental considerations. *Ecological Studies*.
- Miller, W. L., and R. G. Zepp. 1995. Photochemical production of dissolved inorganic carbon from terrestrial organic matter: Significance to the oceanic organic carbon cycle. *Geophys. Res. Lett.* **22**: 417-420.
- Moore, C. A., C. T. Farmer, and R. G. Zika. 1993. Influence of the Orinoco River on Hydrogen Peroxide Distribution and Production in the Eastern Caribbean. *J. Geophys. Res.* **98**: 2289-2298.
- Mopper, K., X. Zhou, R. J. Kieber, D. J. Kieber, R. J. Sikorski, and R. D. Jones. 1991. Photochemical degradation of dissolved organic carbon and its impact on the oceanic carbon cycle. *Nature* **353**: 60-62.
- Moran, M. A., and R. G. Zepp. 1997. Role of Photoreactions in the Formation of Biologically Labile Compounds from Dissolved Organic Matter. *Limnology and Oceanography* **42**: 1307-1316.

- Morris, D. P., and B. R. Hargreaves. 1997. The Role of Photochemical Degradation of Dissolved Organic Carbon in Regulating the UV Transparency of Three Lakes on the Pocono Plateau. *Limnology and Oceanography* **42**: 239-249.
- Osburn, C. L., H. E. Zagarese, D. P. Morris, B. R. Hargreaves, and W. E. Cravero. 2001. Calculation of Spectral Weighting Functions for the Solar Photobleaching of Chromophoric Dissolved Organic Matter in Temperate Lakes. *Limnology and Oceanography* **46**: 1455-1467.
- Prairie, Y. 2008. Carbocentric limnology: looking back, looking forward. *Can J Fish Aquat Sci* **65**: 543-548.
- Reche, I., M. L. Pace, and J. J. Cole. 1999. Relationship of Trophic and Chemical Conditions to Photobleaching of Dissolved Organic Matter in Lake Ecosystems. *Biogeochemistry* **44**: 259-280.
- Sikorski, R. J., and R. G. Zika. 1993. Modeling Mixed-Layer Photochemistry of H<sub>2</sub>O<sub>2</sub>: Optical and Chemical Modeling of Production. *J. Geophys. Res.* **98**: 2315-2328.
- Soumis, N., R. Canuel, and M. Lucotte. 2008. Evaluation of Two Current Approaches for the Measurement of Carbon Dioxide Diffusive Fluxes from Lentic Ecosystems. *Environmental Science & Technology* **42**: 2964-2969.
- Soumis, N., É. Duchemin, R. Canuel, and M. Lucotte. 2004. Greenhouse gas emissions from reservoirs of the western United States. *Global Biogeochem. Cycles* **18**: GB3022.
- Soumis, N. and others 2005. Hydroelectric Reservoirs as Anthropogenic Sources of Greenhouse Gases. *Water Encyclopedia*. John Wiley & Sons, Inc.
- Soumis, N., M. Lucotte, C. Larose, F. Veillette, and R. Canuel. 2007. Photomineralization in a boreal hydroelectric reservoir: a comparison with natural aquatic ecosystems. *Biogeochemistry* **86**: 123-135.
- Teisserenc, R., M. Lucotte, and S. Houel. 2011. Terrestrial organic matter biomarkers as tracers of Hg sources in lake sediments. *Biogeochemistry* **103**: 235-244.
- Tranvik, L. J., and S. Bertilsson. 2001. Contrasting effects of solar UV radiation on dissolved organic sources for bacterial growth. *Ecology Letters* **4**: 458-463.
- Vähätalo, A. V., M. Salkinoja-Salonen, P. Taalas, and K. Salonen. 2000. Spectrum of the Quantum Yield for Photochemical Mineralization of Dissolved Organic Carbon in a Humic Lake. *Limnology and Oceanography* **45**: 664-676.

- Waiser, M., and R. Robarts. 2004. Photodegradation of DOC in a shallow prairie wetland: evidence from seasonal changes in DOC optical properties and chemical characteristics. *Biogeochemistry* **69**: 263-284.
- Weissenberger, S. 2007. Émissions de gaz à effet de serre et cycle du carbone de réservoirs hydroélectriques du moyen Nord québécois Université du Québec à Montréal.
- Zafiriou, O. C., J. Jousot-Dubien, R. G. Zepp, and R. G. Zika. 1984. Photochemistry of natural waters. *Environmental Science & Technology* **18**: 358A-371A.
- Zepp, R. G., and D. M. Cline. 1977. Rates of direct photolysis in aquatic environment. *Environmental Science & Technology* **11**: 359-366.

Tables captions

**Table 1.1** Average values of the main physical and chemical parameters

**Table 1.2** The photochemical mineralization depending on different wavelengths

**Table 1.1** Average values of the main physical and chemical parameters

<b>ENVIRONMENTAL CONDITIONS</b>	<b>DOC (mgC.l<sup>-1</sup>)</b>	<b>Fe (μmol.l<sup>-1</sup>)</b>	<b>[P]total (μg.l<sup>-1</sup>)</b>	<b>pH</b>
<b>RNAL</b>	5,13±1,30	0,98±0,63	8,05±2,17	6,7±0,33
<b>RAL</b>	7,75±1,38	2,73±0,79	13,16±3,59	6,39±0,2
<b>LNAL</b>	3,99±1,10	0,54±0,32	10,16±2,84	7,18±0,48
<b>LAL</b>	5,85±1,09	1,89±0,79	9,34±3,35	6,39±0,28
<b>Reservoirs</b>	6,46±1,86	1,89±1,00	10,86±3,95	6,51±0,31
<b>Lakes</b>	4,61±1,40	1,05±0,83	9,76±2,98	6,94±0,56

**Table 1.2** The photochemical mineralization depending on different wavelenghts

<b>SCENARIOS</b>	$\frac{pm_{UV-B}(0-.04)}{pm(0-.04)}$	$\frac{pm_{UV-A}(0-.04)}{pm(0-.04)}$	$\frac{pm_{PAR}(0-.04)}{pm(0-.04)}$
<b>RNAL</b>	4,32 % ± 0,0068	90,16 % ± 0,0099	5,52 % ± 0,0165
<b>RAL</b>	2,59 % ± 0,0021	85,63 % ± 0,0050	11,77 % ± 0,063
<b>LNAL</b>	4,41 % ± 0,0081	91,06 % ± 0,0194	4,53 % ± 0,0274
<b>LAL</b>	3,12 % ± 0,0006	87,50 % ± 0,0021	9,38 % ± 0,0027

Figures captions

**Figure 1.1** Amount of CO<sub>2</sub> produced by photochemical mineralization across different aquatic environments

**Figure 1.2a** Relationship between amount of CO<sub>2</sub> produced by photochemical mineralization  $PM_{CO_2}(0)$  and DOC concentrations

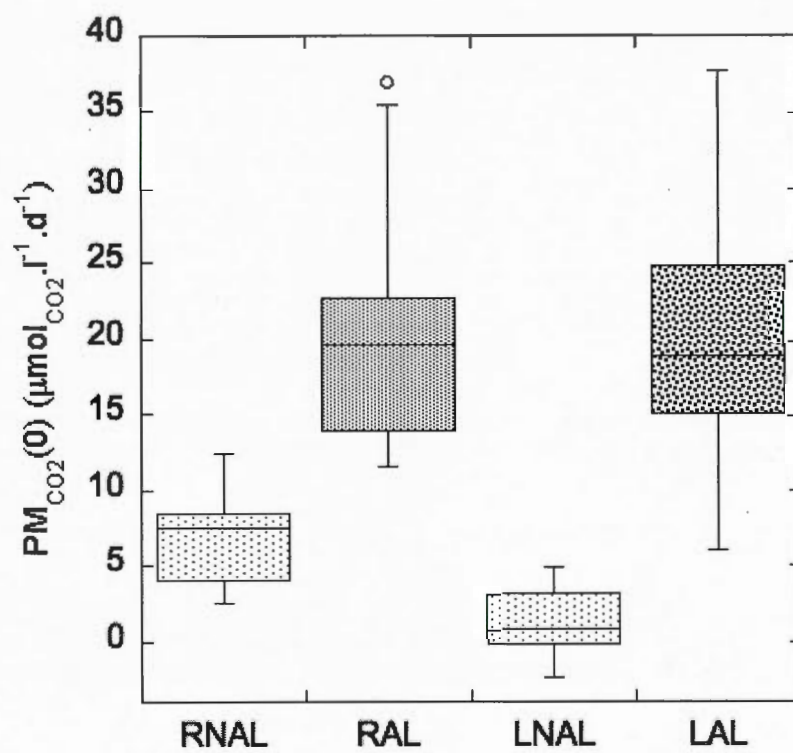
**Figure 1.2b** Relationship between amount of CO<sub>2</sub> produced by photochemical mineralization  $PM_{CO_2}(0)$  and  $pm(0 - .04)$

**Figure 1.3** Relationship between the theoretical amount of CO<sub>2</sub> produced by photochemical mineralization integrated over the top four centimeters  $pm(0 - .04)$  and the standardized amount of CO<sub>2</sub> produced by photochemical mineralization integrated over in the top four centimeters  $\overline{pm}(0 - .04)$

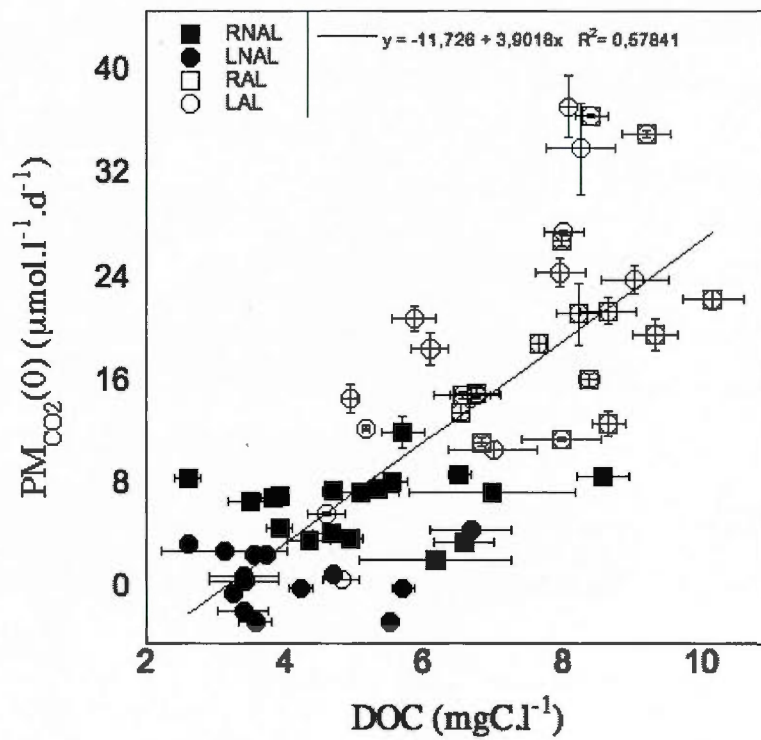
**Figure 1.4** Relationship between the standardized amount of CO<sub>2</sub> produced by photochemical mineralization in the top four centimeters  $\overline{PM}_{CO_2}(0)$  and DOC concentrations in the surface of the bodies of water (*DOC*)

**Figure 1.5** Relationship between the daily quantity of photodegraded DOM  $PM_{CO_2}(0)/DOC$  and Fe concentrations

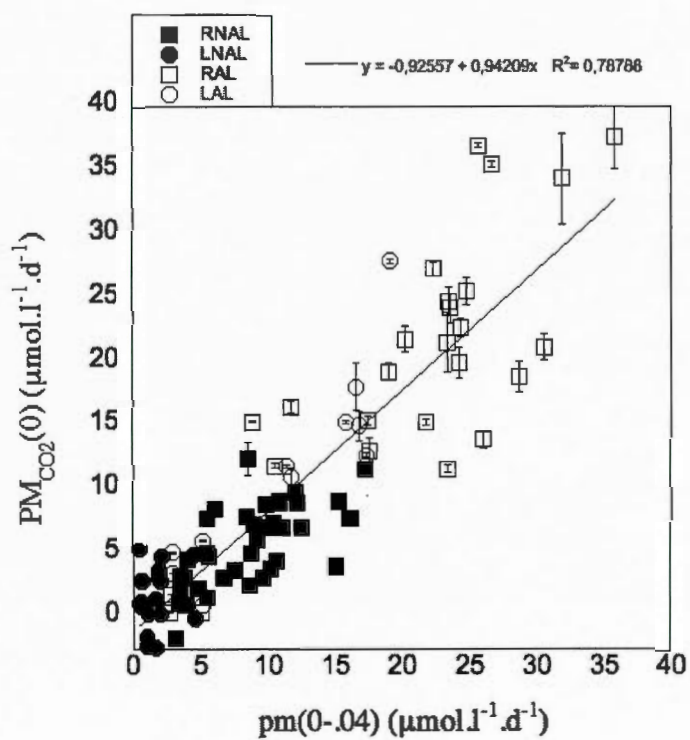
**Figure 1.6** Relationship between the standardized amount of CO<sub>2</sub> produced by photochemical mineralization in the top four centimeters  $\overline{PM}_{CO_2}(0)$  and the total diffusive fluxes of CO<sub>2</sub> ( $f_{CO_2}$ )



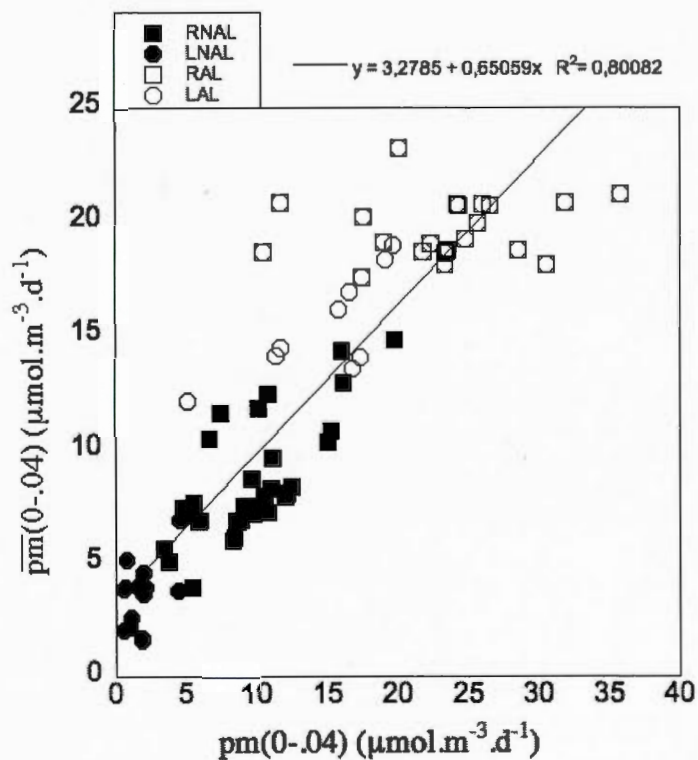
**Figure 1.1** Amount of CO<sub>2</sub> produced by photochemical mineralization across different aquatic environments



**Figure 1.2a** Relationship between amount of CO<sub>2</sub> produced by photochemical mineralization  $PM_{CO_2}(0)$  and DOC concentrations



**Figure 1.2b** Relationship between amount of  $\text{CO}_2$  produced by photochemical mineralization  $PM_{CO_2}(0)$  and  $pm(0-.04)$



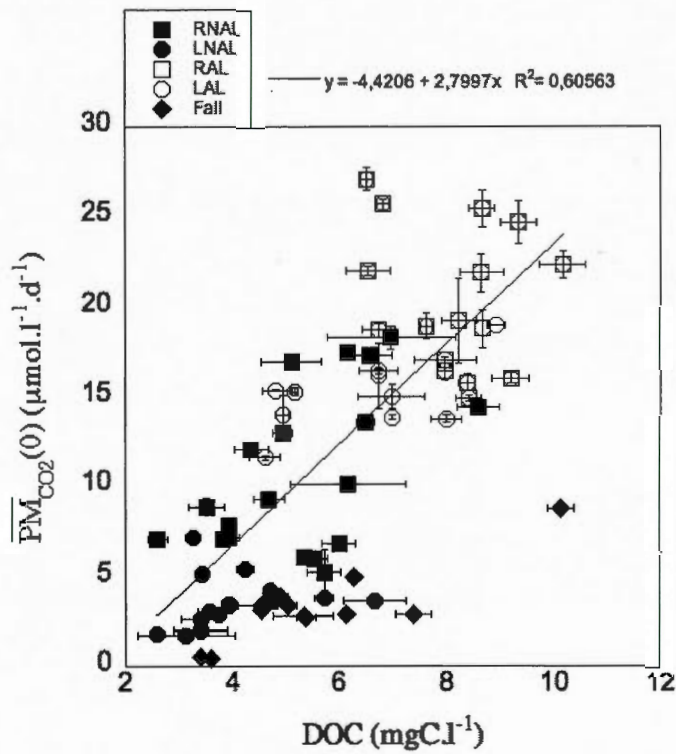


**Figure 1.4** Relationship between the standardized amount of  $\text{CO}_2$  produced by photochemical mineralization in the top four centimeters  $\overline{PM}_{\text{CO}_2}(0)$  and DOC concentrations in the surface of the bodies of water ( $\text{DOC}$ )

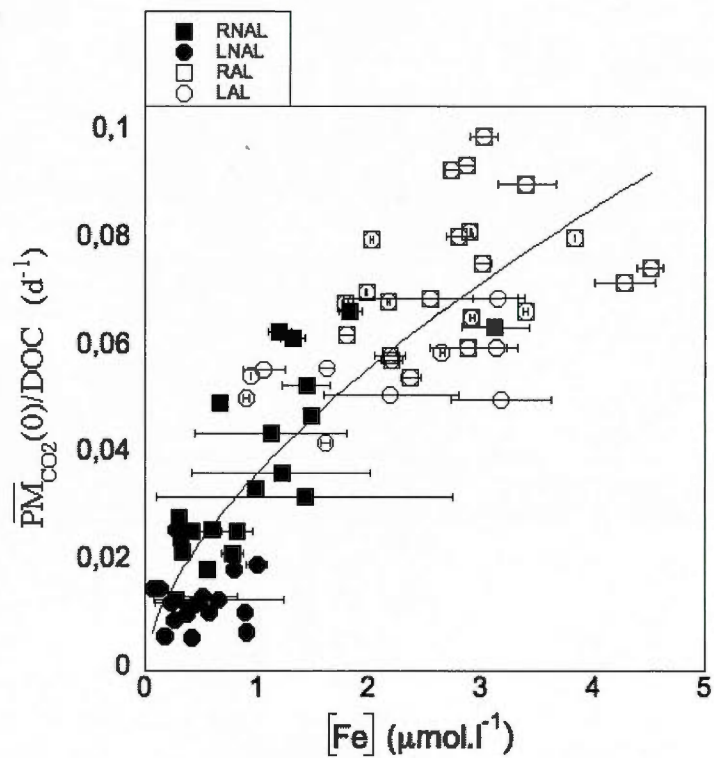


**Figure 1.5** Relationship between the daily quantity of photodegraded DOM  $\overline{PM}_{\text{CO}_2(0)}/\text{DOC}$  and Fe concentrations

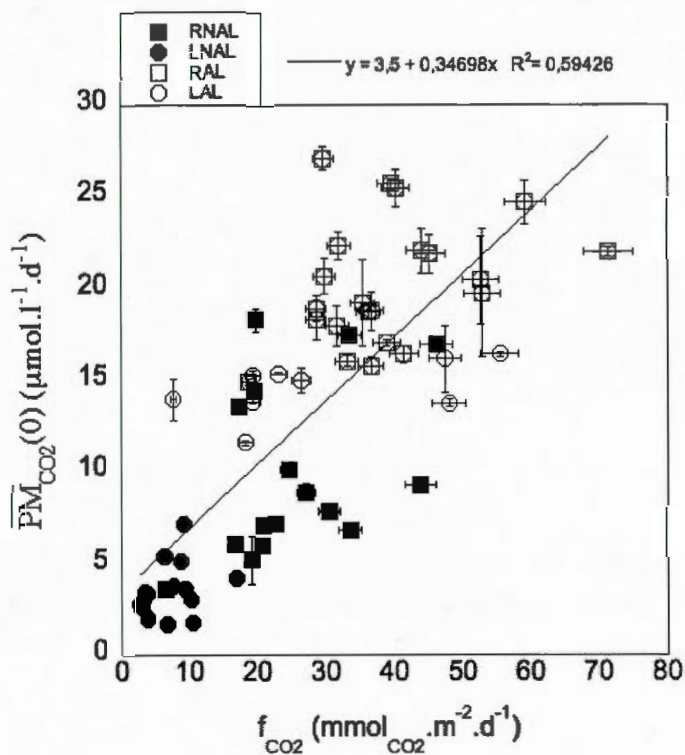


**Figure 1.6** Relationship between the standardized amount of  $CO_2$  produced by photochemical mineralization in the top four centimeters  $\overline{PM}_{CO_2}(0)$  and the total diffusive fluxes of  $CO_2$  ( $f_{CO_2}$ )

## CHAPITRE II

CONTRIBUTION DE LA PHOTODÉGRADATION DE LA MATIÈRE  
ORGANIQUE TERRIGÈNE À L'HÉTÉROTROPHIE DES ÉCOSYSTÈMES  
AQUATIQUES EN RÉGION BORÉALE QUÉBÉCOISE (CANADA)

PHOTODEGRADATION OF TERRIGENOUS ORGANIC MATTER  
CONTRIBUTES TO HETEROTROPHY IN BOREAL AQUATIC  
ECOSYSTEMS

Jean-Baptiste Plouhinec<sup>1</sup>, Marc Lucotte<sup>1</sup>, Alexandre Ouellet<sup>2</sup> and Yves Gélinas<sup>2</sup>

<sup>1</sup>GEOTOP and Institute of Environmental Sciences, UQAM, C.P. 8888, Succursale Centre-Ville, Montréal, Québec, Canada, H3C-3P8

<sup>2</sup>GEOTOP and Department of Chemistry and Biochemistry, Concordia University, 7141 Sherbrooke Street West, Montréal, Québec, Canada, H4B-1R6

Corresponding author:  
Jean-Baptiste PLOUHINEC  
Université du Québec à Montréal  
GEOTOP-UQAM-McGill  
CP 8888 Succ. Centre-Ville,  
Montréal, Québec, Canada  
H3C 3P8

Phone number: 514-987-3000 #5662  
Fax: 514-987-3635  
Email: plouhinec.jean-baptiste@uqam.ca

## Acknowledgments

We thank the Natural Science and Engineering Research Council of Canada (NSERC) and the *Fonds Québécois de la recherche sur la nature et les technologies* (FQRNT). The authors thank Nicolas Soumis (UQAM) for his precious advice on experimental protocols, as well as Sophie Chen from UQAM for her help in the laboratory. This study was funded through grants (M.L. and Y.G.) and scholarships (A.O. and J.B.P.) from BIOCAP-Canada and NSERC. This is GEOTOP contribution 2012-XXXX.

## Résumé

Afin de faire la lumière sur quelques-uns des facteurs qui contrôlent l'hétérotrophie des lacs et réservoirs situés en région boréale, nous avons évalué l'importance de la minéralisation photochimique de la matière organique dissoute (MOD) par rapport à d'autres sources de production de CO<sub>2</sub> dans six lacs naturels ou perturbés par l'exploitation forestière de leurs bassins versants ainsi que de deux réservoirs situés au Québec (Canada). Les taux de production de CO<sub>2</sub> dans la colonne d'eau ont été mesurés selon un système d'incubation / irradiation pour distinguer l'importance relative de la minéralisation par photodégradation, de la respiration bactérienne, et de l'absorption de CO<sub>2</sub> par la photosynthèse. Nous avons ensuite estimé les flux théoriques de CO<sub>2</sub> émis selon la production dans la zone photique ( $f^*_{CO_2}$ ). On obtient la production quotidienne de CO<sub>2</sub> par minéralisation photochimique de la MOD, intégrée sur la colonne d'eau ( $DIPM_{CO_2}$ ) à l'aide du calcul d'un indicateur de rendement quantique ( $\phi_\lambda$ ).  $DIPM_{CO_2}$  semble être un indicateur fiable fortement corrélé au coefficient d'absorption spectral de la MOD mesuré à 360 nm ( $R^2 = 0.81$ ,  $p < 0.01$ ).  $DIPM_{CO_2}$  représente  $15.1 \pm 14.1\%$  du flux diffusif total de CO<sub>2</sub> émis vers l'atmosphère, indépendamment du type de masse d'eau ou de la nature de la perturbation du plan d'eau. Nos données suggèrent également que la minéralisation photochimique et la photosynthèse soient fortement intercorrélées ( $R^2 = 0.79$ ,  $p < 0.01$ ), ce qui proviendrait du fait de l'atténuation du rayonnement photosynthétiquement actif imputable à la matière organique d'origine terrestre (MOT) lessivée du bassin versant vers la colonne d'eau. Enfin, les flux diffusifs mesurés ( $f_{CO_2}$ ) dépassent régulièrement  $f^*_{CO_2}$  de  $10 \text{ mmol. CO}_2 \cdot \text{m}^{-2} \cdot \text{d}^{-1}$  ( $R^2 = 0.97$ ,  $p < 0.001$ ), ce qui suggère une production de CO<sub>2</sub> dans l'hypolimnion qui soit indépendante des conditions environnementales.

Mots-clés: Minéralisation photochimique, Processus hétérotrophes, Gaz à effet de serre, Respiration bactérienne, Cycle du carbone aquatique.

## Abstract

To shed light on some of the factors controlling heterotrophy in lakes and reservoirs of the boreal region, we evaluated the importance of photochemical mineralization of dissolved organic matter (DOM) relative to other sources of CO<sub>2</sub> production in six natural or human-perturbed lakes through logging on their watersheds and two reservoirs in Quebec (Canada). Rates of CO<sub>2</sub> production in the water column were measured through incubation/irradiation experiments to distinguish the importance of photochemical mineralization, bacterial respiration, and CO<sub>2</sub> uptake by photosynthesis. We then estimated theoretical CO<sub>2</sub> fluxes emitted from the photic zone ( $f_{CO_2}$ ). We obtained the daily integrated production of CO<sub>2</sub> through photochemical mineralization ( $DIPM_{CO_2}$ ) of DOM over the entire water column using the calculation of the spectrum yield ( $\phi_\lambda$ ).  $DIPM_{CO_2}$  appeared to be a robust indicator strongly correlated to the absorption coefficient of chromophoric DOM at 360 nm ( $R^2=0.81$ ,  $p<0.01$ ).  $DIPM_{CO_2}$  accounted for  $15.1 \pm 14.1$  % of the total diffusive flux of CO<sub>2</sub> to the atmosphere, independently of the water body type or the nature of the perturbation of the water body. Our data also suggest that photochemical mineralization and photosynthesis are strongly correlated ( $R^2=0.79$ ,  $p < 0.01$ ), which is due to the fact that the strong photosynthetically active radiation attenuation derives from terrestrial organic matter (TOM) inputs into the water column. Finally, the measured diffusive fluxes towards the atmosphere ( $f_{CO_2}$ ) steadily exceeds  $f_{CO_2}$  by  $10 \text{ mmol.CO}_2\text{.m}^{-2}\text{.d}^{-1}$  ( $R^2=0.97$ ,  $p < 0.001$ ), suggesting CO<sub>2</sub> production in the hypolimnion independent of the environmental conditions.

Keywords: photochemical mineralization, heterotrophic processes, greenhouse gases, bacterial respiration, freshwater, boreal forest

## 2.1 Introduction

The growing need for rigorous quantification of CO<sub>2</sub> emissions produced by aquatic ecosystems, at a global scale, makes it essential to understand the mechanisms controlling the total diffusive fluxes of CO<sub>2</sub> produced by natural lakes, reservoirs and other water bodies affected by human activities (Weissenberger et al. 2010). A first hypothesis to explain the considerable differences observed in CO<sub>2</sub> emissions between reservoirs, natural lakes and water bodies affected by logging activities, targets the quality, or freshness, of terrigenous organic matter (TOM) that is processed by bacterial communities thus leading to the production of CO<sub>2</sub> in the water column. Inputs of fresher TOM would result in higher CO<sub>2</sub> emissions (Miller et al. 2002; Ouellet 2010). A second hypothesis for the differences in emissions between the different water bodies pertains to the photochemical mineralization of TOM in the aquatic environment, which could have a significant impact on the total diffusive flux of CO<sub>2</sub> to the atmosphere (Huttunen et al. 2003; Soumis et al. 2007). The water bodies of the boreal forest domain included in this study were: (i) lakes not affected by logging activities (LNAL), also defined as pristine lakes, (ii) lakes affected by logging activities on their watershed (LAL), (iii) a reservoir not affected by logging activities (RNAL), and (iv) a reservoir affected by logging activities (RAL).

The major goal of this study was to test this second hypothesis by calculating the daily production of CO<sub>2</sub> by photochemical mineralization of dissolved organic matter (DOM), integrated over the entire water column ( $DIPM_{CO_2}$ ), of distinct water bodies representing various environmental scenarios. This quantity was determined using the calculation of the spectrum quantum yield ( $\phi_\lambda$ ) proposed by Vähätalo et al. (2000). As  $\phi_\lambda$  is determined by two constants c and d ( $\phi_\lambda = c \cdot \exp(-d\lambda)$ ), we measured the photochemical mineralization at two depths (just below the surface and at 1 meter,

defined as  $PM_{CO_2}(0)$  and  $PM_{CO_2}(1)$  respectively). In order to evaluate ( $DIPM_{CO_2}$ ), we have also measured the downward vector irradiance spectrum ( $I_{d,c,0+,\lambda}$ ) and the absorption coefficient of chromophoric dissolved organic matter (CDOM) at  $\lambda$ , ( $a_{CDOM,\lambda}$ ) for each water body sampled. As the total diffusive fluxes of  $CO_2$  from the water surface to the atmosphere ( $f_{CO_2}$ ) were measured using the thin boundary layer method (TBL), we were able to calculate the relative contribution of the daily production of  $CO_2$  by photochemical mineralization integrated over the entire water column to the total emission of  $CO_2$  to the atmosphere at the water surface ( $DIPM_{CO_2} / f_{CO_2}$ ).

On the other hand, the main processes controlling the inorganic carbon cycle in aquatic systems represented by the photochemical mineralization, the bacterial respiration and the  $CO_2$  uptake by photosynthesis were also measured. We then propose to integrate those  $CO_2$  production and uptake into an empirical model that will allow us to quantify the relative importance of those processes to the total diffusive fluxes of  $CO_2$  from the water surface to the atmosphere.

## 2.2 Methods

### 2.2.1 Sampling sites

All water bodies considered in this study are located on the Canadian Shield in mid northern Québec, a region mostly characterized by thin soils covering metamorphic and igneous rocks, and belonged to the boreal ecosystem, a region of mixed forest consisting primarily of conifers and some broad-leaved trees. We selected six lakes, located in the Forêt de l'Aigle conservation area, and two reservoirs, Decelles and Cabonga, located in the La Vérendrye wildlife reserve. The six lakes (Mary, Ellard,

Jean, Claire, Brock, and Bouleau) and the two reservoirs represented the four environmental scenarios listed above (see Ouellet et al. 2008, for details). The surface area of each lake is relatively small, ranging from 0.280 km<sup>2</sup> for L. Ellard to 1.879 km<sup>2</sup> for L. Jean. The Cabonga and Decelles reservoirs were impounded in 1928 and 1941 respectively, and the latter was expanded in 1949. This study therefore relates to relatively old reservoirs, considered stabilized (Tremblay et al. 2004). They were sampled in the spring, summer and fall of 2006 and 2007.

#### 2.2.2 Measurements of the total diffusive fluxes of CO<sub>2</sub> from the water surface to the atmosphere using the thin boundary layer method

Different methods have been developed to measure the fluxes of CO<sub>2</sub> between water bodies and the atmosphere, most notably static chambers (Duchemin et al. 1999) and the TBL method based on the measurement of concentrations of gases present in dissolved form in a thin layer of surface water (Cole et al. 1994). However, Soumis et al. (Soumis et al. 2008) have shown that the use of static chambers introduces a significant bias into the calculation of diffusive fluxes because of disturbances in the water column concentration gradients. Given the size of the reservoirs, the static chamber approach also requires a significant logistical effort, and thus we opted for the TBL method in this project. The calculation of the diffusive fluxes of CO<sub>2</sub> with the TBL method is based on four factors: wind speed, air temperature, water temperature, and the concentration of both gases in the water samples (Duchemin et al. 1999; Kelly et al. 1997; Weissenberger 2007). These four variables were used to evaluate  $f_{CO_2}$  as proposed by Cole and Caraco (1998) and modified by Soumis et al. (2004). In order to account for limits in the applicability of this model, we assumed that surface waters were well mixed and that transfer of CO<sub>2</sub> across the interface took place through molecular diffusion (Liss and Slater 1974; Macintyre et al. 1995).

The values of  $f_{CO_2}$  were calculated according to Fick's first law (Equation 2.1):

$$f_{CO_2} = k_{CO_2} \cdot ([CO_2]_{surf} - pCO_{2atm} \cdot K_H) \quad (2.1)$$

where  $k_{CO_2}$  the piston velocity,  $K_H$  Henry's constant adjusted according to temperature and  $pCO_{2atm}$  the partial atmospheric pressure. The piston velocity is defined by the equation 2:

$$k_{CO_2} = k_{600} \cdot (600 / Sc_{CO_2})^{0.67} \quad (2.2)$$

where  $k_{600}$  represents the constant of piston velocity normalized for a Schmidt number ( $Sc_{CO_2}$ ) of 600. We used a value of the constant  $k_{600}$ , which is determined using the model developed by Cole et al. (1994), where  $U_{10}$  is the wind speed at 10 m over the surface of the lake. The constant for piston velocity is thus obtained from the empirical equation 3:

$$k_{600} = 2.07 + (0.215 \cdot U_{10}^{1.7}) \quad (2.3)$$

Finally, the Schmidt number for carbon dioxide is calculated according to the equation of Wanninkhof (1992):

$$Sc_{CO_2} = 1911.1 - 118.11 \cdot T_w^\circ - 3.4527 \cdot (T_w^\circ)^2 - 0.04132 \cdot (T_w^\circ)^3 \quad (2.4)$$

where ( $T_w^\circ$ ) is the temperature at the surface of the water.

The values of  $f_{CO_2}$  were calculated on the basis of 30-mL samples taken from the first two centimeters of the water column. Using 60-mL syringes, four samples were

collected at each site in order to assure the representativeness of the samples. Then, 30 mL of ultrapure N<sub>2</sub> were added to each syringe. The four syringes were shaken for one minute and the liquid part of the sample was discarded. Upon shaking, CO<sub>2</sub> equilibrates with the N<sub>2</sub> headspace according to the equations developed by Duchemin (2000). Concentrations were analyzed using a Varian Star-3400 gas chromatograph (GC) fitted with a 1-mL sampling loop and a stainless steel Hayesep-Q column (200 mm long, 3 mm in diameter, 80/100 mesh, isothermal oven at 50°C). Helium was used as the carrier gas at a flow rate of 30 mL.min<sup>-1</sup>. Quantification of the gases was done using a thermal conductivity detector.

### 2.2.3 Measurements of CO<sub>2</sub> from photochemical mineralization, bacterial respiration, and CO<sub>2</sub> uptake by photosynthesis

The various processes of production of CO<sub>2</sub> i.e. photochemical mineralization, bacterial respiration, and consumption of CO<sub>2</sub> during photosynthesis, were measured using an incubation/irradiation system approach validated by Soumis (Soumis 2006). Using filtration at different porosities, this system allows measuring three forms of CO<sub>2</sub> production in water samples irradiated *in-situ* just below the water surface (0.02m) and at a depth of one meter. Dark cells and transparent quartz cells of 200 mm length and 20 mm internal radius were irradiated during 24 hours to quantify the daily production of CO<sub>2</sub> by photochemical mineralization, bacterial respiration, and consumption of CO<sub>2</sub> during photosynthesis. The UV-PAR transmittance of the cells of quartz used in this work varies between 88 % and 94 % for the entire spectral length considered here (305 to 700 nm). The cells were filled with water that was first filtered through a 0.2 µm nylon filter (Pall®) for the S samples (sterile), at 1.2 µm for B samples (bacterial) and at 210 µm for P samples (planktonic). The cells were sealed using rubber corks and Parafilm. Once filtered, each sample was placed in duplicate dark cells (DS, DB, DP) or transparent quartz cells (TS, TB, TP), and then irradiated

for 24 hours. CO<sub>2</sub> production by photochemical mineralization ( $PM_{CO_2}$ ), bacterial respiration ( $BR_{CO_2}$ ) and CO<sub>2</sub> uptake by photosynthesis ( $PH_{CO_2}$ ), for each sampling site, are defined by equations 5 and 6:

$$PM_{CO_2}(z) = TS_{CO_2}(z) - DS_{CO_2}(z) \quad (2.5)$$

$$BR_{CO_2}(z) = DB_{CO_2}(z) - DS_{CO_2}(z) \quad (2.6)$$

Where,  $TS_{CO_2}(z)$ ,  $DB_{CO_2}(z)$  and  $DS_{CO_2}(z)$  represent the concentrations of dissolved CO<sub>2</sub> expressed in  $\mu\text{mol.L}^{-1}$  after 24 hours of incubation, for the TS, DB, and DS cells, irradiated at a depth of z. The values of gross CO<sub>2</sub> production by photochemical mineralization ( $PM_{CO_2}(z)$ ), and bacterial respiration  $BR_{CO_2}(z)$ , are thus expressed in  $\mu\text{mol CO}_2.\text{L}^{-1}.\text{d}^{-1}$ . The concentrations of dissolved CO<sub>2</sub> produced by each irradiated sample were measured as above for the TBL method.

We also evaluated the CO<sub>2</sub> uptake by photosynthesis (Equation 2.7):

$$PH_{CO_2}(z) = (TP_{CO_2}(z) - DS_{CO_2}(z)) - BR_{CO_2}(z) - PM_{CO_2}(z) \quad (2.7)$$

where  $TP_{CO_2}(z)$  represents the concentrations of dissolved CO<sub>2</sub> expressed in  $\mu\text{mol.L}^{-1}$  after 24 hours of incubation for TP cells, irradiated at a depth of z (just below the surface and at 1 meter depth).

#### 2.2.4 Theoretical model for the daily production of CO<sub>2</sub> by photochemical mineralization, integrated over the entire water column

As a first step, we measured the average absorbance of CDOM at  $\lambda$  ( $A_{CDOM,\lambda}$ ) at wavelengths of 305, 313, 320, 340, 380, 395, 400, 550, and 700 nm. The absorbance of filtered samples was measured using a Beijing Purkinge General Instrument

TU-18005 UV-PAR spectrophotometer. The average absorption coefficient of CDOM at  $\lambda$  ( $a_{CDOM,\lambda}$ ) was then calculated based on measurements of spectral absorbance of CDOM before irradiation ( $A_{CDOM,\lambda}_{ini}$ ) and after irradiation ( $A_{CDOM,\lambda}_{end}$ ), to take into account the fact that the absorbance of samples can decrease with the photodegradation of DOM (Lindell et al. 2000; Reche et al. 1999). The value ( $A_{CDOM,\lambda}$ ) is based on the mean values of absorbance  $A_{CDOM,\lambda} = \left( \left( A_{CDOM,\lambda}_{ini} + A_{CDOM,\lambda}_{end} \right) / 2 \right)$ . The average absorbance of CDOM at  $\lambda$  was then used to determine the average absorption coefficient of CDOM at  $\lambda$  ( $a_{CDOM,\lambda}$ ), using Equation 2.1 (Kirk 1994). In this equation,  $l$  is the length of the optical path corresponding to the quartz cells of the spectrophotometer ( $l = 0.1$  m):

$$a_{CDOM,\lambda} = 2,303 \cdot A_{CDOM,\lambda} / l \quad (2.8)$$

The second step consisted in measuring the downward vector photon flux density at the surface and at  $\lambda$  to which each sample was exposed over the course of irradiation ( $Q_{d,v,0+,\lambda}$ ). Those values were collected using a PUV-2500/2510 radiometric probe. As the absorption coefficient of CDOM at  $\lambda$  ( $a_{CDOM,\lambda}$ ) was determined, we were able to calculate the scalar photon flux density at depth  $z$  and at  $\lambda$  ( $Q_{s,z,\lambda}$ ) for each sample (Miller 1998). To evaluate the daily production of  $CO_2$  by photochemical mineralization, integrated over the entire water column ( $DIPM_{CO_2}$ ), we used the theoretical model developed by Vähätalo et al. (2000):

$$DIPM_{CO_2} = \int_z \int_{\lambda_{\min}}^{\lambda_{\max}} \phi_{\lambda} Q_{s,z,\lambda} a_{CDOM,\lambda} d\lambda dz \quad (2.9)$$

Each term of this equation has previously been described. The factors  $\lambda_{\min}$  and  $\lambda_{\max}$  represent the wavelengths at 300 nm and 700 nm respectively. As suggested by Vähätalo et al. (2000), the spectrum of apparent quantum yield for photochemical mineralization  $\phi_{\lambda}$  (number of CO<sub>2</sub> mol produced / number of mol of absorbed photons) related to natural DOM, decreases exponentially with increasing wavelength (Moore et al. 1993; Sikorski and Zika 1993; Vähätalo et al. 2000) and can be generalized to:

$$\phi_{\lambda} = c \times 10^{-d\lambda} \quad (2.10)$$

with  $c$  (dimensionless) and  $d$  (nm<sup>-1</sup>) being positive constants and  $\lambda$ , the wavelength in nanometers. As measured by Vähätalo et al. (2000), the constants  $c$  and  $d$  will be determined according to the measurements of the photochemical mineralization just below the surface ( $PM_{CO_2}(0)$ ) and at one meter depth ( $PM_{CO_2}(1)$ ). The mathematical optimization was done with the Stella Software (see systems Releases STELLA® and iThink® Version 9.0). As shown in Equation 2.9,  $DIPM_{CO_2}$  is expressed as a daily flux of CO<sub>2</sub> produced by DOM mineralization (mmol.CO<sub>2</sub>.m<sup>-2</sup>.d<sup>-1</sup>).

In order to state that the variations of the amounts of CO<sub>2</sub> produced by photochemical mineralization could be linked to the various environmental conditions, we first verified that the variations in the photon flux density ( $Q_{d,y,0+, \lambda}$ ) did not substantially affect the  $DIPM_{CO_2}$  values. We verified that the variations in photochemical mineralization did not depend upon daily differences in radiation

intensity. For this purpose, we used the Vähätalo et al. (2000) equations wherein  $pm_z$  is defined. We merely changed the photon flux value ( $Q_{d,v,0+, \lambda}$ ) that came from the PUV-2500/2510 to the average photon flux value ( $\bar{Q}_{d,v,0+, \lambda}$ ), calculated as the average values of  $Q_{d,v,0+, \lambda}$  measured during summer and spring field campaigns. Thus, the daily flux of  $CO_2$  produced by DOM mineralization and standardized according to the average of the scalar photon flux density can be evaluated as  $\overline{DIPM}_{CO_2} = \int_z \int_{\lambda \min}^{\lambda \max} \phi_{\lambda} \bar{Q}_{s,z, \lambda} a_{CDOM, \lambda} d\lambda dz$ , where  $\bar{Q}_{s,z, \lambda}$  comes from  $\bar{Q}_{d,v,0+, \lambda}$  as the average of the scalar photon flux density.

### 2.2.5 Empirical model of $CO_2$ diffusive fluxes

The empirical model for uptake and production of  $CO_2$  over the water column ( $f_{CO_2}$ ) was built in keeping with the system of irradiation and incubation developed by Soumis et al. (2007). To do this, we evaluated the constants c and d included in the spectrum of the quantum yield for photochemical mineralization formula ( $\phi_{\lambda}$ ) according to the photochemical mineralization measurements just below the surface and at one meter depth ( $PM_{CO_2}(0)$  and  $PM_{CO_2}(1)$  respectively). Then, we calculated  $\overline{DIPM}_{CO_2}$ , the daily production of  $CO_2$  integrated over the entire water column. Bacterial respiration ( $BR_{CO_2}$ ) was integrated over the epilimnetic zone in order to calculate the daily-integrated flux of  $CO_2$  arising from bacterial respiration ( $DIBR_{CO_2}$ ). This calculation was based on the depth of the mixed layer ( $z_{ML}$ ) as proposed by Hanson et al. (2004):

$$z_{ML} = 10^{(1.16 - 0.066 * \log_{10} ([DOC] + 1))} \quad (2.11)$$

The fact that  $BR_{CO_2}$  is not significantly different according to spectral exposure (Soumis 2006) led us to define  $DIBR_{CO_2}$  as follow:

$$DIBR_{CO_2} = (BR_{CO_2}(0) + BR_{CO_2}(1))/2 * z_{ML} \quad (2.12)$$

Finally, the amount of  $CO_2$  fixed during the photosynthesis, was also evaluated over the entire mixed layer depth, based on the quantity of  $CO_2$  measured just below the surface ( $PH_{CO_2}(0)$ ) and at one meter depth ( $PH_{CO_2}(1)$ ). To evaluate the quantity of carbon fixed by photosynthesis over the entire water column, we used the downward attenuation coefficient of irradiance over the photosynthetically active radiation range ( $K_{d,I,PAR}$ ). We assumed that the amount of  $CO_2$  fixed by photosynthesis is proportional to the amount of the scalar photon flux density for the PAR range ( $Q_{s,z,PAR}$ ) reaching the depth  $z$  over the depth of the photic zone ( $z_{pz}$ ). Our calculation, summarized in equation 11, is therefore based on the fraction of  $Q_{s,z,PAR}$  (the scalar photon flux density for the PAR) over  $Q_{d,v,0+,PAR}$  (the spectrum of downward vector photon flux density for the PAR just below the surface) multiplied by the  $CO_2$  fixed by photosynthesis at one meter depth:

$$PH_{CO_2}(z) = \frac{Q_{s,z,PAR}}{Q_{d,v,0+,PAR}} * PH_{CO_2}(1) \quad \text{for } z_{pz} \geq z \geq 1 \quad (2.13a)$$

$$PH_{CO_2}(z) = ((1 - z) * PH_{CO_2}(0) + z * PH_{CO_2}(1))/2 \quad \text{for } 1 \geq z > 0 \quad (2.13b)$$

In these equations, the amount of  $CO_2$  fixed by photosynthesis ( $DIPH_{CO_2}$ ) is defined as follows:

$$DIPH_{CO_2} = \int_{0+}^{z_{pz}} PH_{CO_2}(z) dz * 1000 \quad (2.14)$$

It is therefore possible to propose a flux of CO<sub>2</sub> at the water-air interface arising from the combination of photochemical mineralization, bacterial respiration and CO<sub>2</sub> uptake by photosynthesis:

$$f_{CO_2}^* = DIPM_{CO_2} + DIBR_{CO_2} + DIPH_{CO_2} \quad (2.15)$$

### 2.2.6 Evaluation of the dissolved and particulate organic matter terrigenous fractions

The  $C/N$  ratios and a two-component mixing model were used to determine the DOM and particulate organic matter (POM) terrigenous fractions in each water body. The end-member values were obtained from pure terrigenous sources by sampling the organic and inorganic horizons of local soils of the boreal forest, and fixed at 13 for the autochthonous source (Weissenberger 2007). All samples were freeze-dried and then analyzed for organic carbon and total nitrogen contents using a Carlo Erba NA-1500 elemental analyzer. To determine the terrigenous fraction ( $f_{terr}$ ) in DOM and POM samples, we used the following Equation (16):

$$f_{terr} = \left( \frac{C}{N}_{mix} - \frac{C}{N}_{aut} \right) / \left( 0.8 \cdot \frac{C}{N}_{hor} + 0.2 \frac{C}{N}_{hin} - \frac{C}{N}_{aut} \right) \quad (2.16)$$

where  $\frac{C}{N}_{mix}$  is the value of the atomic  $C/N$  ratios for the DOM, POM or sedimentary material (SED), and where  $\frac{C}{N}_{aut}$  refers to the autochthonous source,  $\frac{C}{N}_{hor}$  to the organic horizon, and  $\frac{C}{N}_{hin}$  to the inorganic horizon.

## 2.3 Results

### 2.3.1 Diffusive fluxes of CO<sub>2</sub>

The average  $f_{CO_2}$  values measured in reservoirs were twice those measured in lakes:  $30.94 \pm 23.34 \text{ mmol.m}^{-2}.\text{d}^{-1}$  vs.  $16.38 \pm 17.46 \text{ mmol.m}^{-2}.\text{d}^{-1}$ , respectively (Figure 2.1), and the effect of logging on the watershed was even larger. The type of water body with the highest CO<sub>2</sub> emissions was therefore the RAL ( $34.74 \pm 26.14 \text{ mmol.m}^{-2}.\text{d}^{-1}$ ), followed by the LAL ( $32.27 \pm 17.99 \text{ mmol.m}^{-2}.\text{d}^{-1}$ ), the RNAL ( $24.38 \pm 15.54 \text{ mmol.m}^{-2}.\text{d}^{-1}$ ) and finally the LNAL ( $9.69 \pm 12.11 \text{ mmol.m}^{-2}.\text{d}^{-1}$ ).

### 2.3.2 Daily production of CO<sub>2</sub> by photochemical mineralization integrated over the water column

Once the downward vector irradiance spectrum ( $I_{d,v,0+,\lambda}$ ) was measured by PUV2500/2510 probes, those values were converted to a photon flux density ( $Q_{d,v,0+,\lambda}$ ). As we have also measured the absorption coefficient of CDOM at  $\lambda$  ( $a_{CDOM,\lambda}$ ), we were able to quantify the daily production of CO<sub>2</sub> by photochemical mineralization integrated over the entire water column from the theoretical model developed by Vähätalo et al. (2000). Indeed, the c and d parameters of the quantum yield for photochemical mineralization at  $\lambda$  ( $\phi_\lambda$ ), shown in the Equation 2.10, were evaluated by iteration with the STELLA® and iThink® Version 9.0 softwares. First, we fixed the constant c to 7.52 (obtained from the Swedish Valkea-Kotinen Lake) as suggested by Vähätalo et al. (2000). Moreover, the parameter d was deduced by iteration from the  $PM_{CO_2}(1)$  values. In order to minimize the variation of  $PM_{CO_2}(1)$  attributable to the analytical error of  $I_{d,v,0+,\lambda}$  values, we decided to evaluate the parameter d from the average value of  $PM_{CO_2}(1)$  calculated for each environmental condition. Thus, the constant d was evaluated with the following average values of

$PM_{CO_2}(1)$  for reservoirs affected or not by logging,  $1.45 \pm 0.85 \mu\text{mol.l}^{-1}.\text{d}^{-1}$  for RNAL, and  $5.09 \pm 3.81 \mu\text{mol.l}^{-1}.\text{d}^{-1}$  for RAL. The constant  $d$  was also evaluated for lakes affected or not by logging with the following average values of  $PM_{CO_2}(1)$ ,  $0.10 \pm 0.15 \mu\text{mol.l}^{-1}.\text{d}^{-1}$  for LNAL and  $2.68 \pm 2.56 \mu\text{mol.l}^{-1}.\text{d}^{-1}$  for LAL. For each of these environmental conditions, the average of the scalar photon flux density ( $\bar{Q}_{d,v,0+, \lambda}$ ) as well as the average absorption coefficient of CDOM at  $\lambda$  ( $\bar{a}_{CDOM, \lambda}$ ) and the average of the amount of  $CO_2$  produced by photochemical mineralization at one meter depth ( $PM_{CO_2}(1)$ ) was used to determine the parameter  $d$ . We observed that the parameter  $d$  varied greatly between environmental conditions. Thus, the quantum yield evaluated for the RNAL scenario is very similar to that obtained by Vähätalo et al. (2000) wherein  $\phi_{\lambda, V\ddot{a}h\ddot{a}talo} = 7.52 \times 10^{-0.0122 \lambda}$ . Indeed, in our case  $\phi_{\lambda, RNAL} = 8.56 \times 10^{-0.0124 \lambda}$ , the other quantum yield for reservoir affected by logging was higher with  $\phi_{\lambda, RAL} = 12.56 \times 10^{-0.0107 \lambda}$  (Figure 2.1). For the other scenarios, we obtained  $\phi_{\lambda, LNAL} = 6.49 \times 10^{-0.0139 \lambda}$  for lakes non-affected by logging and finally  $\phi_{\lambda, LAL} = 12.05 \times 10^{-0.0111 \lambda}$  for lakes with logged watersheds (Figure 2.1).

It was then possible to calculate the daily production of  $CO_2$  by photochemical mineralization, integrated over the entire water column ( $DIPM_{CO_2}$ ). The  $DIPM_{CO_2}$  value, which corresponds to the area under the curve defined by the product of  $\phi_{\lambda}$  and  $\bar{Q}_{d,v,0+, \lambda}$ , also strongly depends on the environmental conditions (Figure 2.2). The average values of  $DIPM_{CO_2}$  for the four different environmental scenarios are presented at Figure 2.3. RAL has the highest value of average daily production of  $CO_2$  by photochemical mineralization integrated over the entire water column with a  $DIPM_{CO_2}$  value of  $9.38 \pm 2.59 \text{ mmol.CO}_2.\text{m}^{-2}.\text{d}^{-1}$ . This is followed by LAL ( $5.16 \pm 2.30 \text{ mmol.CO}_2.\text{m}^{-2}.\text{d}^{-1}$ ), RNAL ( $2.51 \pm 0.49 \text{ mmol.CO}_2.\text{m}^{-2}.\text{d}^{-1}$ ), and finally LNAL ( $0.24 \pm 0.16 \text{ mmol.CO}_2.\text{m}^{-2}.\text{d}^{-1}$ ). As such, an average LNAL produces only a little

over  $2.5 \pm 1.9$  % of the amount of  $\text{CO}_2$  produced by photochemical mineralization over the entire water column in the RAL. Seasonality also plays an important role due to changes in the photon flux density ( $Q_{d,r,0+\lambda}$ ). Thus, the average values of  $DIPM_{\text{CO}_2}$  during spring and summer regardless of the environmental conditions is equal to  $3.68 \pm 3.95 \text{ mmol.CO}_2.\text{m}^{-2}.\text{d}^{-1}$  while these values are  $1.08 \pm 0.73 \text{ mmol.CO}_2.\text{m}^{-2}.\text{d}^{-1}$  during the fall.

### 2.3.3 $\text{CO}_2$ uptake by photosynthesis

The  $\text{CO}_2$  uptake by photosynthesis ( $DIPH_{\text{CO}_2}$ ) was evaluated based on  $PH_{\text{CO}_2}(z)$  values where  $z$  takes a value of 0 or 1 based on whether the TP solutions was irradiated at the surface level or at a depth of 1 m. To quantify the  $\text{CO}_2$  uptake, we used Equation 14. As such,  $PH_{\text{CO}_2}(z)$  provided an average value of  $\text{CO}_2$  taken up by photosynthesis over the first meter of the water column. By definition, the photosynthetic yield is equal to the plankton respiration, at the point of compensation ( $I_C$ ), we considered the downward attenuation coefficient of irradiance over the photosynthetically active radiation range ( $K_{d,I,PAR}$ ) equivalent to ( $I_C$ ) in order to extrapolate the  $\text{CO}_2$  uptake over the epilimnetic zone. First, we observed that the depth of the photic zone ( $z_{pz}$ ) submitted to a Kruskal Wallis test, provided a significant difference between the environmental conditions ( $df=3$ ,  $p<0.001$ ). However, when a Kruskal Wallis test was applied to the depth of the photic zone grouped by season, the results were not significant ( $df=2$ ,  $p=0.296$ ). According to a Kruskal Wallis test, the  $DIPH_{\text{CO}_2}$  values restricted to the first cubic meter ( $DIPH_{\text{CO}_2,1m}$ ) could not be differentiated among the various scenarios, even though the average values of  $DIPH_{\text{CO}_2,1m}$  were quite distinct. The  $DIPH_{\text{CO}_2,1m}$  values fell in

the same range as those of  $f_{CO_2}$  or  $DIPM_{CO_2}$ . The  $DIPH_{CO_2,1m}$  values were  $-0.13 \pm 6.72 \mu\text{mol.l}^{-1}.\text{d}^{-1}$  for RAL,  $-1.57 \pm 5.57 \mu\text{mol.l}^{-1}.\text{d}^{-1}$  for RNAL,  $-3.24 \pm 5.95 \mu\text{mol.l}^{-1}.\text{d}^{-1}$  for LAL and  $-3.69 \pm 6.54 \mu\text{mol.l}^{-1}.\text{d}^{-1}$  for LNAL.

#### 2.3.4 CO<sub>2</sub> production by bacterial respiration

Bacterial respiration also contributes substantially to CO<sub>2</sub> emissions (Biddanda and Benner 1997). We therefore measured CO<sub>2</sub> production by bacterial respiration ( $BR_{CO_2}(z)$ ) in the first of the water column as it was previously described (Equation 2.6). The application of a Kruskal Wallis to  $BR_{CO_2}(z)$ , according to the environmental conditions, resulted in a significant outcome (df=3, p<0.001). Average values of  $\overline{BR_{CO_2}(z)}$ , the average value of  $BR_{CO_2}(0)$  and  $BR_{CO_2}(1)$ , defined by respiration in the first meter of the water column, were  $4.31 \pm 4.54 \mu\text{mol.l}^{-1}.\text{d}^{-1}$  for RAL,  $3.33 \pm 4.19 \mu\text{mol.l}^{-1}.\text{d}^{-1}$  for LAL,  $2.78 \pm 3.17 \mu\text{mol.l}^{-1}.\text{d}^{-1}$  for RNAL, and  $0.03 \pm 2.39 \mu\text{mol.l}^{-1}.\text{d}^{-1}$  for LNAL. It is noticeable that the presence or absence of logging in the watershed, in these results, has a larger effect than the distinction between reservoirs and lakes. The  $\overline{BR_{CO_2}(z)}$  values associated with RNAL were approximately 60% of the corresponding value for RAL, and almost zero for LNAL.

#### 2.3.5 Terrigenous organic matter in the water column

Because we are considering water bodies that vary according to logging in the watershed, we found intrinsically relevant to measure quantities of terrigenous organic matter present in the water column, as this could have an effect on the CO<sub>2</sub> production by photochemical mineralization (Bertilsson and Tranvik 2000). The analysis of the terrigenous fraction of the organic matter was calculated according to

mixing equation (Equation 16), based on the  $C/N$  ratio. Table 2.1 presents these results, across different environmental scenarios, including the following data: organic and inorganic horizons of soil samples from the watershed of each water body ( $C/N_{hor}$  and  $C/N_{in}$ , respectively); POM and DOM present in the water column ( $C/N_{DOC}$  and  $C/N_{POC}$ , respectively) and the average ratios over the top five centimeters of sediment ( $C/N_{SED}$ ).  $C/N$  ratios were lower for the inorganic horizons than for the organic ones across all environmental scenarios. Similarly,  $C/N$  ratios for POM were smaller than those for DOM while the lowest  $C/N$  ratios were observed in sediments. Results of the calculation of the terrigenous fractions ( $f_{terr}$ ) of organic carbon, among the various scenarios, are presented in Table 2.2. We found that according to the mixing equation, almost all dissolved carbon ( $< 0.45 \mu m$ ) is of terrigenous origin, regardless of the scenario. The terrigenous fraction of POM, on the other hand, showed a strong variability among the various scenarios. The fraction of terrigenous material forming POM appeared much larger for RAL ( $\approx 58\%$ ) than for LNAL ( $\approx 28\%$ ). Similarly, the terrigenous fraction of POM are much larger in the case of RAL ( $\approx 34\%$ ) than in LNAL ( $\approx 6\%$ ).

#### 2.4 Discussion

The ultimate photodegradation of DOM results in the photochemical mineralization, which mainly constitutes of a production of  $CO_2$ . However, the photodegradation of DOM also provides compounds that are labile for bacteria (Del Giorgio and Davis 2003). Upon photodegradation, the absorbance of the DOM will decrease (Osburn et al. 2001). It has been observed that the production of dissolved inorganic carbon (DIC) by photochemical mineralization is strongly correlated to the color of the DOM

(Bertilsson and Tranvik 2000). According to our observations, this result remains valid for the daily flux of  $\text{CO}_2$  deriving from the DOM mineralization for an average photon flux value over the water column, as indicated by the coefficient of correlation  $R^2 = 0.81$  between  $\overline{DIPM}_{\text{CO}_2}$  and  $a_{360}$  ( $p < 0.001$ ) (Figure 2.4). Moreover, it appears that during the fall season, the  $\overline{DIPM}_{\text{CO}_2}$  (calculated with a  $\overline{Q}_{s,z,\lambda}$  corresponding to the average photon flux measured during the fall season) remains strongly correlated with  $a_{360}$  ( $R^2 = 0.65, p < 0.001$ ) (Figure 2.4). Finally,  $\overline{DIPM}_{\text{CO}_2}$  values were also evaluated from  $PM_{\text{CO}_2}(z)$  values obtained during a summer field campaign on La Grande reservoir sites (LG) (Soumis et al. 2007). The  $\overline{DIPM}_{\text{CO}_2}$  values and  $a_{360}$  are then well correlated for a vast series of water bodies distributed from  $46^\circ\text{N}$  to  $54^\circ\text{N}$ . As the CDOM is linked to the quantity of terrigenous matter by the presence of aromatic molecules (Graneli et al. 1996), we may assume that an important part of the DOM photochemical mineralization derives from these molecules. While there are limitations to the conclusions we can draw from the  $C/N$  ratios observations, it seems nonetheless that the DOM terrigenous fraction ( $f_{\text{terr}}$ ) is comparable among the various environmental scenarios considered. We can therefore hypothesize that the TOM freshness (estimated thanks to the parameter  $d$  of the quantum yield  $\phi_\lambda$ ) in addition to the quantity of terrigenous organic matter present in the water column, can have an important influence on the daily production of  $\text{CO}_2$  by photochemical mineralization of DOM standardized for an average photon flux value over the water column.

#### 2.4.1 $\text{CO}_2$ diffusive fluxes and $DIPM_{\text{CO}_2}$

The measurements of  $f_{\text{CO}_2}$  with the TBL method are systematically higher for the reservoirs than for the lakes. This observation can be made independently of any other environmental factor. Taking into account the importance of wind speed according to the equations of Cole and Caraco (1994), it is likely that the fetch

explains part of this higher production at the surface of reservoirs (Soumis et al. 2004). Despite this effect, the emissions must be sustained by a higher level of CO<sub>2</sub> production in the water column or in sediments (Houel et al. 2006; Soumis et al. 2005). The fact that  $DIPM_{CO_2}$  is higher in the case of RAL than LNAL led us to compare  $\overline{DIPM}_{CO_2}$  to  $f_{CO_2}$ . As  $\overline{DIPM}_{CO_2}$ , the standardized value of  $DIPM_{CO_2}$  by photon flux value is expressed in mmol.m<sup>-2</sup>.d<sup>-1</sup>, we are able to determine the contribution of the amount of CO<sub>2</sub> produced by photochemical mineralization integrated over the entire water column to total CO<sub>2</sub> diffusive fluxes towards the atmosphere. We observed a relationship, which is evaluated with a linear regression, between the non-standardized value of the daily flux of CO<sub>2</sub> deriving from the mineralization of DOM ( $DIPM_{CO_2}$ ) and  $f_{CO_2}$  (R<sup>2</sup>=0.49, p<0.001). The equations defined by these regressions can be expressed as follows:

$$f_{CO_2} = 12.68 + 2.77 \cdot \overline{DIPM}_{CO_2} \quad (2.17)$$

$$f_{CO_2} = 15.7 + 1.92 \cdot DIPM_{CO_2} \quad (2.18)$$

According to this equation, the production of by CO<sub>2</sub> the photodegradation of DOM amounts to approximately 15.13 ± 14.1 % of total CO<sub>2</sub> emissions. Except for the LNAL scenario that corresponds to small CO<sub>2</sub> fluxes from photochemical mineralization, this percentage seems to be independent of our varying environmental scenarios. This result highlights the fact that the CO<sub>2</sub> production deriving from the photochemical mineralization of DOM cannot be the only heterotrophic process but it contributes in an important way to total CO<sub>2</sub> diffusive fluxes towards the atmosphere.

#### 2.4.2 Relation between photochemical mineralization of DOM and bacterial respiration

The results for the daily production of CO<sub>2</sub> by bacterial respiration show a significant difference in average values across the various environmental scenarios. The highest bacterial production ( $\overline{BR}_{CO_2}(z)$ ) corresponds to the RAL scenario with  $4.50 \pm 3.33 \mu\text{mol.l}^{-1}.\text{d}^{-1}$ ; while in contrast, the values of CO<sub>2</sub> production ( $\overline{BR}_{CO_2}(z)$ ) for LNAL are the lowest values with  $1.39 \pm 1.83 \mu\text{mol.l}^{-1}.\text{d}^{-1}$ . Values of bacterial respiration are however not correlated with the phosphorus concentrations ( $R^2 = 0.079$ ,  $p = 0.0639$ ). It seems reasonable to assume that a bias associated with analytical methods explains the similar ordering of scenarios in the cases of CO<sub>2</sub> production either by photochemical mineralization or by bacterial respiration. One might think that a possible source of this bias is the filtering of water samples on 0.2  $\mu\text{m}$  filters, which may have resulted in the presence of non-negligible amounts of degraded organic matter in the DB and TB cells. However, this hypothesis is contradicted by the fact that transparent and dark cells that were filtered on 1,2  $\mu\text{m}$  filters do not present significant differences, according to a Kruskal Wallis test. Therefore photodegradation of DOM particles with sizes comprised between 0.2  $\mu\text{m}$  and 1.2  $\mu\text{m}$  does not occur at a detectable level over 24h of irradiation under natural conditions.

As previously defined in Equation 6, the average values of the bacterial respiration produced in the first meter  $\overline{BR}_{CO_2}(z)$  follow a pattern that is similar to the daily standardized production of CO<sub>2</sub> by photochemical mineralization, integrated over the entire water column ( $\overline{DIPM}_{CO_2}$ ) (Table 2.3). However, when all sampling sites are considered, CO<sub>2</sub> production by bacterial respiration, over the entire water column ( $\overline{DIBR}_{CO_2}$ ), shows no relationship with  $\overline{DIPM}_{CO_2}$ . This result may derive from the fact that bacterial respiration is homogeneous over a well-mixed epilimnion (Del Giorgio et al. 1997). Consequently, by construction,  $\overline{DIBR}_{CO_2}$  and  $\overline{BR}_{CO_2}(z)$  differ

from each other by the factor  $z_{ML}$ . It is remarkable that  $\overline{BR}_{CO_2}(z)$  and  $\overline{DIPM}_{CO_2}$  follow the same trends and, according to the hypothesis suggested by Anesio et al. (2005), there would be an effect of humics photodegradation on bacterial growth and respiration in lake water. However, this effect seems much more detectable in the first meter of the water column. It therefore seems that significant differences in the amounts of terrigenous material brought to water bodies result in significant differences in the photodegradation of DOM, as Huttunen et al. (2003) already noticed. Nevertheless, the main contribution of labile compounds does not seem to come from the degradation of terrigenous compounds. Indeed, contrary to what was expected,  $DIBR_{CO_2}$  is not correlated with the level of the human activities, although the lakes with watersheds without logging provide the lowest bacterial respiration rate (Table 2.3). We finally evaluated the  $CO_2$  uptake by photosynthesis over the epilimnion ( $DIPH_{CO_2}$ ) (Figure 2.5, Table 2.3). It appears, when the average of each scenario is considered, that  $\overline{DIPM}_{CO_2}$  and  $DIPH_{CO_2}$  are strongly correlated ( $R^2 = 0.79$ ,  $p < 0.01$ ). This follows the fact that the more anthropogenically disturbed an ecosystem is, the less  $CO_2$  is fixed by photosynthesis (Figure 2.6) and the less deep its photic zone is (Table 2.3).

#### 2.4.3 Diffusive flux of $CO_2$ among various incubation experiments

Using Equation 15, it is possible to compare the flux of  $CO_2$  at the water-air interface deriving from photochemical mineralization, bacterial respiration and the  $CO_2$  uptake by photosynthesis ( $f_{CO_2}^*$ ) to the diffusive flux values calculated using the TBL method ( $f_{CO_2}$ ) (Figure 2.6). The  $f_{CO_2}^*$  and the  $f_{CO_2}$  values are significantly correlated, with  $R^2 = 0.97$  ( $p < 0.001$ ). Our system of incubation therefore appears as quite reliable to estimate total  $CO_2$  diffusive fluxes except for the intercept value. Indeed, it

is furthermore interesting to note that  $f_{CO_2}^*$  is very often lower than  $f_{CO_2}$ , which could imply that there is another production process of  $CO_2$ . This cannot be explained by planktonic respiration not occurring within the photic zone. The difference between  $f_{CO_2}^*$  and  $f_{CO_2}$  could be explained by the production of  $CO_2$  in sediments, however, this contribution reaching an average value of  $10 \text{ mmol.m}^{-2}.\text{d}^{-1}$  appears much higher than the  $0.08 \text{ mmol.m}^{-2}.\text{d}^{-1}$  value reported by Duchemin et al. (2006). The most likely would be that, regardless of environmental conditions, an appreciable and relatively constant amount of dissolved  $CO_2$  reaches the aquatic ecosystems by percolation or runoff waters (Hanson et al. 2004). It is also possible that, although water bodies are stratified, some  $CO_2$  situated in the hypolimnetic zone of the water bodies diffuses through the metalimnion. Finally, it is noteworthy that for oligotrophic lakes, where emissions of  $CO_2$  are very low and the  $CO_2$  uptake by photosynthesis is large, the TBL method of sampling appears to measure passive diffusive fluxes of  $CO_2$  that does not stem from a production in the epilimnetic zone.

## 2.5 Conclusion

As several studies have already suggested (Granéli et al. 1998; Lindell et al. 2000), the photodegradation of dissolved organic matter in the water column can make an important contribution to the heterotrophy of boreal water bodies. Other researchers (Carignan et al. 2000; Del Giorgio et al. 1999) showed however that, for oligotrophic lakes of the Canadian Shield, the gross primary production often exceeded bacterial respiration, an observation that, according to these authors, would imply a less important role for terrigenous carbon. In contrast, Tranvik and Bertilsson (2001), ascribe to allochthonous carbon a large role, at least in bacterial metabolic processes. Our results show that photodegradation of dissolved allochthonous carbon can play a significant role in  $CO_2$  emissions. Indeed, photoproduction of  $CO_2$  seems more important when the water body is perturbed by human activities. For example, we

found that a long time impounded reservoir affected by recent logging in its watershed emitted, near four times more  $\text{CO}_2$  by photodegradation during the spring and summer than nearby pristine lakes. It is also noteworthy that the contribution of the photodegradation of DOM ( $\overline{DIPM}_{\text{CO}_2}$ ) to the total emissions ( $f_{\text{CO}_2}$ ) seems to be independent of the presence or absence of logging, or of the distinction between lakes and reservoirs. Photodegradation of DOM oscillates around  $15.13 \pm 14.1\%$  of the total diffusive flux of  $\text{CO}_2$ . This research made it possible to evaluate photochemical flux, using various values of photochemical quantum yield. The photobleaching may be an explanation of the variations in photochemical yield according to various environmental conditions. The CDOM may be more or less photodegraded, making DOM more or less photoreactive. On the other hand, it is possible that the concentration of CDOM in the water column can affect the photochemical mineralization of the CDOM. The fact of having considered, in the same study, bacterial respiration, photochemical mineralization and  $\text{CO}_2$  uptake by photosynthesis allowed us to demonstrate a clear relationship between these various processes. The terrestrial organic matter freshness is linked to the spectrum quantum yield ( $\phi_\lambda$ ) and provides more labile compounds available for bacterial respiration, although the photodegradation of terrigenous material does not seem to represent the major contribution of the total diffusive fluxes of  $\text{CO}_2$ . On the other hand, the input of TOM by logging reduces the depth of the photic zone, which generates a lower photosynthesis active zone. While we do not have an exact measurement of origins of the organic matter affecting the photodegradation process, it is clear that terrestrial organic matter has a significant impact, as other authors suggested (Anesio et al. 2005; Vähätalo et al. 2003).  $\text{CO}_2$  uptake by photosynthesis does not counter balance the other processes of  $\text{CO}_2$  production for the water bodies considered (Del Giorgio et al. 1997). Finally, while validating our experimental system of incubation, we were also able to demonstrate the importance of the photochemical mineralization in the overall process of  $\text{CO}_2$  emissions from water bodies. Indeed, the activity of

photodegradation acts either as a catalyst of CO<sub>2</sub> production by bacterial respiration, or as a composite indicator of the photoreactivity of the allochthonous and autochthonous matter present in the water column.

## References:

- Anesio, A. M., W. Granéli, G. R. Aiken, D. J. Kieber, and K. Mopper. 2005. Effect of Humic Substance Photodegradation on Bacterial Growth and Respiration in Lake Water. *Applied and Environmental Microbiology* **71**: 6267-6275.
- Bertilsson, S., and L. J. Tranvik. 2000. Photochemical Transformation of Dissolved Organic Matter in Lakes. *Limnology and Oceanography* **45**: 753-762.
- Biddanda, B., and R. Benner. 1997. Carbon, Nitrogen, and Carbohydrate Fluxes During the Production of Particulate and Dissolved Organic Matter by Marine Phytoplankton. *Limnology and Oceanography* **42**: 506-518.
- Carignan, R., P. D'arcy, and S. Lamontagne. 2000. Comparative impacts of fire and forest harvesting on water quality in Boreal Shield lakes. *Can J Fish Aquat Sci* **57**: 105-117.
- Cole, J. J., and N. F. Caraco. 1998. Atmospheric Exchange of Carbon Dioxide in a Low-Wind Oligotrophic Lake Measured by the Addition of SF<sub>6</sub>. *Limnology and Oceanography* **43**: 647-656.
- Cole, J. J., N. F. Caraco, G. W. Kling, and T. K. Kratz. 1994. Carbon Dioxide Supersaturation in the Surface Waters of Lakes. *Science* **265**: 1568-1570.
- Del Giorgio, P. A., J. J. Cole, N. F. Caraco, and R. H. Peters. 1999. Linking planktonic biomass and metabolism to net gas fluxes in northern temperate lakes. *Ecology* **80**: 1422-1431.
- Del Giorgio, P. A., J. J. Cole, and A. Cimleris. 1997. Respiration rates in bacteria exceed phytoplankton production in unproductive aquatic systems. *Nature* **385**: 148-151.
- Del Giorgio, P. A., and J. Davis. 2003. Patterns in dissolved organic matter lability and consumption across aquatic ecosystems, Findlay SEG, Sinsabaugh RL ed. Academic Press, San Diego.
- Duchemin, É. 2000. Hydroélectricité et gaz à effet de serre évaluation des émissions des différents gaz et identification des processus biogéochimiques de leur production. Thèse (Ph.D). Université du Québec à Montréal.

- Duchemin, E., M. Lucotte, and R. Canuel. 1999. Comparison of Static Chamber and Thin Boundary Layer Equation Methods for Measuring Greenhouse Gas Emissions from Large Water Bodies—β. *Environmental Science & Technology* **33**: 350-357.
- Duchemin, É., M. Lucotte, R. Canuel, and N. Soumis. 2006. First assessment of methane and carbon dioxide emissions from shallow and deep zones of boreal reservoirs upon ice break-up. *Lakes & Reservoirs: Research & Management* **11**: 9-19.
- Granéli, W., M. Lindell, B. M. De Faria, and F. De Assis Esteves. 1998. Photoproduction of dissolved inorganic carbon in temperate and tropical lakes – dependence on wavelength band and dissolved organic carbon concentration. *Biogeochemistry* **43**: 175-195.
- Graneli, W., M. Lindell, and L. Tranvik. 1996. Photo-Oxidative Production of Dissolved Inorganic Carbon in Lakes of Different Humic Content. *Limnology and Oceanography* **41**: 698-706.
- Hanson, P. C., A. I. Pollard, D. L. Bade, K. Predick, S. R. Carpenter, and J. A. Foley. 2004. A model of carbon evasion and sedimentation in temperate lakes. *Global Change Biology* **10**: 1285-1298.
- Houel, S., P. Louchouart, M. Lucotte, R. Canuel, and B. Ghaleb. 2006. Translocation of Soil Organic Matter Following Reservoir Impoundment in Boreal Systems: Implications for In situ Productivity. *Limnology and Oceanography* **51**: 1497-1513.
- Huttunen, J. T. and others 2003. Fluxes of methane, carbon dioxide and nitrous oxide in boreal lakes and potential anthropogenic effects on the aquatic greenhouse gas emissions. *Chemosphere* **52**: 609-621.
- Kelly, C. A. and others 1997. Increases in Fluxes of Greenhouse Gases and Methyl Mercury following Flooding of an Experimental Reservoir†. *Environmental Science & Technology* **31**: 1334-1344.
- Kirk, J. T. 1994. *Light and photosynthesis in aquatic ecosystems*. Cambridge Univ. Press.
- Lindell, M., W. Granéli, and S. Bertilsson. 2000. Seasonal photoreactivity of dissolved organic matter from lakes with contrasting humic content. *Can J Fish Aquat Sci* **57**: 875-885.

- Liss, P. S., and P. G. Slater. 1974. Flux of Gases across the Air-Sea Interface. *Nature* **247**: 181-184.
- Macintyre, S., A. L. Alldredge, and C. C. Gotschalk. 1995. Accumulation of Marine Snow at Density Discontinuities in the Water Column. *Limnology and Oceanography* **40**: 449-468.
- Miller, W. L. 1998. Effects of UV radiation on aquatic humus: Photochemical principles and experimental considerations. Springer.
- Miller, W. L., M. A. Moran, W. M. Sheldon, R. G. Zepp, and S. Opsahl. 2002. Determination of Apparent Quantum Yield Spectra for the Formation of Biologically Labile Photoproducts. *Limnology and Oceanography* **47**: 343-352.
- Moore, C. A., C. T. Farmer, and R. G. Zika. 1993. Influence of the Orinoco River on Hydrogen Peroxide Distribution and Production in the Eastern Caribbean. *J. Geophys. Res.* **98**: 2289-2298.
- Osburn, C. L., H. E. Zagarese, D. P. Morris, B. R. Hargreaves, and W. E. Cravero. 2001. Calculation of Spectral Weighting Functions for the Solar Photobleaching of Chromophoric Dissolved Organic Matter in Temperate Lakes. *Limnology and Oceanography* **46**: 1455-1467.
- Ouellet, A. 2010. Assessing carbon dynamics in natural and human-perturbed boreal aquatic systems. Concordia University.
- Reche, I., M. L. Pace, and J. J. Cole. 1999. Relationship of Trophic and Chemical Conditions to Photobleaching of Dissolved Organic Matter in Lake Ecosystems. *Biogeochemistry* **44**: 259-280.
- Sikorski, R. J., and R. G. Zika. 1993. Modeling Mixed-Layer Photochemistry of H<sub>2</sub>O<sub>2</sub>: Optical and Chemical Modeling of Production. *J. Geophys. Res.* **98**: 2315-2328.
- Soumis, N. 2006. Émissions de gaz à effet de serre à partir des réservoirs hydroélectriques : aspects méthodologiques et évaluation des processus photochimiques. Thèse (Ph.D). Université du Québec à Montréal.
- Soumis, N., R. Canuel, and M. Lucotte. 2008. Evaluation of Two Current Approaches for the Measurement of Carbon Dioxide Diffusive Fluxes from Lentic Ecosystems. *Environmental Science & Technology* **42**: 2964-2969.

- Soumis, N., É. Duchemin, R. Canuel, and M. Lucotte. 2004. Greenhouse gas emissions from reservoirs of the western United States. *Global Biogeochem. Cycles* **18**: GB3022.
- Soumis, N. and others 2005. Hydroelectric Reservoirs as Anthropogenic Sources of Greenhouse Gases. *Water Encyclopedia*. John Wiley & Sons, Inc.
- Soumis, N., M. Lucotte, C. Larose, F. Veillette, and R. Canuel. 2007. Photomineralization in a boreal hydroelectric reservoir: a comparison with natural aquatic ecosystems. *Biogeochemistry* **86**: 123-135.
- Tranvik, L. J., and S. Bertilsson. 2001. Contrasting effects of solar UV radiation on dissolved organic sources for bacterial growth. *Ecology Letters* **4**: 458-463.
- Tremblay, A., M. Lambert, and L. Gagnon. 2004. Do Hydroelectric Reservoirs Emit Greenhouse Gases? *Environmental Management* **33**: S509-S517.
- Vähätalo, A. V., M. Salkinoja-Salonen, P. Taalas, and K. Salonen. 2000. Spectrum of the Quantum Yield for Photochemical Mineralization of Dissolved Organic Carbon in a Humic Lake. *Limnology and Oceanography* **45**: 664-676.
- Vähätalo, A. V., K. Salonen, U. MüNster, M. Jarvinen, and R. G. Wetzel. 2003. Photochemical transformation of allochthonous organic matter provides bioavailable nutrients in a humic lake. *Archiv für Hydrobiologie* **156**: 287-314.
- Weissenberger, S. 2007. Émissions de gaz à effet de serre et cycle du carbone de réservoirs hydroélectriques du moyen Nord québécois Université du Québec à Montréal.
- Weissenberger, S., M. Lucotte, S. Houel, N. Soumis, R. Duchemin, and R. Canuel. 2010. Modeling the carbon dynamics of the La Grande hydroelectric complex in northern Quebec. *Ecological Modelling* **221**: 610-620.

## TABLES CAPTIONS

**Table 2.1**  $C/N$  ratios according to the environmental scenarios for soil and the POC, DOC, or SED material

**Table 2.2** Terrigenous fraction for POC, DOC and SED material

**Table 2.3**  $CO_2$  production and  $CO_2$  fluxes according to photochemical mineralization ( $DIPM_{CO_2}$ ), bacterial respiration ( $DIBR_{CO_2}$ ), and consumption by photosynthesis ( $DIPH_{CO_2}$ )

**Table 2.1**  $C/N$  ratios according to the environmental scenarios for soil and the POC, DOC, or SED material

Scenario	$C/N_{hor}$	$C/N_{hin}$	$C/N_{POC}$	$C/N_{DOC}$	$C/N_{SED}$
RAL	40	30	29	41	21
RNAL	37	32	22	35	17
LAL	38	27	22	35	14
LNAL	29	19	16	30	13

**Table 2.2** Terrigenous fraction for POC, DOC and SED material

<b>Environmental scenario</b>	<b><math>f_{terr}(\text{POC})</math></b>	<b><math>f_{terr}(\text{DOC})</math></b>	<b><math>f_{terr}(\text{SED})</math></b>
<b>RAL</b>	<b><math>58 \pm 10\%</math></b>	<b><math>112 \pm 15\%</math></b>	<b><math>33 \pm 10\%</math></b>
<b>RNAL</b>	<b><math>44 \pm 10\%</math></b>	<b><math>93 \pm 15\%</math></b>	<b><math>19 \pm 10\%</math></b>
<b>LAL</b>	<b><math>40 \pm 10\%</math></b>	<b><math>92 \pm 15\%</math></b>	<b><math>9 \pm 10\%</math></b>
<b>LNAL</b>	<b><math>28 \pm 10\%</math></b>	<b><math>113 \pm 15\%</math></b>	<b><math>6 \pm 10\%</math></b>

**Table 2.3** CO<sub>2</sub> production and CO<sub>2</sub> fluxes according to photochemical mineralization (DIPM<sub>CO2</sub>), bacterial respiration (DIBR<sub>CO2</sub>), and consumption by photosynthesis (DIPH<sub>CO2</sub>)

SCENARIOS	RB <sub>CO2</sub>	PH <sub>CO2</sub>	Z <sub>ph</sub>
<b>RAL</b>	4,50 ± 3,33	1,48 ± 9,57	2,78 ± 0,44
<b>RNAL</b>	3,29 ± 2,45	-1,24 ± 5,54	5,37 ± 1,52
<b>LAL</b>	2,91 ± 2,30	-1,67 ± 5,10	4,51 ± 1,79
<b>LNAL</b>	1,39 ± 1,83	-3,68 ± 6,54	7,54 ± 2,02

SCENARIOS	DIPM <sub>CO2</sub>	DIBR <sub>CO2</sub>	DIPH <sub>CO2</sub>	f* <sub>CO2</sub>
<b>RAL</b>	12,34 ± 3,19	12,54 ± 0,75	4,13 ± 4,29	29,02 ± 8,23
<b>RNAL</b>	2,18 ± 0,46	17,66 ± 1,88	-3,36 ± 8,48	16,49 ± 10,83
<b>LAL</b>	5,20 ± 3,93	13,13 ± 2,07	-3,77 ± 9,16	14,56 ± 15,15
<b>LNAL</b>	0,15 ± 0,10	10,51 ± 1,86	-13,91 ± 13,2	-3,24 ± 15,23

Figures captions

**Figure 2.1** Quantum yield ( $\phi_\lambda$ ) across different aquatic environments

**Figure 2.2** Photochemical mineralization over the entire water column across different aquatic environments

**Figure 2.3** The daily flux of  $\text{CO}_2$  comes from the mineralization of dissolved organic matter standardized for average photon flux value over the water column ( $\overline{DIPM}_{\text{CO}_2}$ ) according to the environmental conditions in spring and summer season

**Figure 2.4** Relationship between the daily flux of  $\text{CO}_2$  comes from the mineralization of dissolved organic matter standardized for average photon flux value over the water column ( $\overline{DIPM}_{\text{CO}_2}$ ) and the absorption coefficient of CDOM at 360nm ( $a_{360}$ )

**Figure 2.5** Relationship between the daily flux of  $\text{CO}_2$  comes from the mineralization of dissolved organic matter over the water column ( $\overline{DIPM}_{\text{CO}_2}$ ) and total diffusive fluxes of  $\text{CO}_2$  ( $f_{\text{CO}_2}$ )

**Figure 2.6** Relationship between the total diffusive fluxes of  $\text{CO}_2$  ( $f_{\text{CO}_2}$ ) and the theoretical diffusive fluxes of  $\text{CO}_2$  ( $f^*_{\text{CO}_2}$ )

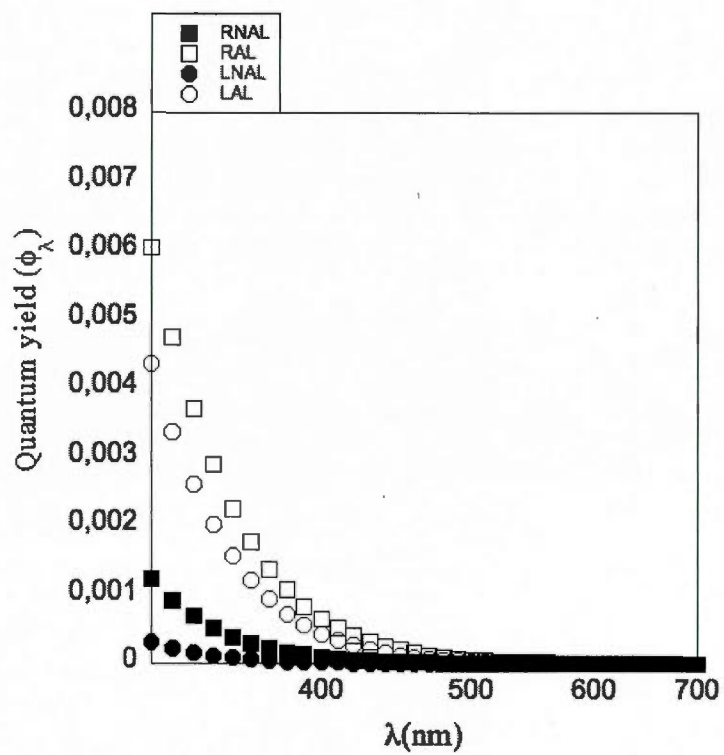
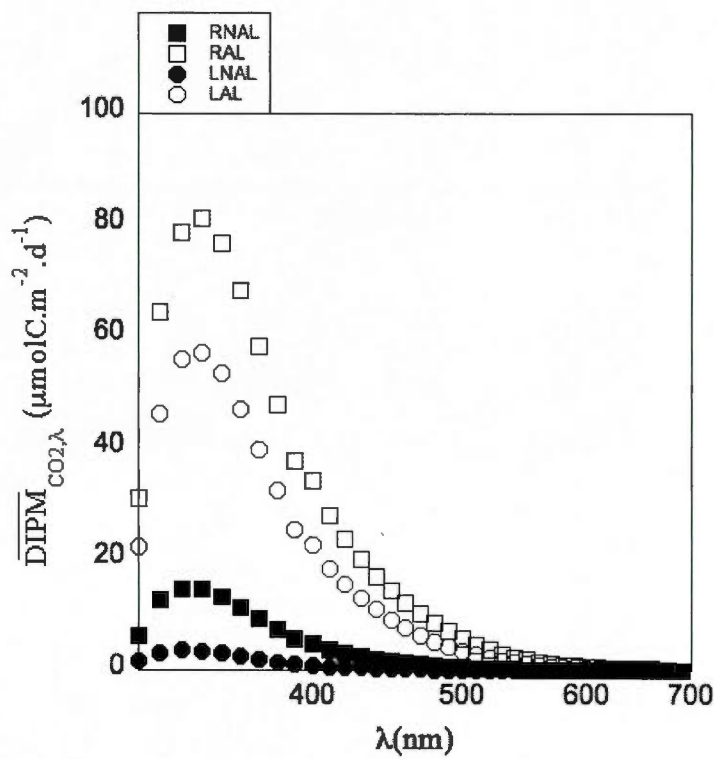
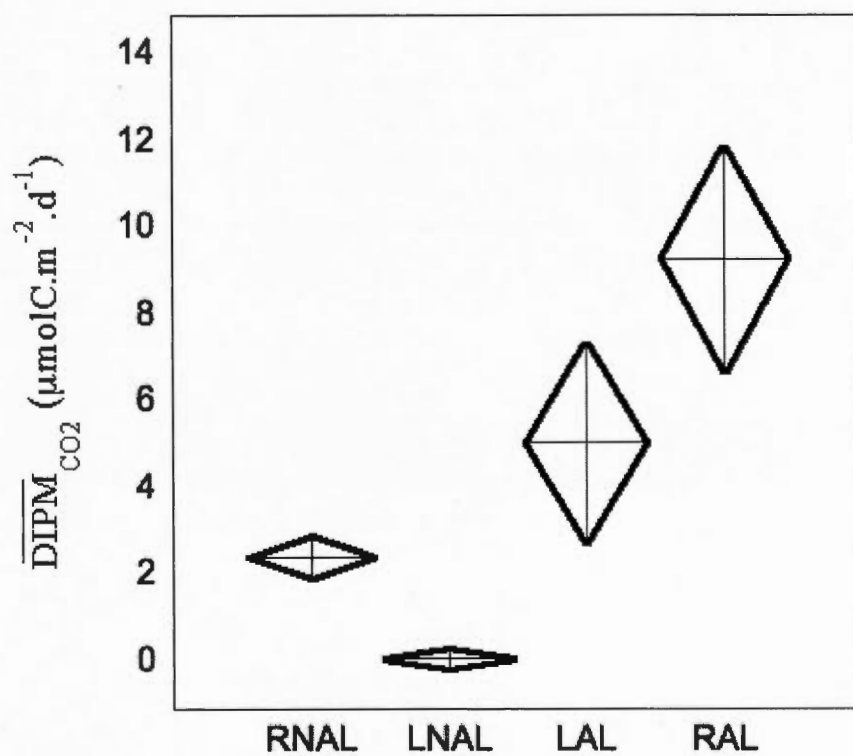


Figure 2.1 Quantum yield ( $\phi_\lambda$ ) across different aquatic environments



**Figure 2.2** Photochemical mineralization over the entire water column across different aquatic environments



**Figure 2.3** The daily flux of  $\text{CO}_2$  comes from the mineralization of dissolved organic matter standardized for average photon flux value over the water column ( $\overline{DIPM}_{CO_2}$ ) according to the environmental conditions in spring and summer season

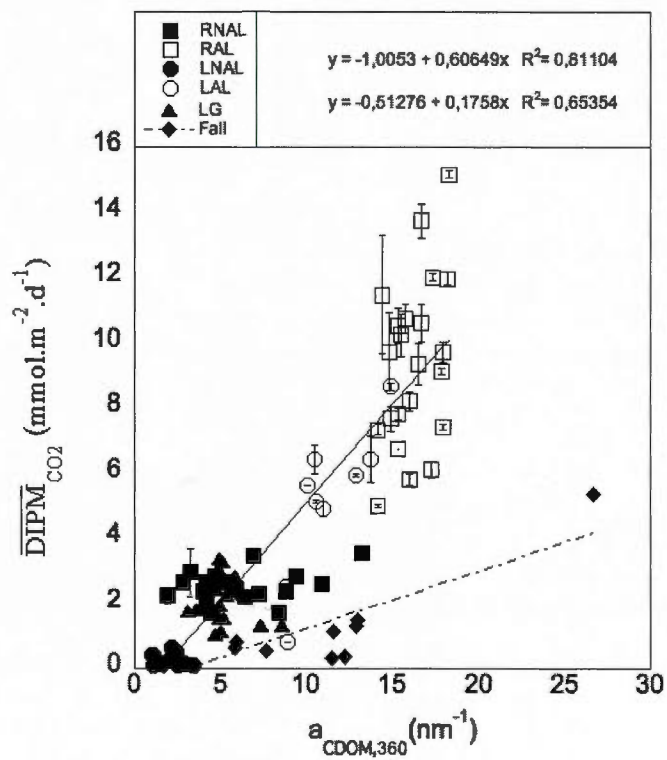


**Figure 2.4** Relationship between the daily flux of  $\text{CO}_2$  comes from the mineralization of dissolved organic matter standardized for average photon flux value over the water column ( $\overline{DIPM}_{CO_2}$ ) and the absorption coefficient of CDOM at 360nm ( $a_{360}$ )

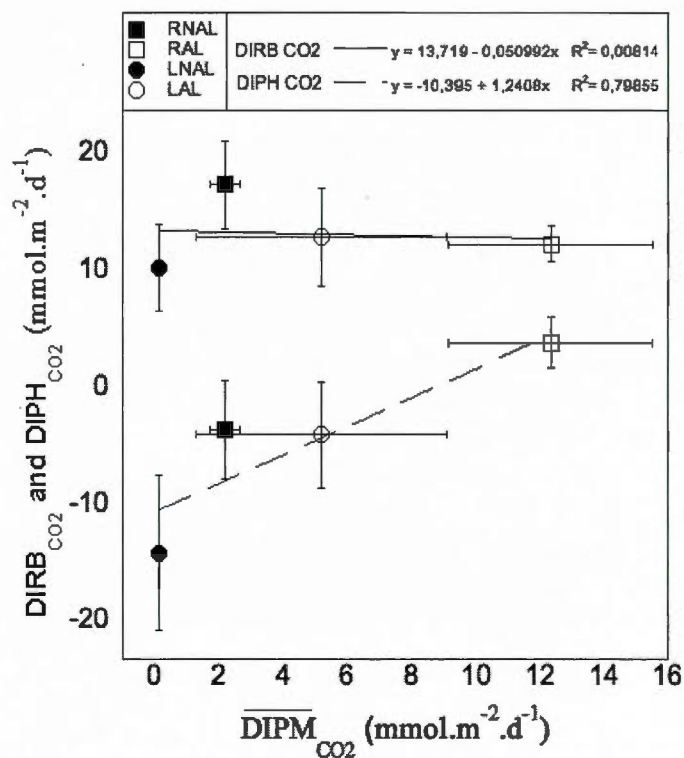


**Figure 2.5** Relationship between the daily flux of CO<sub>2</sub> comes from the mineralization of dissolved organic matter over the water column ( $\overline{DIPM}_{CO_2}$ ) and total diffusive fluxes of CO<sub>2</sub> ( $f_{CO_2}$ )

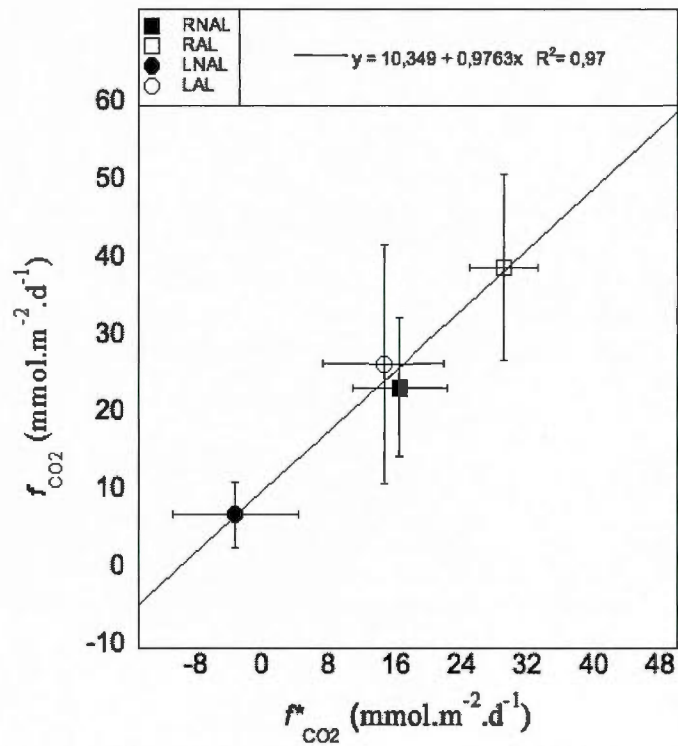


**Figure 2.6** Relationship between the total diffusive fluxes of CO<sub>2</sub> ( $f_{CO_2}$ ) and the theoretical diffusive fluxes of CO<sub>2</sub> ( $f_{CO_2}^*$ )

## CHAPITRE III

L'IMPACT DE L'EXPLOITATION FORESTIÈRE ET DE LA MISE EN EAU  
DU RÉSERVOIR SUR LE CYCLE DU CARBONE ORGANIQUE  
TERRIGÈNE DANS LES BASSINS VERSANTS BORÉAUX DU QUÉBEC  
(CANADA) : UNE APPROCHE BASÉE SUR LES BIOMARQUEURS DE LA  
LIGNINE

IMPACT OF FOREST HARVESTING AND RESERVOIR IMPOUNDMENT ON  
THE TERRIGENOUS ORGANIC CARBON CYCLE IN QUEBEC BOREAL  
WATERSHEDS (CANADA): AN APPROACH BASED ON LIGNIN  
BIOMARKERS

Jean-Baptiste Plouhinec<sup>1</sup>, Marc Lucotte<sup>1</sup>, Alexandre Ouellet<sup>2</sup> and Yves  
Gélinas<sup>2</sup>

<sup>1</sup>GEOTOP and Institute of Environmental Sciences, UQAM, C.P. 8888, Succursale  
Centre-Ville, Montréal, Québec, Canada, H3C-3P8

<sup>2</sup>GEOTOP and Department of Chemistry and Biochemistry, Concordia University,  
7141 Sherbrooke Street West, Montréal, Québec, Canada, H4B-1R6

Corresponding author:

Jean-Baptiste PLOUHINEC  
Université du Québec à Montréal  
GEOTOP-UQAM-McGill  
CP 8888 Succ. Centre-Ville,  
Montréal, Québec, Canada  
H3C 3P8

Phone number: 514-987-3000 #5662

Fax: 514-987-3635

Email: [plouhinec.jean-baptiste@uqam.ca](mailto:plouhinec.jean-baptiste@uqam.ca)

#### Acknowledgments:

We thank the Natural Sciences and Engineering Research Council of Canada (NSERC) and the *Fonds Québécois de la recherche sur la nature et les technologies* (FQRNT). The authors thank Nicolas Soumis (UQAM) for his precious advice on experimental protocols, as well as Sophie Chen (UQAM) for her help in the laboratory. This study was funded through grants (M.L. and Y.G.) and scholarships (A.O. and J.B.P.) from BIOCAP-Canada and NSERC. This is GEOTOP contribution 2012-XXXX.

## Résumé

Le transfert de matière organique terrigène (MOT) d'un bassin versant vers un plan d'eau contribue significativement aux émissions de gaz à effet de serre depuis ces systèmes aquatiques. Dans cette étude, nous relierons la nature de la MOT présente en suspension dans la colonne d'eau, sous forme dissoute ou particulaire, ou dans les sédiments récents aux flux de  $\text{CO}_2$  émis vers l'atmosphère. Nous utilisons des biomarqueurs de la lignine pour caractériser la MOT au niveau moléculaire, ses sources et son état de dégradation. Des lacs non perturbés, des plans d'eau touchés par l'exploitation forestière et par l'inondation de forêts dans la cas de réservoirs ont été échantillonnés dans le cadre de cette étude. Les résultats sont basés sur six campagnes d'échantillonnage effectuées entre 2006 et 2007. La présence de MOT dissoute dans la colonne d'eau, a été obtenue en utilisant le biomarqueur de la lignine  $\lambda_{\text{DOC}}$ , (somme des cinnamyls, syringyls et vanillyls) apparaît hautement corrélée au flux de  $\text{CO}_2$  quotidien provenant de la photodégradation de la matière organique ( $\text{DIPM}_{\text{CO}_2}$ ) pour l'ensemble de la colonne d'eau ( $R^2 = 0.60, p < 0.01$ ). De même, le rapport cinnamyl sur vanillyl ( $C/V$ ), couramment utilisé pour distinguer les tissus boisés et non boisés des plantes vasculaires, indique une relation entre la qualité de la matière organique dans les sédiments et la quantité de  $\text{CO}_2$  totale émise vers l'atmosphère ( $R^2 = 0.83, p < 0.001$ ). Enfin, le rapport ( $C/V$ ) est également corrélé ( $R^2 = 0.75, p < 0.001$ ) aux flux quotidiens de  $\text{CO}_2$  provenant de la photodégradation de la matière organique ( $\text{DIPM}_{\text{CO}_2}$ ) dans l'ensemble de la colonne d'eau. Les transferts de MOT de bassins versants déboisés de lacs naturels ou de réservoirs déclenche des émissions de  $\text{CO}_2$  vers l'atmosphère 2 à 4 fois plus élevées ( $32.27 \pm 17.99$  and  $34.74 \pm 26.14 \text{ mmolCO}_2 \cdot \text{m}^{-2} \cdot \text{d}^{-1}$ ) que celles à la surface de plans d'eau équivalents avec peu de déboisement dans leurs bassins versants ( $9.69 \pm 12.11$  and  $24.38 \pm 15.54 \text{ mmolCO}_2 \cdot \text{m}^{-2} \cdot \text{d}^{-1}$ ).

Mots-clés: Lacs boréaux, Minéralisation photochimique, Récolte forestière, Biomarqueurs de la lignine, Matière organique terrigène.

## Abstract

Terrigenous organic matter (TOM) transfer from a watershed to a waterbody significantly contributes to greenhouse gas emissions from these aquatic ecosystems. In this study, we link the nature of TOM present either in suspension in the water column under dissolved or particulate forms or in recent sediments to CO<sub>2</sub> fluxes emitted into the atmosphere. We use lignin biomarkers to characterize TOM at the molecular level, its sources and state of degradation. Pristine lakes as well as waterbodies impacted by logging and forest impoundment in the case of reservoirs are considered. The results are based on six field sampling campaigns conducted in 2006 and 2007. The presence of dissolved TOM in the water column, which is obtained using the lignin biomarker  $\lambda_{DOC}$  (sum of cinnamyls, syringyls and vanillyls), appears to be highly correlated to the daily flux of CO<sub>2</sub> produced by organic matter photodegradation ( $DIPM_{CO_2}$ ) over the entire water column ( $R^2=0.60$ ,  $p < 0.01$ ). Furthermore, the cinnamyl to vanillyl ratio ( $C/V_p$ ), which is commonly used to distinguish woody and non-woody vascular plant tissues, indicates a relationship between the source of sedimentary organic matter and the total diffusive CO<sub>2</sub> fluxes emitted into the atmosphere ( $R^2 = 0.83$ ,  $p < 0.001$ ). Finally, the ( $C/V_p$ ) ratio is also correlated to the daily flux of CO<sub>2</sub> produced by organic matter photodegradation ( $DIPM_{CO_2}$ ) over the entire water column ( $R^2 = 0.74$ ,  $p < 0.001$ ). TOM transfers from logged watersheds to either natural lakes or reservoir trigger CO<sub>2</sub> emissions to the atmosphere 2 to 4 times higher ( $32.27 \pm 17.99$  and  $34.74 \pm 26.14 \text{ mmolCO}_2 \cdot \text{m}^{-2} \cdot \text{d}^{-1}$ ) than those at the water surface of equivalent waterbodies with limited logging in their watersheds ( $9.69 \pm 12.11$  and  $24.38 \pm 15.54 \text{ mmolCO}_2 \cdot \text{m}^{-2} \cdot \text{d}^{-1}$ ).

Keywords: Boreal lakes, photochemical mineralization, forestry, reservoirs, lignin biomarkers, terrigenous organic matter.

### 3.1 Introduction

Since the mid 1990s, a significant part of limnological research has been concentrated on increasing our understanding of the processes involved in the production of greenhouse gases (GHG) from natural and artificial waterbodies (Duchemin et al. 2006; Tremblay et al. 2004). First of all, the emissions at the water surface had to be quantified in order to integrate CO<sub>2</sub> and CH<sub>4</sub> fluxes into national GHG production inventories (Weissenberger 2007). As human activity is now considered to be a dominant factor in climate change as mentioned by the Intergovernmental Panel on Climate Change (2004), the corporations producing energy from water resources have to deal with this new information, and have to release a balance sheet of their greenhouse gas emissions (Tremblay et al. 2005). The massive emission of greenhouse gases that follows reservoir impoundment is undisputable (Duchemin et al. 2006; Hélie and Hillaire-Marcel 2005; Soumis et al. 2007). Studies have also shown that greenhouse gas emissions tend to decrease significantly ten years after impoundment (Tremblay et al. 2004). Furthermore, recent studies (Battin et al. 2009; Ouellet et al. 2012) suggest that the amount of CO<sub>2</sub> emitted by aquatic ecosystems could increase if the watershed is disturbed by logging. The present study evaluates the contribution of terrigenous organic matter (TOM) weathered to lakes and old hydroelectric reservoirs located in the boreal region of Quebec in terms of CO<sub>2</sub> atmospheric emissions from these waterbodies. Some of the watersheds in the study have been subject to logging. Considering our experimental design (six lakes and two reservoirs sampled), we focused on explaining the strong variation in fluxes of CO<sub>2</sub> emitted towards the atmosphere as a result of differing environmental conditions (disturbed vs. undisturbed and lake vs. reservoir).

Following Prairie (2008) and Downing et al. (2006) reviews on the question of the origins of the heterotrophic nature of lakes and reservoirs, the most recent research hypothesizes that the proportion and quality of allochthonous organic matter in boreal ecosystems could explain a large part of the CO<sub>2</sub> fluxes produced by

photodegradation and bacterial degradation processes (Ouellet et al. 2012; Plouhinec et al. submitted). To validate this hypothesis, the TOM cycle must be examined in the dissolved and suspended particulate matter in the water column as well as in the sedimentary matter. In addition, the quality of the terrigenous matter in the water column may influence photoreactivity properties (Soumis et al. 2007). For this reason, we used lignin biomarker analysis to estimate the approximate load of TOM in the aquatic ecosystems and the quality of the carbon photoradiation (Houel et al. 2006; Louchouart 2000; Vähätalo et al. 2003). This analysis, conducted using cupric oxidation, allows us to measure 14 phenolic compounds derived from the lignin compounds. These phenolic compounds are part of four main families: cinnamyls ( $\Sigma_C$ ; ferulic acid and p-coumaric acid), syringyls ( $\Sigma_S$ ; syringaldehyde, acetosyringone and syringic acid), vanillyls ( $\Sigma_V$ ; vanillin, acetovanillon, and vanillic acid), p-hydroxyphenols ( $\Sigma_P$ ; p-hydroxybenzaldehyde, p-hydroxyacetophenone and p-hydroxybenzoic acid), and 3,5 dihydroxybenzoic acid (3,5-Bd). These four main families have recently allowed researchers to develop indicators that to evaluate TOM load ( $\lambda_{vol}$ ) (Weissenberger 2007) and other terrigenous material levels, represented by  $\lambda_8$  and  $\Sigma_8$  (Ouellet et al. 2009). Furthermore, TOM quality, which is related to the state of degradation of terrigenous compounds, can be determined using the  $P/V+S$  and  $3,5Bd/V$  indicators (Teisserenc et al. 2011). In order to understand the precise terrestrial organic carbon cycle, we estimated the volume and the morphometry of the lakes and reservoirs using geographical information systems. Finally, various TOM quality and quantity indicators were compared to the data presented by Plouhinec et al. (submitted), which lists the amount of CO<sub>2</sub> produced daily by photochemical mineralization in the water column, as well as the total diffusive fluxes of CO<sub>2</sub> emitted from the waterbodies towards the atmosphere.

## 3.2 Material and Methods

### 3.2.1 Sampling sites

Six Quebec lakes, located in the Forêt de l'Aigle conservation area, and two reservoirs, Decelles and Cabonga, located in the La Vérendrye wildlife reserve, were selected for this study (Figures 3.1 and 3.2). The sampled aquatic ecosystems include Lakes Mary, Ellard, Jean, Claire, Brock and Bouleau (Table 3.1) and the Cabonga and Decelles reservoirs (Table 3.2 and Table 3.3). Each waterbody was classified according to the four following environmental conditions: (1) pristine lakes not affected by logging (LNAL); (2) lakes affected by logging in the watershed (LAL); (3) Cabonga, a 85 years old reservoir that has not been affected by logging (RNAL) and (4) Décelles, a 71 years old reservoir affected by logging in the watershed (RAL). All these waterbodies are located on the Canadian Shield, in the boreal region. The plant cover of the zone studied is mixed forest, consisting mainly of conifers. The coniferous species found in the region include white spruce (*picea glauca*), black spruce (*picea mariana*), grey pine (*pinus banksiana*) and balsam fir (*abies balsamea*). The broad-leaved trees in the region include balsam poplar (*populus balsamifera*), trembling poplar (*populus tremuloides*), paper birch (*betula papyrifera*) and Tamarack larch (*larix laricina*). The volumes of the lakes included in this study vary between  $6.9 \cdot 10^5 \text{ m}^3$  and  $198.7 \cdot 10^5 \text{ m}^3$  (Table 3.1). The lakes are therefore all relatively small in volume (Downing et al. 2006) and relatively similar in size. Lake Jean has the greatest volume ( $198.7 \cdot 10^5 \text{ m}^3$ ), which is around 30 times larger than the volume of the smallest lake, Lake Ellard ( $6.9 \cdot 10^5 \text{ m}^3$ ). However, the drainage ratio ( $DR = LA/WA$ ), defined as lake area over watershed area, varies greatly from one waterbodies to the next. The area of Lake Mary represents 29.8% of its watershed area, while the drainage ratio of Lake Claire is estimated at only 3.7%. Both hydroelectric reservoirs (Decelles and Cabonga) are located in the Ottawa River watershed (Figure 3.3). The Cabonga reservoir, which is also located on the Gatineau

River watershed, is spread over an area of 434  $km^2$ . It is located in a watershed with an approximate area of 2616  $km^2$ , and a storage capacity of  $1.5 \cdot 10^9 m^3$ . We can deduct from these values that the average depth of the Cabonga reservoir is 3.59 m, and the drainage ratio is presumably 16.6%. The Decelles reservoir is spread over an area of 202.8  $km^2$ , and is located in a 13,131  $km^2$  watershed. Its storage capacity is estimated at  $4.97 \cdot 10^9 m^3$ , which allows us to deduct an average depth of 24.5 m. much deeper than the Cabonga reservoir. The drainage ratio (DR) for Decelles is estimated to be 1.53%.

### 3.2.2 Lignin Biomarkers

Molecular biomarkers specific to lignin organic matter were measured by oxidation, according to the cupric oxide (CuO) method developed by Gofñi and Montgomery (2000). These analyses, resulting from cupric oxidation, allow us to measure 14 phenolic compounds derived from lignin compounds, and grouped in the four main families previously mentioned. Various combinations of these phenolic compounds allow us to use the following six indicators: (i) Lambda ( $\lambda_8$ ), the sum of  $\Sigma_C$ ,  $\Sigma_S$ , and  $\Sigma_V$  normalized for 100 mg organic carbon, used as a concentration indicator of terrestrial organic matter from the sediment or the water column; (ii) Sigma ( $\Sigma_8$ ), the sum of  $\Sigma_C$ ,  $\Sigma_S$ , and  $\Sigma_V$  normalized for 10g of samples, which is also a good relative indicator of TOM proportion; (iii) the  $C/V$  ratio, used to differentiate between woody and non-woody vascular plant tissues (Hedges and Mann 1979a); (iv) the  $S/V$  ratio, used to distinguish between the organic matter of angiosperms and gymnosperms (Hedges and Mann 1979a); (v) the  $P/V+S$  ratio, an indicator of diagenetic alterations (that is, of the state of degradation of lignin compounds) (Dittmar and Lara 2001; Teisserenc et al. 2011); and (vi) the  $3,5Bd/V$  ratio, used to differentiate between organic and inorganic soil horizons (Houel et al. 2006; Teisserenc et al. 2010).

### 3.2.3 Data collection, processing and analysis

Lignin biomarkers are used to measure the specific signature of TOM discharge into each aquatic ecosystem. To collect, concentrate and analyze the lignin biomarkers, we adopted a long-accepted analytical method (Farella et al. 2001; Houel et al. 2006; Teisserenc et al. 2010). The water samples were first filtered ( $< 70 \mu m$ ) and then concentrated using a Tangential Flow Filtration (TFF) system, allowing us to collect the particulate organic matter (POM) (between 0.45 and  $70 \mu m$ ). The dissolved organic matter (DOM) (particles  $< 0.45 \mu m$ ) was then demineralized using a cation exchange resin (Chelex-200) and concentrated through a portable reverse osmosis system (Ouellet et al. 2008). To determine the percentage of organic carbon and the atomic ratio of carbon over nitrogen (C/N), including both DOM and POM, water samples were concentrated, freeze-dried, and analyzed with a Carlo Erba system (NA-1500). The samples were then extracted, derivatized and finally analyzed using a gas chromatograph (Varian 3800) coupled with a mass spectrometer (Varian Saturn 2000).

A sediment core was also taken from each waterbody, at the focal point of each lake and at several sites at each hydroelectric reservoir, in order to represent the heterogeneity of these immense waterbodies (Figures 3.1 and 3.2). The cores were collected using a pneumatic piston corer (Mackereth 1958). The cores were then sub-sampled every centimeter. To avoid any contamination, the sedimentary organic matter (SOM) that was in contact with the collecting tubes was removed. The sediment samples were freeze-dried, then analyzed for lignin biomarkers. In this study, we were mainly interested in variations in total  $CO_2$  atmospheric diffusive fluxes as well as the  $CO_2$  production resulting from photochemical mineralization (values calculated from the spring and summer sampling in 2006 and 2007). We also wanted to understand the origin of the relationship between TOM input and  $CO_2$  emissions from aquatic ecosystems. Furthermore, as we wanted to consider only watershed disturbances from the last five years, we measured the average lignin

biomarker value from the top three centimeters of SOM. The accumulation rates in the sediment (Figure 3.4) were obtained by radiometric analyses of  $^{210}\text{Pb}$  (Ali et al. 2008; Houel et al. 2006).

Finally, the bathymetric data was collected during the summer of 2008 and generated from a Halltech Environmental bathymetric/GPS system, which was connected, to a Fujitsu PenCentra 200 data recorder. The MID/MIF files were run through GRASS/GIS software, allowing us to obtain volumes for the lakes in the zone studied.

### 3.3 Results

Table 3.1 shows the main morphometric characteristics of the six lakes included in this study, their average total phosphorus concentrations and the dissolved organic carbon concentrations for each waterbody. These values are the product of four rounds of sampling, from the spring and summer of 2006 and 2007. For each lake, four sample sites were chosen. The dissolved organic carbon concentrations (DOC) were measured with a Shimadzu TOC 5000A analyzer. The DOC concentrations were estimated for each waterbody, and appeared higher in the lakes whose surrounding forest had been harvested, namely, Bouleau, Claire and Ellard, with respective values of  $8.98 \pm 2.08 \text{ mgC.l}^{-1}$ ,  $5.96 \pm 1.05 \text{ mgC.l}^{-1}$  and  $5.74 \pm 1.44 \text{ mgC.l}^{-1}$ . This concentration was recorded at only  $3.17 \pm 0.43 \text{ mgC.l}^{-1}$ ,  $5.04 \pm 1.44 \text{ mgC.l}^{-1}$  and  $3.88 \pm 1.08 \text{ mgC.l}^{-1}$  respectively for lakes Brock, Jean and Mary, which were not subjected to major human disturbances. Total phosphorus concentrations ( $[TP]$ ) were determined using a Bran and Luebbe TRAACS (Model 800) auto-analyzer according to standard protocols. In light of these results, we observe no relationship between  $[TP]$ , which ranges from  $7,36 \pm 0,95 \mu\text{g. L}^{-1}$  to

$12,94 \pm 2,19 \mu\text{g. L}^{-1}$ , and DOC concentrations, nor between  $[TP]$  and forest harvesting around the waterbodies.

The DOC concentrations and  $[TP]$  for the Decelles and Cabonga reservoirs, recorded at thirteen sampling sites, appear in Table 3.2 and 3.3. The seven sampling sites of the Cabonga reservoir, for which lignin biomarkers were also analyzed, are presented in Table 3.2. Sites RCAB-7 and RCAB-8 are located on the former Cabonga River, while sites RCAB-3, RCAB-4, RCAB-5 and RCAB-6 correspond to former lakes. Finally, site RCAB-10 is situated in an area that was flooded when the reservoir was impounded.  $[TP]$  obtained for the Cabonga sites (Table 3.2) range between  $6.76 \pm 0.51 \mu\text{g.L}^{-1}$  and  $10.57 \pm 1.61 \mu\text{g.L}^{-1}$ . Although slightly lower, these concentrations are comparable to the ones obtained for lakes. On the other hand, the DOC concentrations vary between  $2.59 \pm 0.18 \text{mgC.L}^{-1}$  and  $7.55 \pm 1.46 \text{mgC.L}^{-1}$ . These DOC concentrations are in an intermediate range situated between those observed for the RNAL and RAL scenarios.

Three out of the six sampling sites of the Decelles reservoir are situated in the littoral zone (RDEC-2, RDEC-3, RDEC-9), whereas the others are situated in the pelagic zone coinciding with the former bed of the Ottawa River (RDEC-1, RDEC-4, RDEC-6).  $[TP]$  for Decelles are between  $8.94 \pm 0.82 \mu\text{g.L}^{-1}$  and  $15.74 \pm 4.1 \mu\text{g.L}^{-1}$ , which are higher than the concentrations observed for other scenarios. The DOC concentrations follow a similar trend, with highest values varying between  $5.87 \pm 0.31 \text{mgC.L}^{-1}$  and  $9.15 \pm 0.79 \text{mgC.L}^{-1}$  depending on the sampling site in the Decelles Reservoir.

To examine as closely as possible the carbon cycle of each waterbody, we also considered sedimentation rates, which were estimated using radiometric  $^{210}\text{Pb}$  analyses (Ali et al. 2008). These rates were presented in a recent study (Ouellet

2011), and show that they vary widely from one waterbody to the next, being much higher in hydroelectric reservoirs (5.5 mm/yr and 5.8 mm/yr in Decelles Reservoir and Cabonga Reservoir respectively) than in lakes (from 0.34 to 1.35 mm/yr) (Table 3.4).

The results concerning the TOM quality for each sampling site are presented in Figures 3.4, 3.5 and 3.6. The graphs show the  $S/V$  ratio in relation with the  $C/V$  ratio for the various fractions (sedimentary in Figure 3.4; particulate in Figure 3.5; dissolved in Figure 3.6). To compare the values of the different horizons of soil and the values of the water column, we present the  $S/V$  ratio and the  $C/V$  ratio in organic and inorganic soil horizons for angiosperms and gymnosperms located in the boreal forest (Teisserenc et al. 2011). These results suggest that the lignin signature of the sedimentary organic matter varies strongly according to environmental conditions (Figure 3.4). Indeed, the undisturbed lakes (LNALs) have a signature strongly influenced by the characteristic values of gymnosperm species, while their  $S/V$  ratios show a weak but significant contribution to lignin content by angiosperm species. For RNAL and LAL sites, it seems as though angiosperm and gymnosperm contribution is fairly similar. Finally, in the case of the Decelles (RAL) sampling sites, lignin content is mainly provided by angiosperm species, as the  $C/V$  ratio is particularly low. In Figures 3.5 and 3.6, which show  $C/V$  and  $S/V$  ratios in the water column, each point on the charts represents the average value of a given sampling site. For the majority of the sampling sites, it appears that the  $S/V$  ratios correspond to an organic or inorganic soil horizon in an angiosperm-dominated area. The  $C/V$  ratios for the studied sites were measured between 0.02 (for RDEC-6) and 0.16 (for RCAB-10). Only the results from Lake Mary do not fall into the category of an organic or inorganic soil horizon dominated by angiosperms. Indeed, the lignin signature of the particulate fraction for Lake Mary corresponds

rather to that of a peatland. According to this analysis, almost all sampling sites exhibit data for the dissolved fraction that is consistent with the lignin content of an inorganic soil horizon dominated by angiosperm species. We measured  $C/V$  ratios between 0 and 0.07 for each sampled sites, the only exception being Lake Ellard, which recorded  $C/V$  and  $S/V$  ratios that were much closer to those observed in peatlands (Teisserenc 2009). The  $C/V$  and  $S/V$  ratios for Lake Ellard were 0.18 and 0.73 respectively.

We used lignin biomarker values to analyze the TOM sampled from each waterbody (water column and sediment), looking for similarities that could exist between the lignin signatures of the various fractions. The sums of the studied phenolic compounds ( $\Sigma_V$ ,  $\Sigma_C$ ,  $\Sigma_S$ ,  $\Sigma_P$ ), which correspond to a TOM content indicator similar to  $\lambda_8$  (except that p-hydroxy was also added), are given in Figure 3.7. These values were obtained for both DOM and POM as well as for sediment, and are listed in Figure 3.7 according to the various scenarios (LAL, LNAL, RAL, RNAL). It appears that, regardless of the scenario, the lignin content is much higher in the sedimentary fraction than in the dissolved or particulate organic matters. Furthermore, the  $\Sigma_V$  value, measured for DOM and POM, which are exclusively constituted of terrigenous compounds, are the main contributors to the lignin content.

The cinnamyl ( $\Sigma_C$ ) compounds are measured at an extremely low proportion of the total lignin content measured in the dissolved and particulate fractions, although cinnamyl content is significant in the sedimentary samples. The para-hydroxyphenol content in the lignin signature is fairly similar, regardless of the fraction, while the syringyl phenols follow a trend similar to that observed for the vanillyl phenols (q.v. Figures 3.8e and Figure 3.8g). Indeed, although ( $\Sigma_S$ ) represents less than 10% of the total lignin content in DOM, it represents approximately 20% in POM and sediments.

The general results presented in Figure 3.7 are also shown in a more detailed way in Figures 3.8a to 3.8l. According to lignin biomarker  $\lambda_g$ , the total quantity of TOM is lower in the dissolved and particulate fractions than those evaluated in the sedimentary fraction. Biomarker  $\Sigma_g$  (Figure 3.8b) does not follow the same trend as  $\lambda_g$ . The quantity of TOM, represented by  $\Sigma_g$ , which is normalized for 10g of sedimentary material, is much more concentrated in the particulate fraction than in the dissolved fraction or in the sediment (except for in the LNAL scenario). The cinnamyl phenolic compounds ( $\Sigma_c$ ) (Figure 3.8e) vary substantially depending on the fraction analyzed: these compounds are almost exclusively present in the sediment, while para-hydroxyphenol ( $\Sigma_p$ ) values (Figure 3.8f) seem to be consistent regardless of the fraction. However, we observe an increase in  $\Sigma_p$  in all scenarios, depending on the size of the fraction ( $\Sigma_{DOC} < \Sigma_{POC} < \Sigma_{SED}$ ). The vanillyl ( $\Sigma_v$ ) (Figure 3.8g) and syringyl ( $\Sigma_s$ ) (Figure 3.8h) phenolic compounds show similar trends, although the concentration of vanillyl compounds is approximately twice that of the syringyl compounds for all scenarios and fractions. Finally, Figures 3.8i, 3.8j, 3.8k and 3.8l, which correspond respectively to degradation indicators  $P/V+S$ ,  $3,5Bd/V$ ,  $(A_c/A_d)_v$  and  $(A_c/A_d)_s$ , show the same trend, regardless of the fraction. We observe, according to the environmental conditions, a much more advanced state of degradation for the dissolved fraction and a slightly fresher matter for the particulate fraction, with the freshest TOM measured in the sedimentary fraction.

To better understand the TOM cycle in the water column, we show in Figure 3.9 the  $\lambda_g$  values estimated for the dissolved and particulate fractions of each sampling site.  $\lambda_g$  is an indicator of TOM content corresponding to the sum of the vanillyl, cinnamyl and syringyl compounds (Houel et al. 2006; Ouellet 2010; Teisserenc et al. 2010). This graph allows us to examine the relationship between lignin from TOM in the

particulate fraction and in the dissolved fraction, which is consistent regardless of the environmental condition ( $R^2 = 0.78$ ,  $p < 0.001$ ). As presented in Figure 3.10, the TOM content in the dissolved fraction of the water column ( $\lambda_{DOC}$ ) is correlated with DOC concentrations ( $R^2 = 0.67$ ,  $p < 0.001$ ).  $\lambda_8$  values range from 0.2 to 1.7 for the particulate fraction, and from 0.1 to 0.8 for the dissolved fraction. The statistical analyses conducted on TOM content ( $\lambda_8$ ) reveal considerable differences from one environmental scenario to the next (Figure 3.11b, 3.12b and 3.13b). The undisturbed lakes (LNAL) show an average  $\lambda_8$  value of  $0.21 \pm 0.036$  for the dissolved fraction, while LAL recorded an average  $\lambda_8$  value of  $0.63 \pm 0.032$  for the same fraction. The average  $\lambda_8$  values measured in hydroelectric reservoirs show a trend similar to that observed in the disturbed and undisturbed lakes. Indeed, the average  $\lambda_8$  value is measured at  $0.43 \pm 0.11$  for the RNAL, and at  $0.65 \pm 0.08$  for the RAL, which is much higher. These four scenarios were subjected to a Kruskal Wallis test ( $df=3$ ,  $p < 0,001$ ), which determined that TOM contents differ among the four scenarios.

In order to compare not only the relative quantity of TOM estimated for a dissolved fraction in the water column according to the environmental conditions, but also the total quantity of TOM located in the water column, we estimated the  $\lambda_{vol}$  biomarker for every scenario (Weissenberger 2007). This measure of volume ( $\lambda_{vol}$ ) is obtained by multiplying the  $\lambda_8$  value by the DOC concentration. This value indicates the total dissolved terrestrial organic matter per unit of volume in the water column.

The  $\lambda_8$  values presented in Figure 3.10 show that DOC concentration correlates with TOM quantity, standardized for the same quantity of carbon ( $R^2=0.67$ ,  $p < 0.001$ ). The average values  $\lambda_{vol}$  are shown for every scenario in Figure 3.12b. A Kruskal Wallis test confirms that the total dissolved TOM concentration in the water column differs according to the scenario ( $df = 3$ ,  $p < 0.001$ ). The total quantity of lignin in

freshwater dissolved organic matter ( $\lambda_{vol}$ ) and the  $\lambda_8$  values follow the same trend. The LNALs thus have an average  $\lambda_{vol}$  value of  $0.70 \pm 0.06$ , while the LAs show a significantly higher average  $\lambda_{vol}$  value of  $4.16 \pm 1.33$ . The scenario with the most pronounced disturbance by human activity (RAL) records a  $\lambda_{vol}$  value of  $4.91 \pm 1.21$ , which is much higher than that observed for the undisturbed reservoir (RNAL), with a  $\lambda_{vol}$  value of  $2.63 \pm 1.64$ . Finally, the same statistical test is used to examine the particulate TOM content in the water column (Figure 3.13b). According to the Kruskal Wallis test, we observed that the quantity of lignin in freshwater particulate organic matter ( $\lambda_8$ ) is different for each scenario ( $df = 3$ ,  $p < 0.01$ ). The particulate TOM concentration in the water column of ecosystems not affected by logging (Figure 3.13b) shows an average  $\lambda_8$  value of  $0.29 \pm 0.07$  for lakes and  $0.93 \pm 0.26$  for the reservoir. These values are lower than the  $\lambda_8$  values observed for the ecosystems affected by logging, which were measured at  $1.40 \pm 0.16$  for the LAL scenario and  $1.42 \pm 0.22$  for the RAL scenario. However, the LAL and RAL scenarios cannot be distinguished.

Figures 3.11a, 3.12a and 3.13a illustrate the correlation observed between TOM quantity and daily integrated  $CO_2$  production through photochemical mineralization ( $DIPM_{CO_2}$ ) of dissolved organic matter in the entire water column (Plouhinec et al. submitted). Integrated  $CO_2$  production through photochemical mineralization ( $DIPM_{CO_2}$ ) is more closely related to dissolved lignin concentration ( $R^2 = 0.74$ ,  $p < 0.01$ ) than particulate lignin concentration ( $R^2 = 0.57$ ,  $p < 0.01$ ). This relation is illustrated by the following logarithmic function:

$$DIPM_{CO_2} = 3.12 + 5.31 \cdot \log(\lambda_{vol}) \quad (3.1)$$

The most striking result concerns the  $C/V$  ratio estimated in the sedimentary fraction of each waterbody (Figures 3.14a and 3.14b). Contrary to previously observed trends, the  $C/V$  ratio is higher in the sedimentary fraction of ecosystems unaffected by logging, and also higher in lakes than in reservoirs. Furthermore, while the  $C/V$  ratio varies between 0.02 and 0.16 for the particulate organic matter in the water column, and between 0 and 0.07 for the dissolved organic matter in the water column, it is higher in the sedimentary fraction, ranging from 0.1 to 0.70. The  $C/V$  ratio is very closely related to the total diffusive fluxes of  $CO_2$  into the atmosphere ( $f_{CO_2}$ ) (Figure 3.14a) ( $R^2 = 0.84$ ,  $p < 0.01$ ). A strong relationship was also observed between the  $C/V$  ratio and the daily integrated production of  $CO_2$  through photochemical mineralization over the entire water column ( $DIPM_{CO_2}$ ) (Figure 3.14b) ( $R^2 = 0.89$ ,  $p < 0.01$ ). The relation between the diffusive fluxes of  $CO_2$  ( $f_{CO_2}$ ) and the  $C/V$  ratio is considered to be a linear regression:

$$\frac{C}{V} = 0.65 - 0.0128 \cdot f_{CO_2} \quad (3.2)$$

The relation between the daily integrated production of  $CO_2$  through photochemical mineralization over the entire water column ( $DIPM_{CO_2}$ ) and the  $C/V$  ratio is considered to be a logarithmic regression (see Equation 3.3):

$$\frac{C}{V} = 0.76 - 0.72 \cdot \log(DIPM_{CO_2}) \quad (3.3)$$

### 3.4 Discussion

According to the characteristics of watersheds, the contribution of terrestrial organic matter is naturally greater for Lake Claire than for Lake Mary. This hypothesis is all the more true when taking into account the average slope of the

watershed for the two lakes, as correlated to the drainage ratio  $\left(\frac{LA}{WA}\right)$  (Table 3.1). The sedimentation rates (mm/yr) in reservoirs are much higher than those observed in lakes. This result is similar to results obtained by other researchers throughout the world (Dean and Gorham 1998). However, as the  $C/N$  ratio and the  $\delta^{13}C$  values show (Table 3.5), the sedimentary organic matter appears to be mainly autochthonous (Brenner et al. 1999; Gu et al. 1996; Ouellet 2010). Furthermore, the allochthonous content, represented by the  $\lambda_8$  measured in the sediment, varies between 0.42 and 4.81, and cannot be distinguished according to environmental conditions by a Kruskal Wallis test. Finally, the total phosphorus concentration  $[TP]$ , which is a very good indicator of the gross primary production (GPP) (Biddanda and Benner 1997; Hanson et al. 2004), does not seem to explain the variation in accumulation rates, since lakes and reservoirs have very different accumulation rates and similar  $[TP]$  concentrations. It is therefore probable that a substantial part of the top centimeters of the sedimentary matter in reservoirs comes from TOM released from the watershed by erosion, and then stored in the reservoir. Indeed, the impoundment of a reservoir affects the residence time of the former waterbody considerably (Downing et al. 2006). This hypothesis is supported by the  $\Sigma_8$  values measured in all fractions (Figure 3.8b). Finally, the input of sedimentary matter spikes dramatically during floods (Jansson 1988; Milliman and Meade 1983); however the data obtained with our samples cannot show this high annual variability.

The various lignin biomarkers provide precious information about the sources of organic matter. In particular, it is possible to determine the angiosperm contribution to the TOM, as angiosperms are constituted of syringyls and vanillyls, while gymnosperms contain only vanillyls (Hedges and Ertel 1982; Hedges and Mann 1979a). Furthermore, the  $C/V$  and  $S/V$  ratios measured for the dissolved and particulate fractions of the water column are much lower than those measured for

pure sources (Goñi and Hedges 1992; Hedges and Mann 1979b). The  $S/V$  values in our study are comparable to those obtained for the organic soil horizon by previous authors (Otto and Simpson 2006; Teisserenc et al. 2010). Dissolved or particulate  $S/V$  ratios above 0.4 can be indicative of the existence of angiosperms or peatlands (Teisserenc 2009). In our study, the  $C/V$  ratio estimated for the dissolved fraction of the water column is not correlated to the relative quantity of angiosperms situated in the watershed. This was also observed for the  $C/V$  ratio measured in the sedimentary fraction (Teisserenc et al. 2010). It is interesting to note that the  $C/V$  ratio varies widely according to the studied fractions. Moreover, the cinnamyl and vanillyl phenolic compounds seem to undergo numerous changes that contribute to the vast differences observed between the ligneous signature of soil horizons and that of sedimentary matter. Indeed, the lignin signatures recorded in the water column in this study correspond closely to those of angiosperm species, despite the fact that species identification via geographical information systems (Teisserenc et al. 2010) indicates that angiosperms only cover between  $\approx 20\%$  (Lake Mary) and  $\approx 60\%$  (Lake Ellard) of the watershed area (Table 3.1). It must be mentioned that the Lake Ellard watershed was partially flooded because of a beaver dam when it was sampled, which may have led to an unusually high contribution of lignin matter from the surrounding peatlands.

Only herbaceous plants, conifer needles and the leaves of angiosperms contain cinnamyls (Hedges and Mann 1979a). Thus, the differences in  $C/V$  ratio from one fraction to the next may be attributed to the fungal degradation of ligneous compounds during transport from the watershed to the aquatic ecosystem (Hedges et al. 1988), photochemical mineralization or microbial respiration (Opsahl and Benner 1995). These relationships can also explain the variations observed between the ligneous signature of pure sources and those of organic or inorganic soil horizons

(Klap et al. 1999; Opsahl and Benner 1998). Although very resistant, the lignin macromolecule can be biodegraded, in which case the  $S/V$  and  $C/V$  ratios will evolve (Dittmar and Lara 2001; Huang et al. 1998; Opsahl and Benner 1995). There are several hypotheses that can explain the decrease in the  $C/V$  ratio during transport from the watershed to the waterbody. For example, it is possible for cinnamyl compounds to be fixed in the deep horizons of soils, resulting in a significant increase in the  $C/V$  ratio in inorganic soil horizons as compared to organic horizons (Houel et al. 2006). We also notice increased storage of degraded lignin compounds in deep mineral soil horizons (Rumpel et al. 2002). A decrease in the  $C/V$  ratio was also reported during pedogenetic and diagenetic soil degradation (Klap et al. 1999; Louchouart et al. 1999; Opsahl and Benner 1995). These various considerations are in accordance with our main hypothesis, which states that the compounds of the cinnamyl family, bound to larger, denser molecules, are only slightly degraded in the watershed. These molecules, once transported to the waterbody by groundwater or surface water, will quickly settle into sediment. As suggested by previous studies, residence time in the watershed seems to be longer for the dissolved fraction than for the particulate fraction of organic matter (Houel et al. 2006). In fact, the terrigenous DOM, may be leached in significant proportions from the inorganic soil horizon. This conclusion is in accordance with the  $^{3,5}Bd/V$  values presented in Figure 3.8j. The dissolved or particulate lignin matter would thus reach the waterbodies carrying different proportions of phenolic compounds than those observed for particles larger than 63  $\mu\text{m}$ . Indeed, the densest fraction of organic matter settles quickly into sediment and includes a much higher quantity of cinnamyl compounds (Figure 3.8e). Other processes such as photo-oxidation may also degrade lignin compounds. The  $S/V$  ratio for dissolved organic matter in rivers and oceans has been observed as decreasing along a gradient of light exposure (Opsahl and Benner 1998). We also

noticed that cinnamyl compounds showed more photorecalcitrant properties than the vanillyl compounds (Opsahl and Benner 1998). The higher  $C/V$  values measured in the dissolved or particulate fraction could also be the result of the preferential photo-oxidation of vanillyl over cinnamyl compounds in the water column. However, the  $C/V$  ratio measured in the sediment is approximately 10 times higher than the ratio obtained in the dissolved or particulate fraction of the water column.

To confirm that the TOM situated in the water column is derived from a different source than the TOM in the sediment, let us suppose, contrary to our abovementioned hypothesis, that the  $C/V$  ratio measured in the sediment is derived from degraded cinnamyl or vanillyl compounds in the water column. It is only possible to measure the relative amount of cinnamyl compounds in the sediment if almost all of the organic carbon is degraded. Therefore, for such an increase to take place for the  $C/V$  ratio measured in the POM fraction and compared to the sedimentary fraction, 85% to 99.5% of the total amount of carbon in the aquatic environment must be mineralized or biodegraded (or transported towards another waterbody). Finally, we observed that the TOM in the sediment is much fresher than the TOM measured in the water column (Figures 3.8i, 3.8j, 3.8k and 3.8l).

Two possible hypotheses can be drawn from this information. Either the different phenol families have different solubility characteristics, or the sedimentary terrigenous material is compositionally different from the material found in the water column. As the lignin biomarkers measured in the sediment are reliable indicators of watershed plant cover (Teisserenc et al. 2010), the first of these two hypotheses is more likely. The degradation indicator values are lower when the TOM is fresher. Thus, it seems that the sedimentary matter is much fresher than the particulate or dissolved organic matter located in the water column.

Finally, the  $\lambda_g$  value is considerably affected by the tree species providing the lignin material (Hedges and Mann 1979a). Therefore, a watershed's angiosperm/gymnosperm ratio will greatly affect the lignin signature in the sediment

(Teisserenc et al. 2011). Similarly, if TOM undergoes fungal or microbial degradation before being transported towards the aquatic ecosystem, some phenolic compound concentrations may be affected more than others. However, while the TOM degradation in the watershed has already been well investigated (Hedges and Ertel 1982; Opsahl and Benner 1998), the study of lignin degradation in the water column or the sediment are far less well-documented (Teisserenc et al. 2010; Weissenberger 2007). One observation that we can make is that there is a greater lignin concentration in the sediment than in the dissolved and the particulate fractions (Figure 3.7). Therefore, although  $\lambda_g$  is a good indicator of the relative quantity of TOM (Houel et al. 2006; Ouellet et al. 2009; Spencer et al. 2009) for each fraction (dissolved, particulate and sedimentary), it is less useful in providing accurate comparisons between the fractions. Indeed, a classical interpretation of  $\lambda_g$  values (see Figure 3.8a) concludes that the relative amount of TOM situated in the sediment is higher than the TOM concentration in the water column. However, the  $\delta^{13}C$  values (Ouellet 2010) and the  $C/N$  ratio (Table 3.5) show that sedimentary ( $-27.88 \pm 1.27$  ‰) and particulate fractions ( $-28.77 \pm 0.76$  ‰) have lower TOM concentrations than the dissolved fraction ( $-26.96 \pm 0.22$  ‰). Moreover, with the exception of Lake Jean, which corresponds to a sedimentary isotopic signature of  $-25.4$  ‰  $\delta^{13}C$ , the ratio measured for the particulate and sedimentary matter are not distinguishable. We deduce from these results that the relative amount of TOM is higher in the sediment than in the water column.

In lakes, the total amount of organic carbon that settles into sediment is generally less than a third of the carbon that is emitted into the atmosphere (Cole et al. 2007). As POM has a shorter residence time than DOM, the majority of terrigenous organic carbon in the water column is in its dissolved form, as shown by Ouellet et al. (2008). Dissolved terrigenous organic carbon generally represents the largest proportion of organic carbon in the water column (Prairie 2008). In this study, the lignin signature of the water column consists mainly of vanillyl compounds (Figure 3.7). As the total

amount of vanillyls is much higher in the water column than in the sediment (standardized for 100mg of OC), if even a small amount of  $\Sigma_V$  were to settle into sediment, the lignin biomarkers  $P/V+S$  and  $3,5Bd/V$  would be strongly affected. As shown in Figures 3.8i, 3.8j and 3.8k, the vanillyl compounds are not derived from organic matter in the water column. Only a small amount of the organic carbon suspended in the water column will reach the sediment, as the majority of the terrestrial sedimentary matter is derived from a dense, little-degraded particulate fraction in the water column. Our results are therefore in accordance with the hypotheses to which the lignin biomarkers signature in sediments properly integrates the watershed signature of the aquatic ecosystem, developed in earlier studies by Teisserenc et al. (2010) and Houel et al. (2006).

The dissolved terrigenous organic carbon is degraded in the water column by various processes. However, according to results of previous studies (Opsahl and Benner 1998; Ouellet et al. 2009), DOM and POM are strongly degraded over time in the water column, causing significant changes in the lignin signature. The vanillyls are most profoundly affected by this degradation as they are the most common lignin compound in the water column (Figure 3.7). As shown in Figures 3.11a, 3.12a and 3.13a,  $CO_2$  production derived from photochemical mineralization evaluated over the entire water column ( $DIPM_{CO_2}$ ) is strongly correlated to the concentration of dissolved or particulate TOM, represented by values  $\lambda_{DOC}$  and  $\lambda_{POC}$ . The results obtained for identical sites in Ouellet (2010) are similar. In the oligotrophic lakes (Mary and Jean), the dissolved organic carbon is mainly composed of autochthonous matter, while in the affected by logging ecosystems, the DOM is mainly terrestrial. Furthermore, the amount of particulate TOM (Figure 3.13a) is less correlated to the amount of  $CO_2$  produced by photochemical mineralization than what was observed for the dissolved fraction. This result is consistent with our hypothesis that the POM fraction is more recalcitrant to degradation.

The  $C/V$  ratio in the sediment was strongly correlated with daily fluxes of  $CO_2$  derived from photochemical mineralization ( $DIPM_{CO_2}$ ) but also with the total diffusive fluxes of  $CO_2$  towards the atmosphere ( $f_{CO_2}$ ) (Figures 3.14a and 3.14b). We observed that the  $C/V$  ratio was lower when the ecosystem was harvested. As a low  $C/V$  ratio indicates a higher amount of lignin in the sediment, this ratio could be considered as a gradient of disturbance for aquatic environments. Therefore, in the Decelles reservoir, whose watershed was disturbed by forest harvesting, the amount of TOM in the sediment is much greater than that observed in undisturbed lakes. It should also be noted a reservoir's  $C/V$  ratio decreases dramatically after it is impounded (Houel et al. 2006). In this study, the lower the  $C/V$  ratio, the higher the TOM load in the water column, as  $C/V$  is negatively correlated with  $\lambda_{DOC}$ ,  $\lambda_{POC}$  and  $\lambda_{Vd}$  values. However, a larger amount of TOM in the water column causes increased photochemical mineralization ( $DIPM_{CO_2}$ ), and increased diffusive fluxes of  $CO_2$  ( $f_{CO_2}$ ) because of a greater availability of labile matter for the bacterial population (Anesio et al. 2005; Ouellet 2011; Tranvik and Bertilsson 2001). Finally, as the  $C/V$  ratio remains constant once a reservoir is filled (Houel et al. 2006), it is likely that the high  $CO_2$  emissions measured in old reservoirs (Duchemin et al. 2006; Soumis et al. 2007), are the result of a permanent change in the watershed, corresponding to a higher supply of dissolved TOM available for degradation.

### 3.5 Conclusion

In this study, it appears that the TOM transfers from a watershed to the water column of a natural or impounded waterbody can be evaluated thanks to lignin biomarkers.

The lambda indicators, sum of vanilyls, cinnamyls and syringyls in the dissolved and particulate organic matters present in suspension in a given water column ( $\lambda_{DOC}, \lambda_{POC}$ ), are well correlated to the daily-integrated photochemical flux of  $CO_2$  ( $R^2 = 0.60$  and  $R^2 = 0.83$  respectively,  $p < 0.001$ ). Our results also show that  $S/V$  and  $C/V$  lignin biomarkers of the sedimentary fraction are radically different from those measured in the dissolved and particulate organic matter found in the water column. Furthermore, the  $C/V$  ratio, which is used to evaluate the TOM quality in the sedimentary fraction, shows that the quantity of woody vascular plant tissues is much higher in the sediment of lakes or reservoirs disturbed by logging activities in their watersheds than equivalent waterbodies with unlogged watersheds. The high fluxes of woody vascular plant tissues in logged environments then trigger  $CO_2$  emissions to the atmosphere 2 to 4 times higher ( $32.27 \pm 17.99 \text{ mmol}CO_2.m^{-2}.d^{-1}$  for natural lakes and  $34.74 \pm 17.46 \text{ mmol}CO_2.m^{-2}.d^{-1}$  for an old reservoir) than those at the surface of aquatic systems with limited logging in their watersheds ( $9.69 \pm 12.11 \text{ mmol}CO_2.m^{-2}.d^{-1}$  for natural lakes and  $24.38 \pm 15.54 \text{ mmol}CO_2.m^{-2}.d^{-1}$  for an old reservoir). The strong correlation observed between the  $C/V$  ratio in recent sediments and the total diffusive fluxes value of  $CO_2$  to the atmosphere ( $f_{CO_2}$ ) may be used in future studies to easily estimate at low cost  $CO_2$  emissions produced by aquatic ecosystems in the boreal region on a large scale.

## References

- Ali, A. A., B. Ghaleb, M. Garneau, H. Asnong, and J. Loisel. 2008. Recent peat accumulation rates in minerotrophic peatlands of the Bay James region, Eastern Canada, inferred by  $^{210}\text{Pb}$  and  $^{137}\text{Cs}$  radiometric techniques. *Applied Radiation and Isotopes* **66**: 1350-1358.
- Anesio, A. M., W. Granéli, G. R. Aiken, D. J. Kieber, and K. Mopper. 2005. Effect of Humic Substance Photodegradation on Bacterial Growth and Respiration in Lake Water. *Applied and Environmental Microbiology* **71**: 6267-6275.
- Battin, T. J., S. Luysaert, L. A. Kaplan, A. K. Aufdenkampe, A. Richter, and L. J. Tranvik. 2009. The boundless carbon cycle. *Nature Geosci* **2**: 598-600.
- Biddanda, B., and R. Benner. 1997. Carbon, Nitrogen, and Carbohydrate Fluxes During the Production of Particulate and Dissolved Organic Matter by Marine Phytoplankton. *Limnology and Oceanography* **42**: 506-518.
- Brenner, M., T. J. Whitmore, J. H. Curtis, D. A. Hodell, and C. L. Schelske. 1999. Stable isotope ( $\delta^{13}\text{C}$  and  $\delta^{15}\text{N}$ ) signatures of sedimented organic matter as indicators of historic lake trophic state. *Journal of Paleolimnology* **22**: 205-221.
- Cole, J. and others 2007. Plumbing the Global Carbon Cycle: Integrating Inland Waters into the Terrestrial Carbon Budget. *Ecosystems* **10**: 172-185.
- Dean, W. E., and E. Gorham. 1998. Magnitude and significance of carbon burial in lakes, reservoirs, and peatlands. *Geology* **26**: 535-538.
- Dittmar, T., and R. J. Lara. 2001. Molecular evidence for lignin degradation in sulfate-reducing mangrove sediments (Amazonia, Brazil). *Geochimica et Cosmochimica Acta* **65**: 1417-1428.
- Downing, J. A. and others 2006. The Global Abundance and Size Distribution of Lakes, Ponds, and Impoundments. *Limnology and Oceanography* **51**: 2388-2397.
- Duchemin, É., M. Lucotte, R. Canuel, and N. Soumis. 2006. First assessment of methane and carbon dioxide emissions from shallow and deep zones of boreal reservoirs upon ice break-up. *Lakes & Reservoirs: Research & Management* **11**: 9-19.

- Farella, N., M. Lucotte, P. Louchouart, and M. Roulet. 2001. Deforestation modifying terrestrial organic transport in the Rio Tapajos, Brazilian Amazon. *Organic Geochemistry* **32**: 1443-1458.
- Goñi, M. A., and J. I. Hedges. 1992. Lignin dimers: Structures, distribution, and potential geochemical applications. *Geochimica et Cosmochimica Acta* **56**: 4025-4043.
- Goñi, M. A., and S. Montgomery. 2000. Alkaline CuO Oxidation with a Microwave Digestion System: Lignin Analyses of Geochemical Samples. *Analytical Chemistry* **72**: 3116-3121.
- Gu, B., C. L. Schelske, and M. Brenner. 1996. Relationship between sediment and plankton isotope ratios  $^{13}\text{C}$  and  $^{15}\text{N}$  and primary productivity in Florida lakes. *Can J Fish Aquat Sci* **53**: 875-883.
- Hanson, P. C., A. I. Pollard, D. L. Bade, K. Predick, S. R. Carpenter, and J. A. Foley. 2004. A model of carbon evasion and sedimentation in temperate lakes. *Global Change Biology* **10**: 1285-1298.
- Hedges, J. I., W. A. Clark, and G. L. Cowie. 1988. Organic Matter Sources to the Water Column and Surficial Sediments of a Marine Bay. *Limnology and Oceanography* **33**: 1116-1136.
- Hedges, J. I., and J. R. Ertel. 1982. Characterization of lignin by gas capillary chromatography of cupric oxide oxidation products. *Analytical Chemistry* **54**: 174-178.
- Hedges, J. I., and D. C. Mann. 1979a. The characterization of plant tissues by their lignin oxidation products. *Geochimica et Cosmochimica Acta* **43**: 1803-1807.
- . 1979b. The lignin geochemistry of marine sediments from the southern Washington coast. *Geochimica et Cosmochimica Acta* **43**: 1809-1818.
- Hélie, J.-F., and C. Hillaire-Marcel. 2005. Diffusive  $\text{CO}_2$  Flux at the Air-Water Interface of the Robert-Bourassa Hydroelectric Reservoir in Northern Québec : Isotopic Approach ( $^{13}\text{C}$ ), p. 339-354. *In* A. Tremblay, L. Varfalvy, C. Roehm and M. Garneau [eds.], *Greenhouse Gas Emissions — Fluxes and Processes*. Environmental Science. Springer Berlin Heidelberg.
- Houel, S., P. Louchouart, M. Lucotte, R. Canuel, and B. Ghaleb. 2006. Translocation of Soil Organic Matter Following Reservoir Impoundment in Boreal Systems: Implications for In situ Productivity. *Limnology and Oceanography* **51**: 1497-1513.

- Huang, Y., G. Eglinton, E. R. E. Van Der Hage, J. J. Boon, R. Bol, and P. Ineson. 1998. Dissolved organic matter and its parent organic matter in grass upland soil horizons studied by analytical pyrolysis techniques. *European Journal of Soil Science* **49**: 1-15.
- I.P.C.C. 2004. Good Practice Guidance For Land Use, Land-Use Change and Forestry (GPG LULUCF). IPCC National Greenhouse Gas Inventories Programme.
- Jansson, M. B. 1988. A Global Survey of Sediment Yield. *Geografiska Annaler. Series A, Physical Geography* **70**: 81-98.
- Klap, V. A., P. Louchouart, J. J. Boon, M. A. Hemminga, and J. V. Soelen. 1999. Decomposition Dynamics of Six Salt Marsh Halophytes as Determined by Cupric Oxide Oxidation and Direct Temperature-Resolved Mass Spectrometry. *Limnology and Oceanography* **44**: 1458-1476.
- Louchouart, P., M. Lucotte, and N. Farella. 1999. Historical and geographical variations of sources and transport of terrigenous organic matter within a large-scale coastal environment. *Organic Geochemistry* **30**: 675-699.
- Louchouart, P., S. Opsahl, and R. Benner. 2000. Isolation and quantification of dissolved lignin from natural waters using solid-phase extraction (SPE) and GC/MS Selected Ion Monitoring (SIM). *Analytical Chemistry* **13**: 2780-2787.
- Mackereth, F. J. H. 1958. A Portable Core Sampler for Lake Deposits. *Limnology and Oceanography* **3**: 181-191.
- Milliman, J. D., and R. H. Meade. 1983. World-Wide Delivery of River Sediment to the Oceans. *The Journal of Geology* **91**: 1-21.
- Opsahl, S., and R. Benner. 1995. Early diagenesis of vascular plant tissues: Lignin and cutin decomposition and biogeochemical implications. *Geochimica et Cosmochimica Acta* **59**: 4889-4904.
- . 1998. Photochemical Reactivity of Dissolved Lignin in River and Ocean Waters. *Limnology and Oceanography* **43**: 1297-1304.
- Otto, A., and M. Simpson. 2006. Evaluation of CuO oxidation parameters for determining the source and stage of lignin degradation in soil. *Biogeochemistry* **80**: 121-142.
- Ouellet, A. 2010. Assessing carbon dynamics in natural and human-perturbed boreal aquatic systems Concordia University.

- Ouellet, A., D. Catana, J.-B. Plouhinec, M. Lucotte, and Y. G elinas. 2008. Elemental, Isotopic, and Spectroscopic Assessment of Chemical Fractionation of Dissolved Organic Matter Sampled with a Portable Reverse Osmosis System. *Environmental Science & Technology* **42**: 2490-2495.
- Ouellet, A., K. Lalonde, J.-B. Plouhinec, N. Soumis, M. Lucotte, and Y. G elinas. 2012. Assessing carbon dynamics in natural and perturbed boreal aquatic systems. *J. Geophys. Res.* **117**: G03024.
- Ouellet, A. P., J.B. Soumis, N. Lucotte, M. G elinas, Y. 2011. Assessing the impact of wood harvesting and reservoir operation on carbon dynamics in boreal aquatic systems: a bulk isotopic approach. *Limnology and Oceanography*.
- Ouellet, J.-F., M. Lucotte, R. Teisserenc, S. Paquet, and R. Canuel. 2009. Lignin biomarkers as tracers of mercury sources in lakes water column. *Biogeochemistry* **94**: 123-140.
- Plouhinec, J. B., M. Lucotte, A. Ouellet, N. Soumis, and Y. G elinas. submitted. Dissolved organic matter photodegradation in surface waters and CO<sub>2</sub> atmospheric diffusion in pristine and perturbed waterbodies of the boreal region in Quebec (Canada). *Limnology and Oceanography*.
- Prairie, Y. 2008. Carbocentric limnology: looking back, looking forward. *Can J Fish Aquat Sci* **65**: 543-548.
- Rumpel, C., I. K ogel-Knabner, and F. Bruhn. 2002. Vertical distribution, age, and chemical composition of organic carbon in two forest soils of different pedogenesis. *Organic Geochemistry* **33**: 1131-1142.
- Soumis, N., M. Lucotte, C. Larose, F. Veillette, and R. Canuel. 2007. Photomineralization in a boreal hydroelectric reservoir: a comparison with natural aquatic ecosystems. *Biogeochemistry* **86**: 123-135.
- Spencer, R. G. M., G. R. Aiken, K. D. Butler, M. M. Dornblaser, R. G. Striegl, and P. J. Hernes. 2009. Utilizing chromophoric dissolved organic matter measurements to derive export and reactivity of dissolved organic carbon exported to the Arctic Ocean: A case study of the Yukon River, Alaska. *Geophys. Res. Lett.* **36**: L06401.
- Teisserenc, R. 2009. Dynamique de la mati re organique terrig ene et du mercure dans les lacs et r eservoirs bor eaux. Universit  du Qu ebec   Montr al.
- Teisserenc, R., M. Lucotte, and S. Houel. 2011. Terrestrial organic matter biomarkers as tracers of Hg sources in lake sediments. *Biogeochemistry* **103**: 235-244.

- Teisserenc, R., M. Lucotte, S. Houel, and J. Carreau. 2010. Integrated transfers of terrigenous organic matter to lakes at their watershed level: A combined biomarker and GIS analysis. *Geochimica et Cosmochimica Acta* **74**: 6375-6386.
- Tranvik, L. J., and S. Bertilsson. 2001. Contrasting effects of solar UV radiation on dissolved organic sources for bacterial growth. *Ecology Letters* **4**: 458-463.
- Tremblay, A., M. Garneau, C. Roehm, and L. Varfalvy. 2005. *Greenhouse Gas Emissions - Fluxes and Processes : Hydroelectric Reservoirs and Natural Environments*. Springer-Verlag Berlin Heidelberg.
- Tremblay, A., M. Lambert, and L. Gagnon. 2004. Do Hydroelectric Reservoirs Emit Greenhouse Gases? *Environmental Management* **33**: S509-S517.
- Vähätalo, A. V., K. Salonen, U. Münster, M. Jarvinen, and R. G. Wetzel. 2003. Photochemical transformation of allochthonous organic matter provides bioavailable nutrients in a humic lake. *Archiv für Hydrobiologie* **156**: 287-314.
- Weissenberger, S. 2007. *Émissions de gaz à effet de serre et cycle du carbone de réservoirs hydroélectriques du moyen Nord québécois*. Université du Québec à Montréal.

Tables captions

**Table 3.1** Summary of data obtained through the GIS (forest cover, watershed morphometry, lakes volume)

**Table 3.2** Main characteristics of the Cabonga reservoir sampled sites

**Table 3.3** Main characteristics of the Decelles reservoir sampled sites

**Table 3.4** Sedimentation rates (Ouellet, 2010) and sedimentary characteristics of the sampled cores

**Table 3.5** Mean  $C/N$  atomic ratio for each environmental conditions evaluated for the organic horizon of soils ( $C/N_{hor}$ ), for the inorganic horizon of soils ( $C/N_{hin}$ ), and for each fraction POC, DOC and SED

Tableau 3.1 Summary of data obtained through the GIS (forest cover, watershed morphometry, lakes volume)

Lakes	Bouveau	Brock	Clair	Ellard	Jean	Mary
Latitude N	46° 14' 19,63"	46° 16' 26,4"	46° 11' 18,94"	46° 17' 28,79"	46° 21' 55,77"	46° 15' 35,70"
Longitude W	76° 27' 25,42"	76° 20' 35,2"	76° 24' 57,00"	76° 13' 12,05"	76° 20' 44,00"	76° 13' 00,30"
Volume (m <sup>3</sup> )	2 024 500	9 261 400	11 673 390	688 150	19 874 790	2 846 730
LA (m <sup>2</sup> )	323 000	823 000	1 750 000	229 000	1 720 000	536 000
WA (m <sup>2</sup> )	8 232 000	6 350 000	47 020 000	2 355 000	7 312 000	1 799 000
Depth Average (m)	6,28	11,25	6,67	3,00	11,56	5,31
Average Slope (%)	7,14	ND	7,75	9,16	5,87	1,27
TP(μg.l <sup>-1</sup> )	8.98 ± 2.08	7.36 ± 0.95	8.02 ± 2.21	13.52 ± 1.09	8.01 ± 2.03	12.94 ± 2.19
DOC (mgC.l <sup>-1</sup> )	8.46 ± 0.64	3.17 ± 0.43	5.96 ± 1.05	5.74 ± 1.44	5.04 ± 1.44	3.88 ± 1.08
% Conifers	38.08	ND	29.22	21.48	20.60	21.88
% Hardwood	35.95	ND	38.41	60.41	44.52	20.33

**Tableau 3.2** Main characteristics of the Cabonga reservoir sampled sites

Cabonga	RCAB-3	RCAB-4	RCAB-5	RCAB-6	RCAB-7	RCAB-8	RCAB-10
Latitude N	47° 13' 53,9"	47° 18' 55,8"	47° 23' 18,4"	47° 35' 31,1"	47° 21' 7,9"	47° 19' 20,0"	47° 17' 24,4"
Longitude W	76° 42' 54,8"	76° 42' 8,2"	76° 44' 3,7"	76° 37' 42,7"	76° 29' 26,4"	76° 30' 47,0 "	76° 36' 24,1"
Depth Average (m)	3,80	10,45	5,30	8,55	85,00	±20	22,23
TP ( $\mu\text{g.l}^{-1}$ )	8,19 ± 2,09	6,76 ± 0,51	10,57 ± 1,61	8,54 ± 1,69	7,71 ± 0,51	5,32 ± 1,20	7,08 ± 3,15
DOC ( $\text{mgC.l}^{-1}$ )	7,55 ± 1,46	6,78 ± 0,28	4,735 ± 0,29	4,77 ± 0,92	5,17 ± 1,11	2,59 ± 0,18	4,66 ± 0,93

Tableau 3.3 Main characteristics of the Decelles reservoir sampled sites

Decelles	RDEC-1	RDEC-2	RDEC-3	RDEC-4	RDEC-6	RDEC-9
Latitude N	47° 45' 44,5"	47° 42' 57,2"	47° 41' 31,6"	47° 44' 42,4"	47° 40' 16,3"	47° 46' 25,5"
Longitude W	78° 18' 45,5"	78° 15' 44,1"	78° 12' 17,2"	78° 14' 56,9"	78° 05' 45,9"	78° 07' 33,6"
Depth Average (m)	6,78	2,75	4,60	6,33	11,2	4,75
TP ( $\mu\text{g.l}^{-1}$ )	12,56 $\pm$ 3,79	15,33 $\pm$ 5,20	12,02 $\pm$ 1,96	11,30 $\pm$ 1,85	8,94 $\pm$ 0,82	15,74 $\pm$ 4,10
DOC ( $\text{mgC.l}^{-1}$ )	6,91 $\pm$ 0,78	7,70 $\pm$ 0,84	8,11 $\pm$ 0,26	9,15 $\pm$ 0,79	5,87 $\pm$ 0,31	8,69 $\pm$ 0,63

**Tableau 3.4** Sedimentation rates (Ouellet, 2010) and sedimentary characteristics of the sampled cores

Waterbodies	Jean	Claire	Bouleau	Mary	Decelles (2)	Cabonga (6)
Sedimentation rate (mm/yr)	0,44	0,72	0,34	1,35	5,8	5,5
Carbon percentage	13	3	14,2	25	7,1	8,6
Total phosphorus ( $\mu\text{g.l}^{-1}$ )	8,01	8,02	8,98	12,94	15,53	8,54
Drainage ratio (LA/WA)	23%	3,7%	3,9%	29%	1,5%	1,6%
Depth average (m)	11,56	6,67	6,28	5,31	2,75	8,55

Tableau 3.5 Mean  $C/N$  atomic ratio for each environmental conditions evaluated for the organic horizon of soils ( $C/N_{hor}$ ), for the inorganic horizon of soils ( $C/N_{hin}$ ), and for each fraction POC, DOC and SED

Scenario	$C/N_{hor}$	$C/N_{hin}$	$C/N_{POC}$	$C/N_{DOC}$	$C/N_{SED}$
RAL	40	30	29	41	21
RNAL	37	32	22	35	17
LAL	38	27	22	35	14
LNAL	29	19	16	30	13

Figures captions

**Figure 3.1** Map of the sampled sites on the Cabonga reservoir

**Figure 3.2** Map of the sampled sites on the Decelles reservoir

**Figure 3.3** Map of the watershed of the Ottawa River ([http:// fr.academic.ru](http://fr.academic.ru))

**Figure 3.4** S / V ratio versus C / V ratio in sediments

**Figure 3.5** S / V ratio versus C / V ratio in the particulate fraction

**Figure 3.6** S / V ratio versus C / V ratio in the dissolved fraction

**Figure 3.7** The various phenolic compounds constituting of the lignin biomarkers, according to the dissolved fraction, the particulate fraction and the sedimentary matter for every environmental conditions

**Figure 3.8a** The lignin biomarkers values of  $\lambda_8$  measured according to various environmental conditions (LNAL, LAL, RNAL, RAL) in the dissolved and the particulate fraction and in the sedimentary matter

**Figure 3.8b** The lignin biomarkers values of  $\Sigma_8$  measured according to various environmental conditions (LNAL, LAL, RNAL, RAL) in the dissolved and the particulate fraction and in the sedimentary matter

**Figure 3.8c** The lignin biomarkers values of the S/V ratio, measured according to various environmental conditions (LNAL, LAL, RNAL, RAL) in the dissolved and the particulate fraction and in the sedimentary matter

**Figure 3.8d** The lignin biomarkers values of the C/V ratio, measured according to various environmental conditions (LNAL, LAL, RNAL, RAL) in the dissolved and the particulate fraction and in the sedimentary matter

**Figure 3.8e** The lignin biomarkers values of  $\Sigma_C$  measured according to various environmental conditions (LNAL, LAL, RNAL, RAL) in the dissolved and the particulate fraction and in the sedimentary matter

**Figure 3.8f** The lignin biomarkers values of  $\Sigma_P$  measured according to various environmental conditions (LNAL, LAL, RNAL, RAL) in the dissolved and the particulate fraction and in the sedimentary matter

**Figure 3.8g** The lignin biomarkers values of  $\Sigma_V$  measured according to various environmental conditions (LNAL, LAL, RNAL, RAL) in the dissolved and the particulate fraction and in the sedimentary matter

**Figure 3.8h** The lignin biomarkers values of  $\Sigma_S$  measured according to various environmental conditions (LNAL, LAL, RNAL, RAL) in the dissolved and the particulate fraction and in the sedimentary matter

**Figure 3.8i** The lignin biomarkers values of the P/(V+S) ratio, measured according to various environmental conditions (LNAL, LAL, RNAL, RAL) in the dissolved and the particulate fraction and in the sedimentary matter

**Figure 3.8j** The lignin biomarkers values of the 3,5 Bd/V ratio, measured according to various environmental conditions (LNAL, LAL, RNAL, RAL) in the dissolved and the particulate fraction and in the sedimentary matter

**Figure 3.8k** The lignin biomarkers values of the (Ac/Ad)<sub>v</sub> ratio, measured according to various environmental conditions (LNAL, LAL, RNAL, RAL) in the dissolved and the particulate fraction and in the sedimentary matter

**Figure 3.8l** The lignin biomarkers values of the (Ac/Ad)<sub>s</sub> ratio, measured according to various environmental conditions (LNAL, LAL, RNAL, RAL) in the dissolved and the particulate fraction and in the sedimentary matter

**Figure 3.9**  $\lambda_8$  values measured in the dissolved fraction in relation with  $\lambda_8$  measured for the particulate fraction

**Figure 3.10** Relationship between the concentration of the dissolved terrigenous matter ( $\lambda_{DOC}$ ) and the total concentration of DOC

**Figure 11a**  $\lambda_{DOC}$  values obtained in the dissolved fraction in relationship with the CO<sub>2</sub> production deriving from the photochemical mineralization

**Figure 11b**  $\lambda_{DOC}$  values obtained in the dissolved fraction according to the environmental conditions

**Figure 3.12a**  $\lambda_{\text{Vol}}$  values obtained in the dissolved fraction in relationship with the  $\text{CO}_2$  production deriving from the photochemical mineralization

**Figure 3.12b**  $\lambda_{\text{Vol}}$  values obtained in the dissolved fraction according to the environmental conditions

**Figure 3.13a**  $\lambda_{\text{POC}}$  values obtained in the dissolved fraction in relationship with the  $\text{CO}_2$  production deriving from the photochemical mineralization

**Figure 3.13b**  $\lambda_{\text{POC}}$  values obtained in the dissolved fraction according to the environmental conditions

**Figure 3.14a** Values of the C/V ratio measured in the sedimentary matter in relationship with the total diffusive fluxes of  $\text{CO}_2$  ( $f_{\text{CO}_2}$ )

**Figure 3.14b** Values of the C/V ratio measured in the sedimentary matter in relationship with the daily production of  $\text{CO}_2$  from photochemical mineralization over the entire water column ( $\text{DIPM}_{\text{CO}_2}$ )

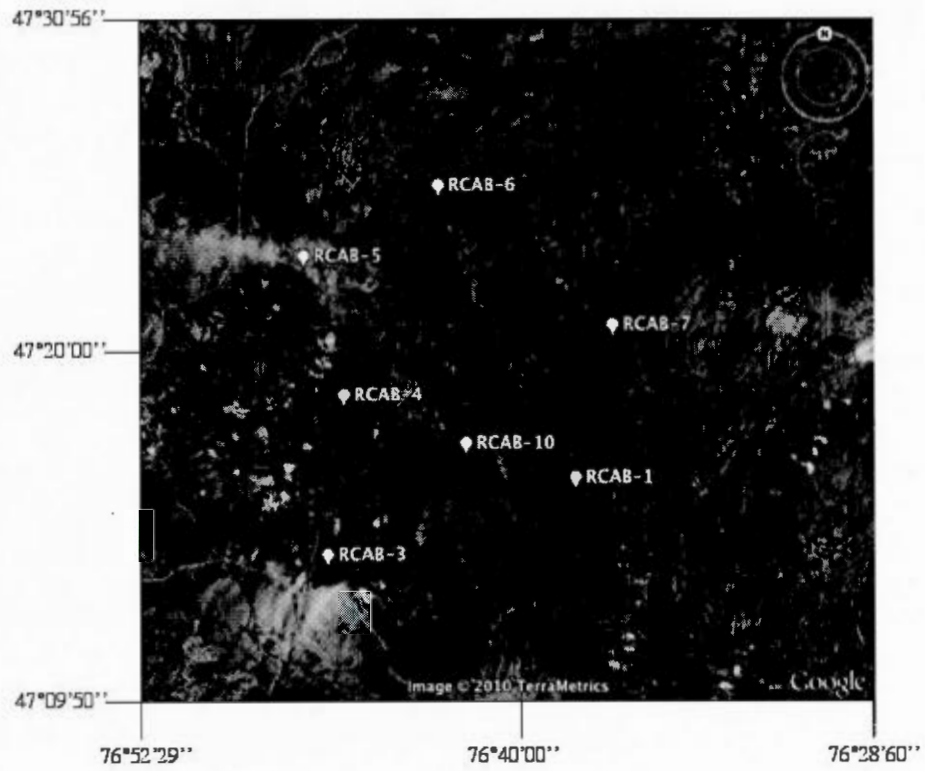


**Figure 3.1** Map of the sampled sites on the Cabonga reservoir

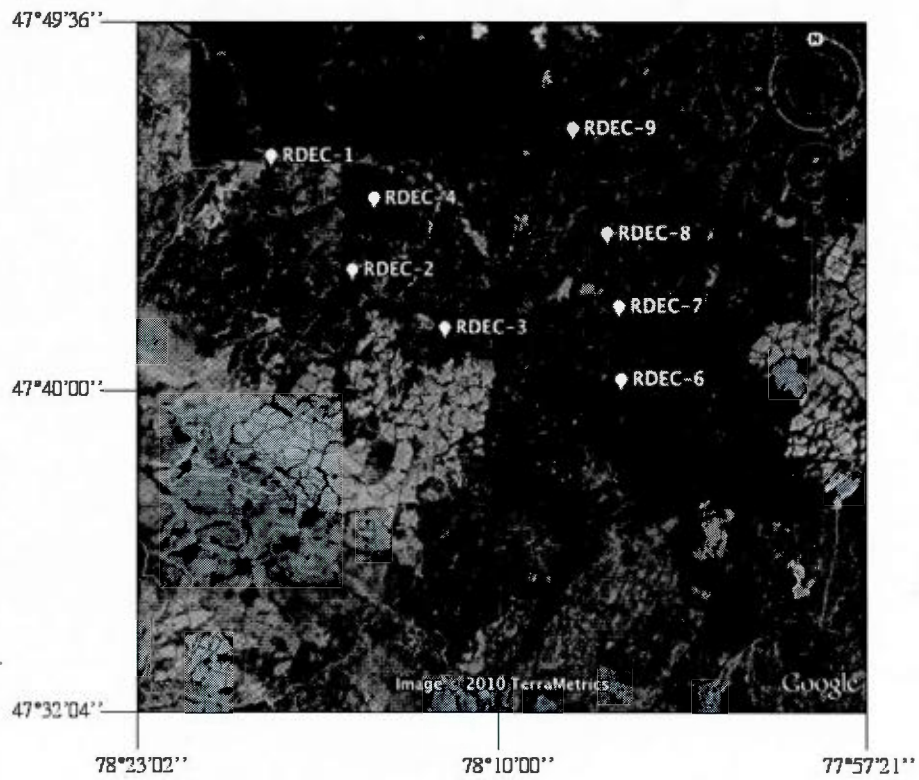


**Figure 3.2** Map of the sampled sites on the Decelles reservoir



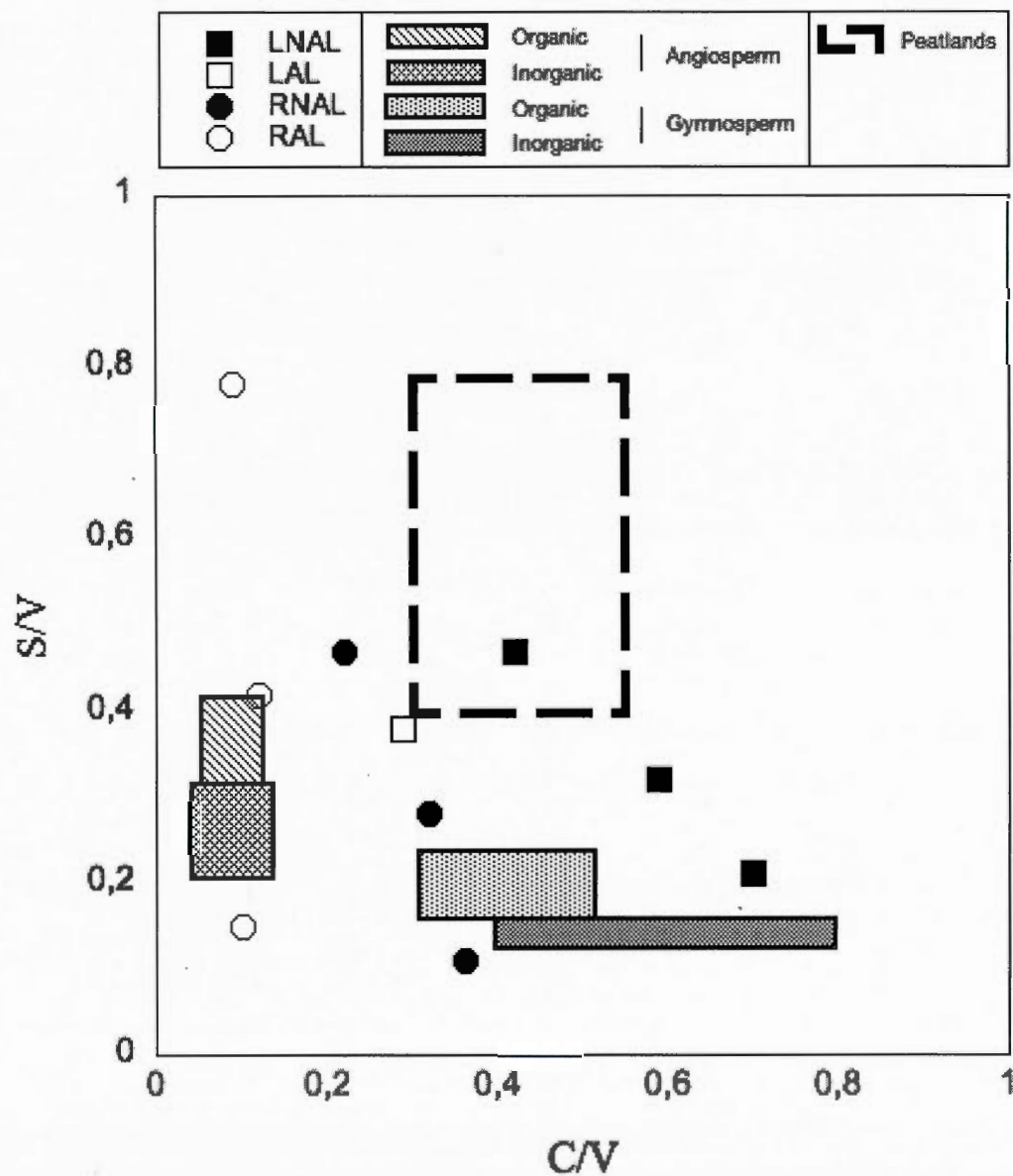


Figure 3.4 S / V ratio versus C / V ratio in sediments

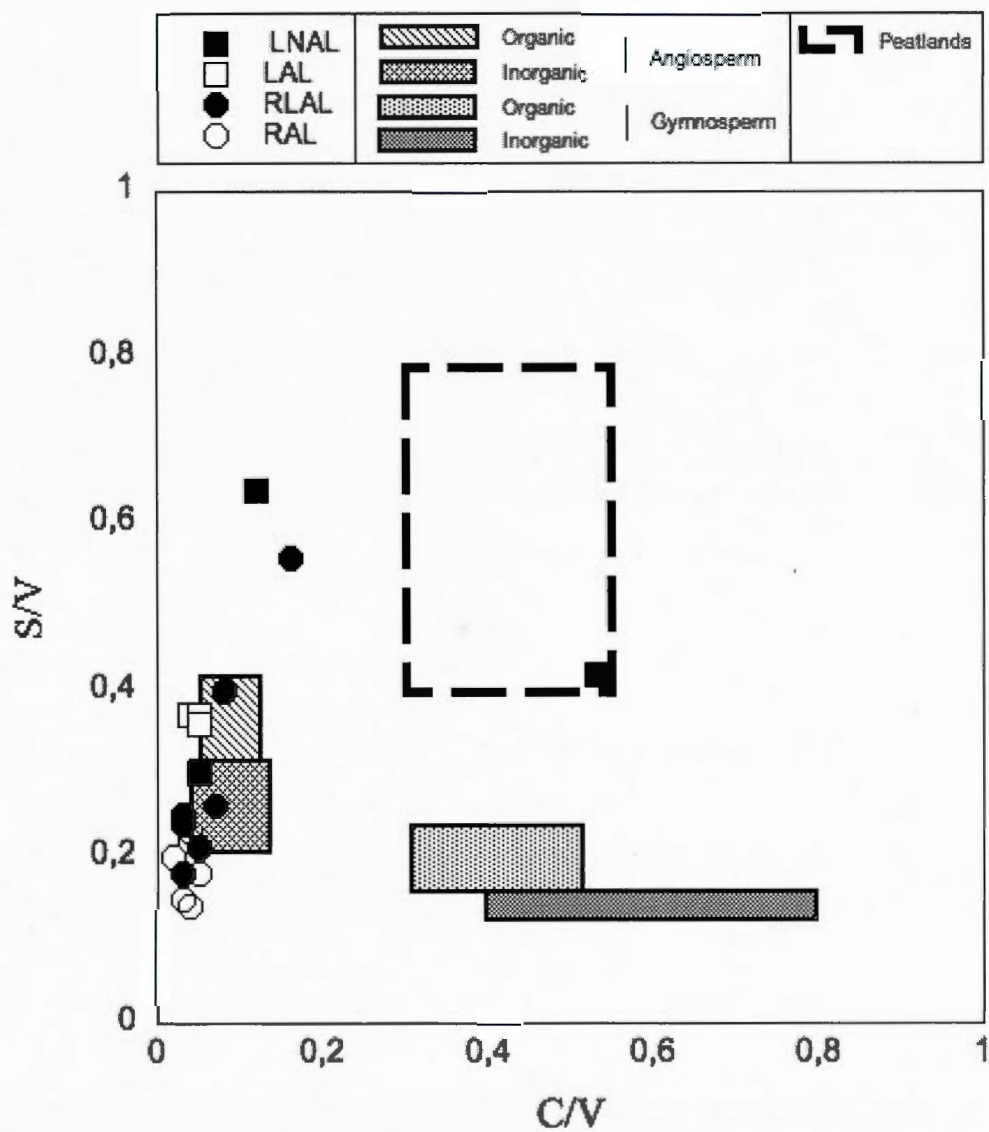


Figure 3.5 S / V ratio versus C / V ratio in the particulate fraction

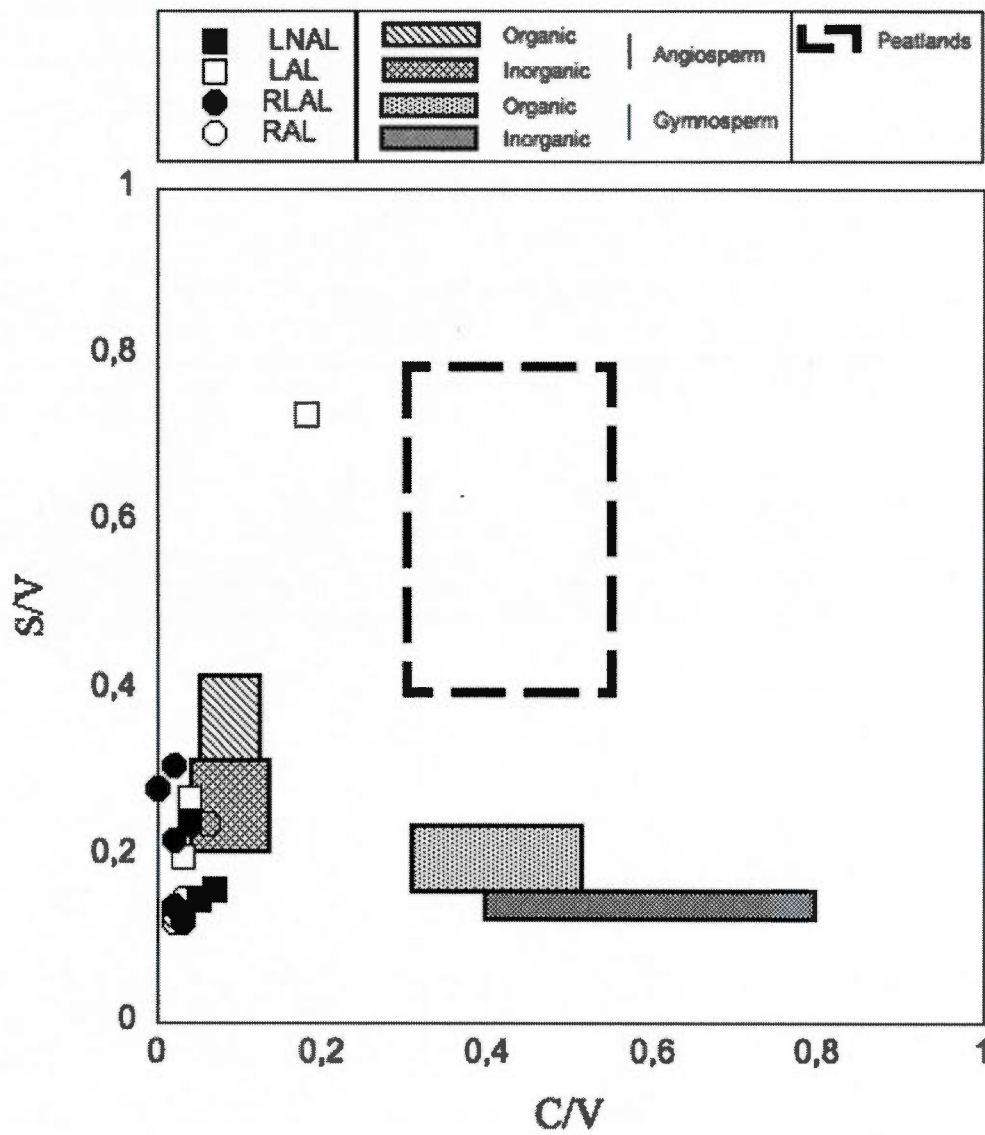
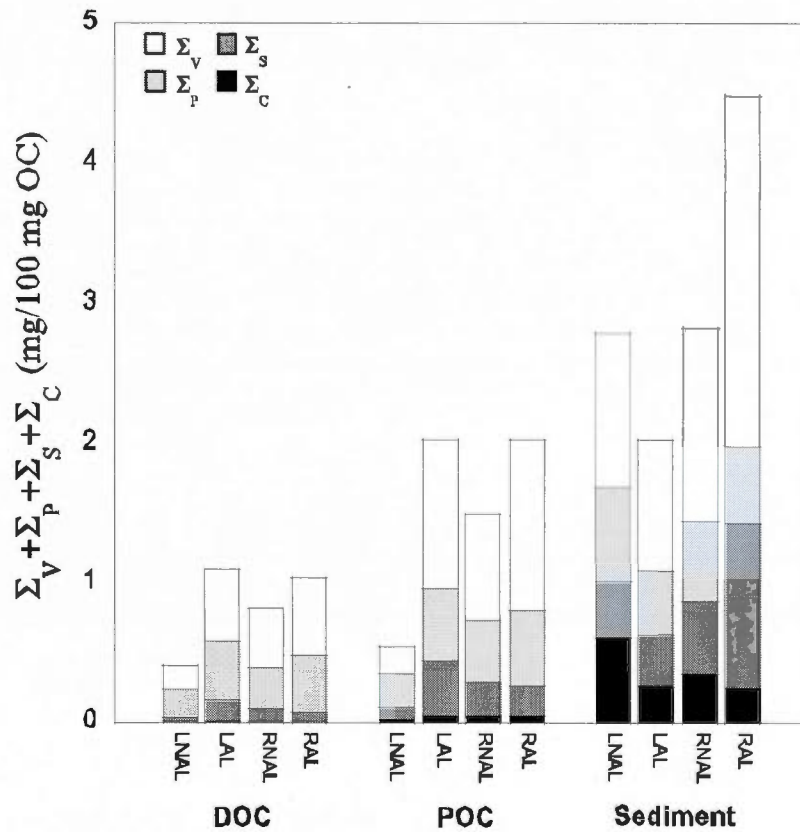
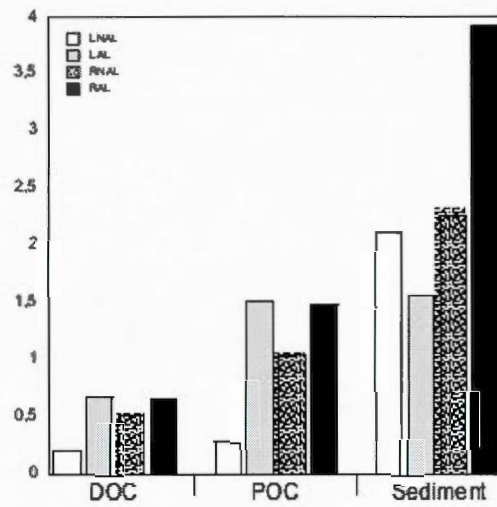


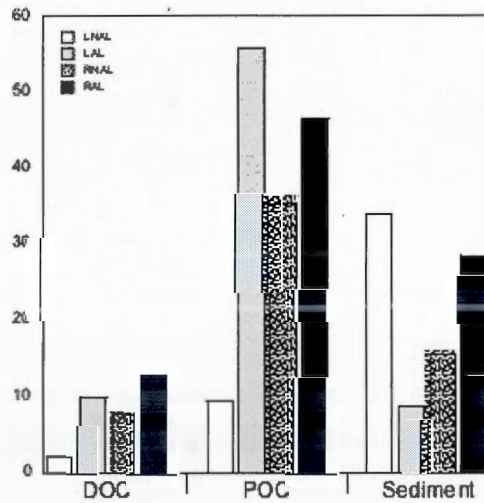
Figure 3.6 S / V ratio versus C / V ratio in the dissolved fraction



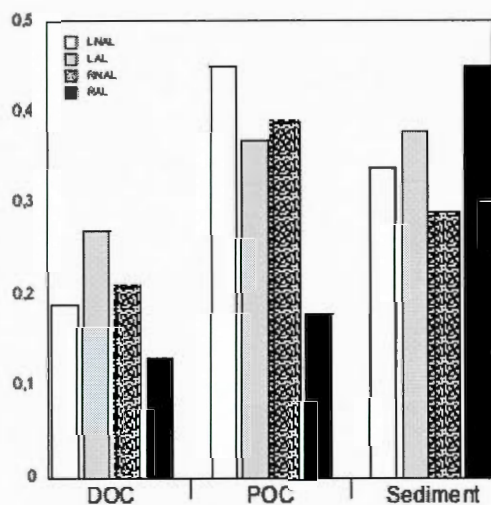
**Figure 3.7** The various phenolic compounds constituting of the lignin biomarkers, according to the dissolved fraction, the particulate fraction and the sedimentary matter for every environmental conditions



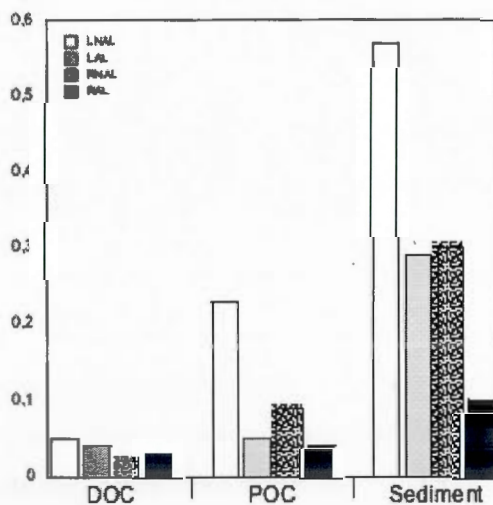
**Figure 3.8a** The lignin biomarkers values of  $\lambda_8$  measured according to various environmental conditions (LNAL, LAL, RNAL, RAL) in the dissolved and the particulate fraction and in the sedimentary matter



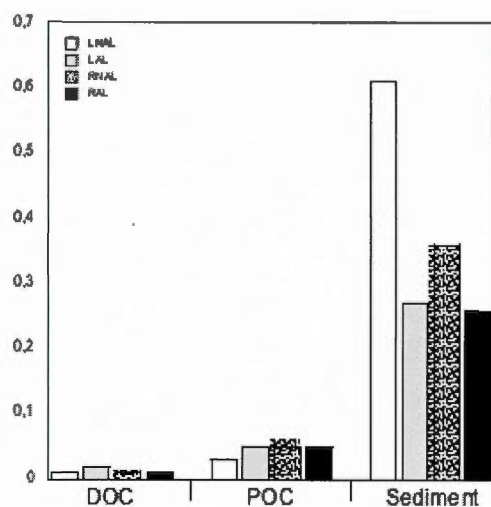
**Figure 3.8b** The lignin biomarkers values of  $\Sigma_8$  measured according to various environmental conditions (LNAL, LAL, RNAL, RAL) in the dissolved and the particulate fraction and in the sedimentary matter



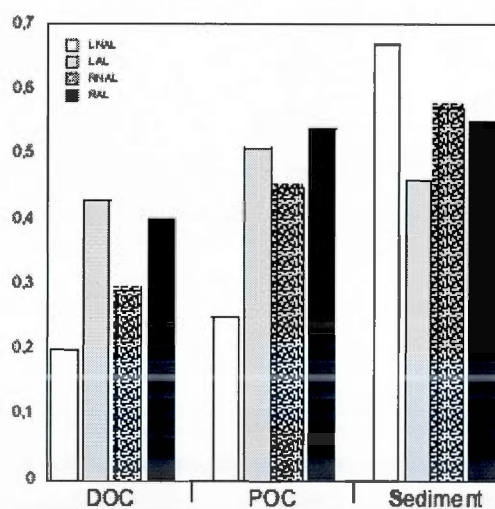
**Figure 3.8c** The lignin biomarkers values of the S/V ratio, measured according to various environmental conditions (LNAL, LAL, RNAL, RAL) in the dissolved and the particulate fraction and in the sedimentary matter



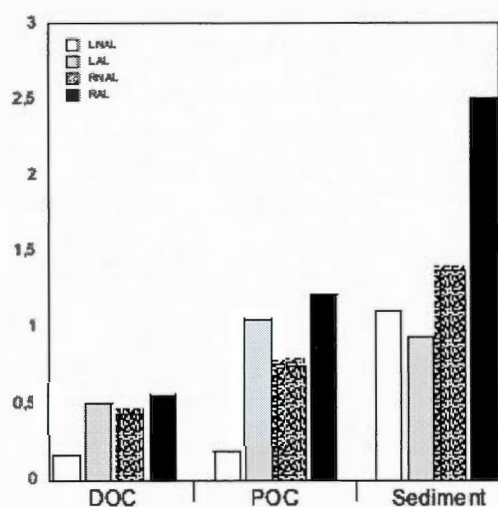
**Figure 3.8d** The lignin biomarkers values of the C/V ratio, measured according to various environmental conditions (LNAL, LAL, RNAL, RAL) in the dissolved and the particulate fraction and in the sedimentary matter



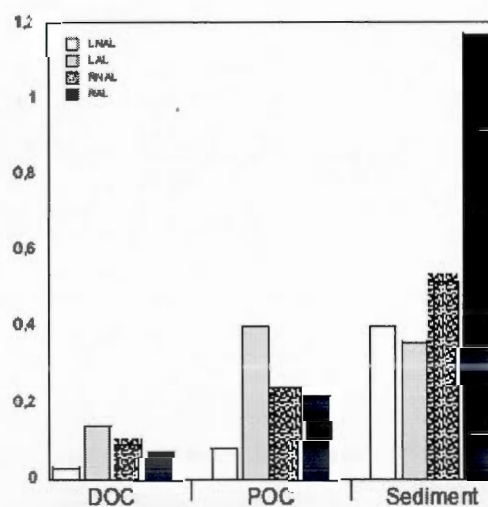
**Figure 3.8e** The lignin biomarkers values of  $\Sigma_C$  measured according to various environmental conditions (LNAL, LAL, RNAL, RAL) in the dissolved and the particulate fraction and in the sedimentary matter



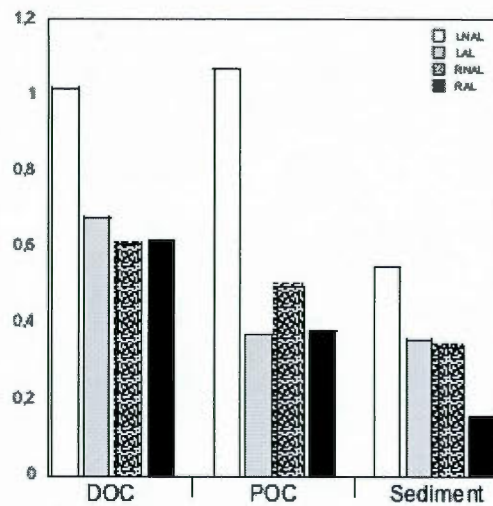
**Figure 3.8f** The lignin biomarkers values of  $\Sigma_P$  measured according to various environmental conditions (LNAL, LAL, RNAL, RAL) in the dissolved and the particulate fraction and in the sedimentary matter



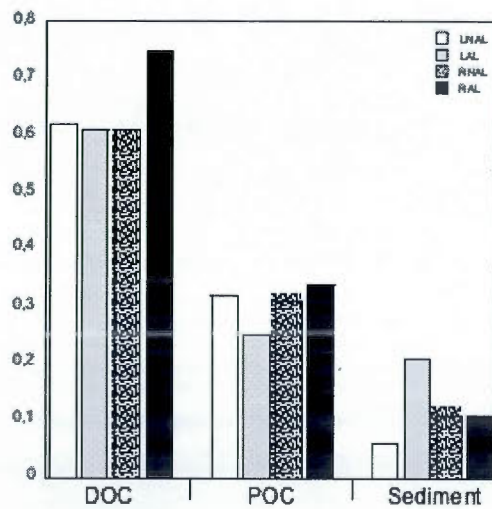
**Figure 3.8g** The lignin biomarkers values of  $\Sigma_V$  measured according to various environmental conditions (LNAL, LAL, RNAL, RAL) in the dissolved and the particulate fraction and in the sedimentary matter



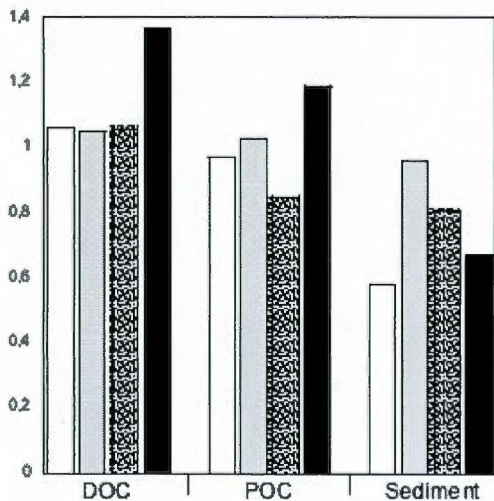
**Figure 3.8h** The lignin biomarkers values of  $\Sigma_S$  measured according to various environmental conditions (LNAL, LAL, RNAL, RAL) in the dissolved and the particulate fraction and in the sedimentary matter



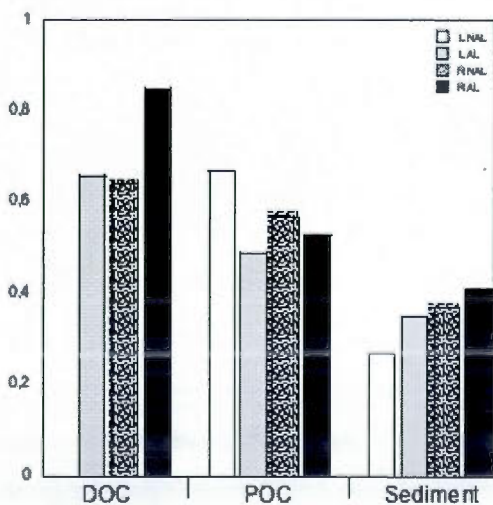
**Figure 3.8i** The lignin biomarkers values of the P/(V+S) ratio, measured according to various environmental conditions (LNAL, LAL, RNAL, RAL) in the dissolved and the particulate fraction and in the sedimentary matter



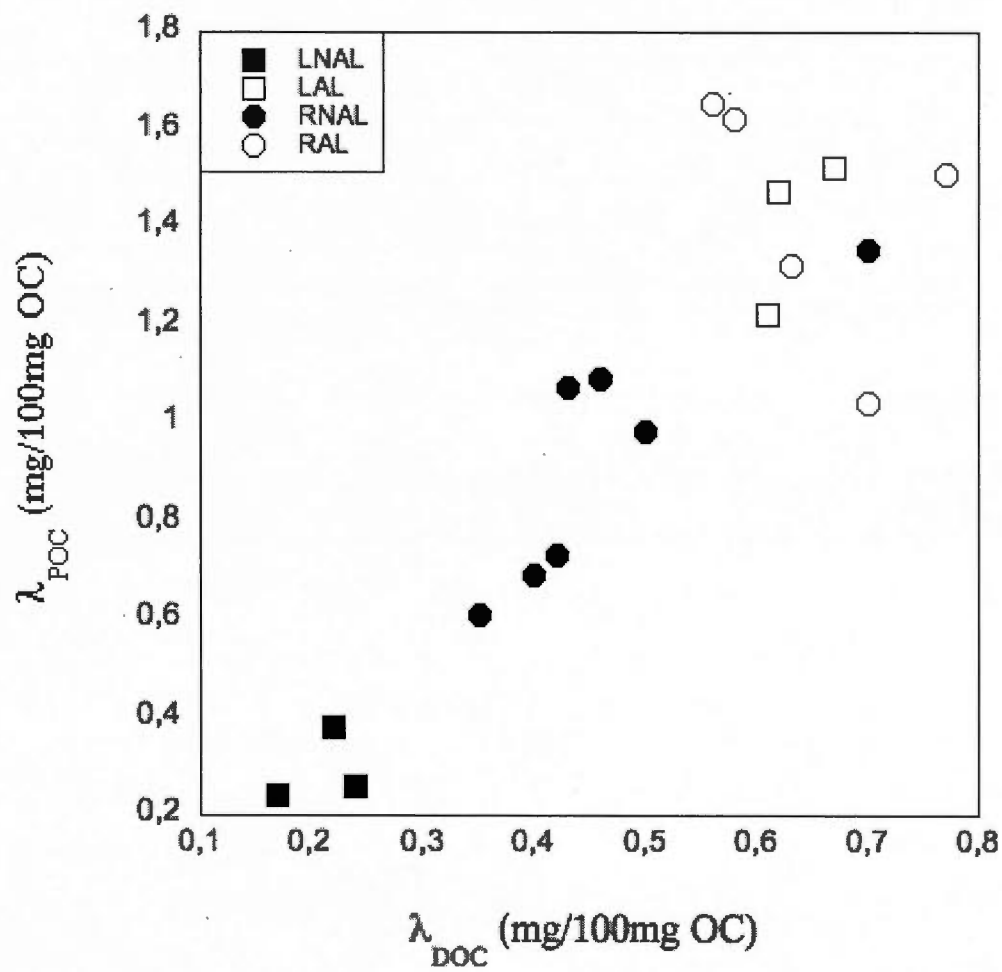
**Figure 3.8j** The lignin biomarkers values of the 3,5 Bd/V ratio, measured according to various environmental conditions (LNAL, LAL, RNAL, RAL) in the dissolved and the particulate fraction and in the sedimentary matter



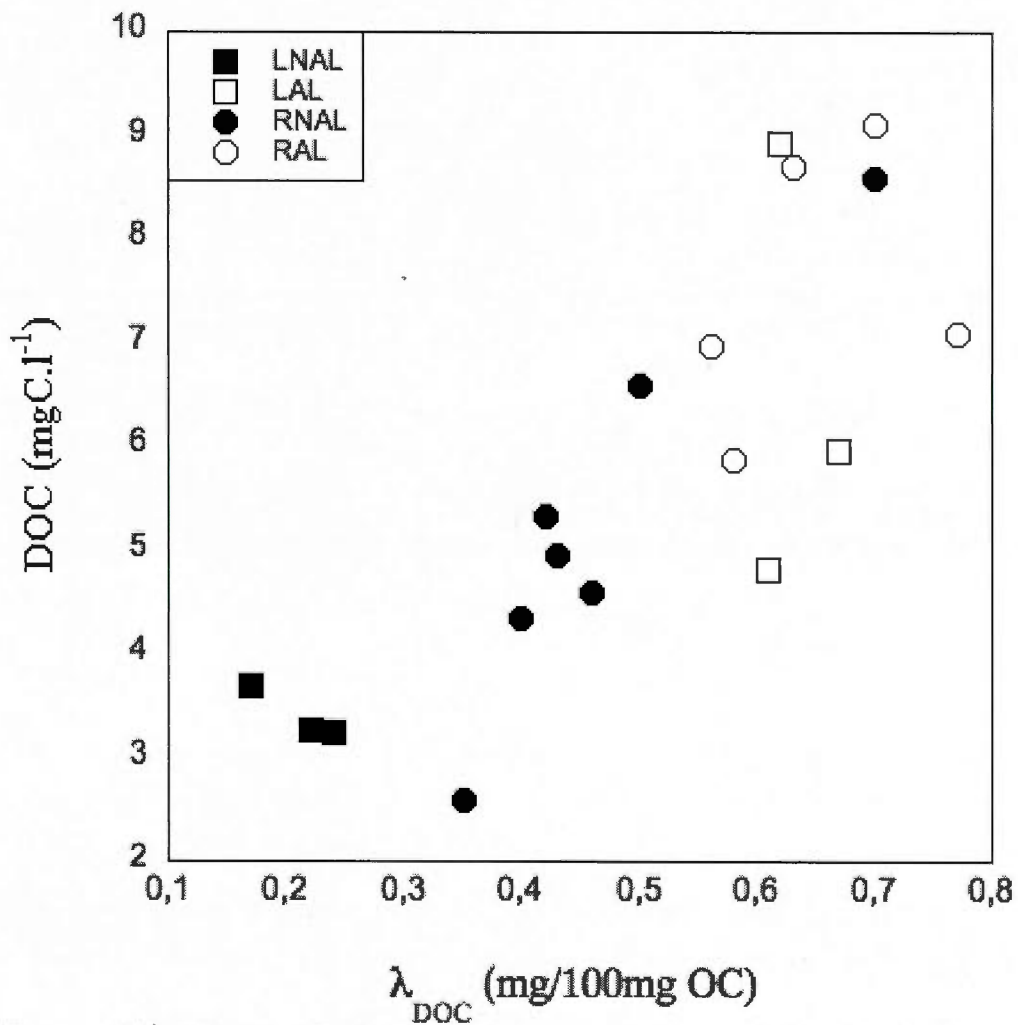
**Figure 3.8k** The lignin biomarkers values of the  $(Ac/Ad)_v$  ratio, measured according to various environmental conditions (LNAL, LAL, RNAL, RAL) in the dissolved and the particulate fraction and in the sedimentary matter



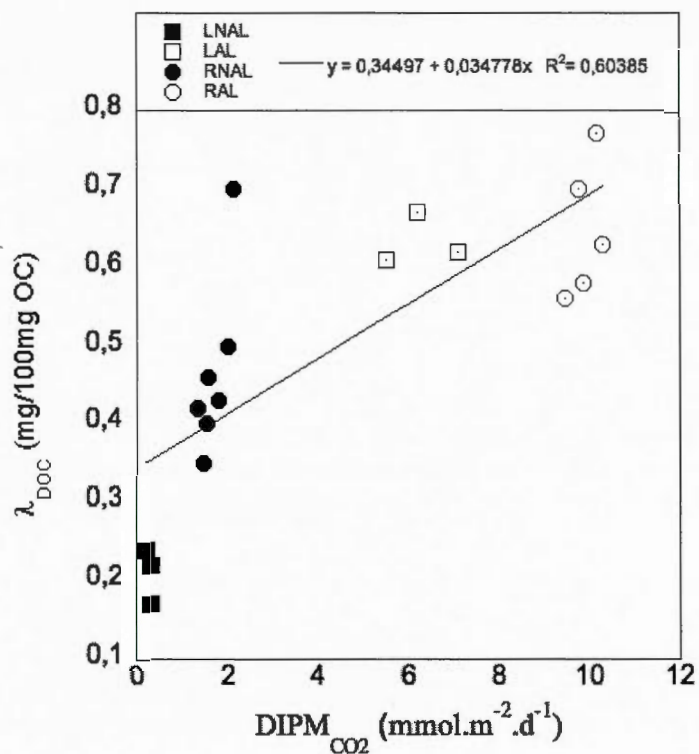
**Figure 3.8l** The lignin biomarkers values of the  $(Ac/Ad)_s$  ratio, measured according to various environmental conditions (LNAL, LAL, RNAL, RAL) in the dissolved and the particulate fraction and in the sedimentary matter



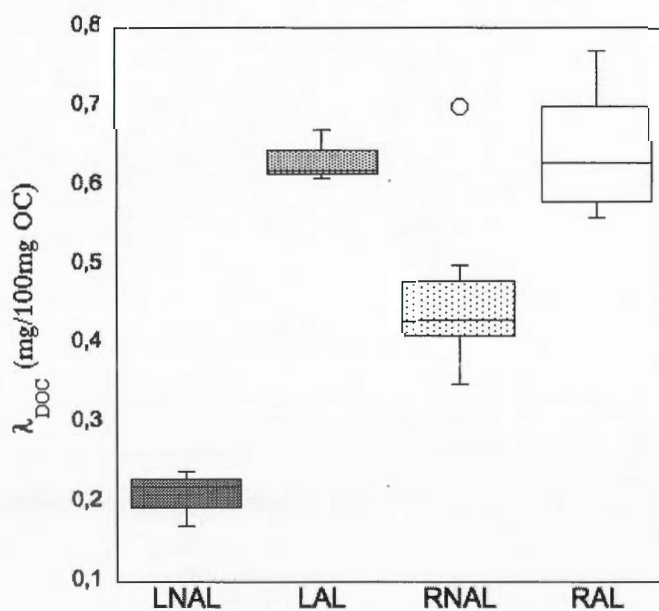
**Figure 3.9**  $\lambda_8$  values measured in the dissolved fraction in relation with  $\lambda_8$  measured for the particulate fraction



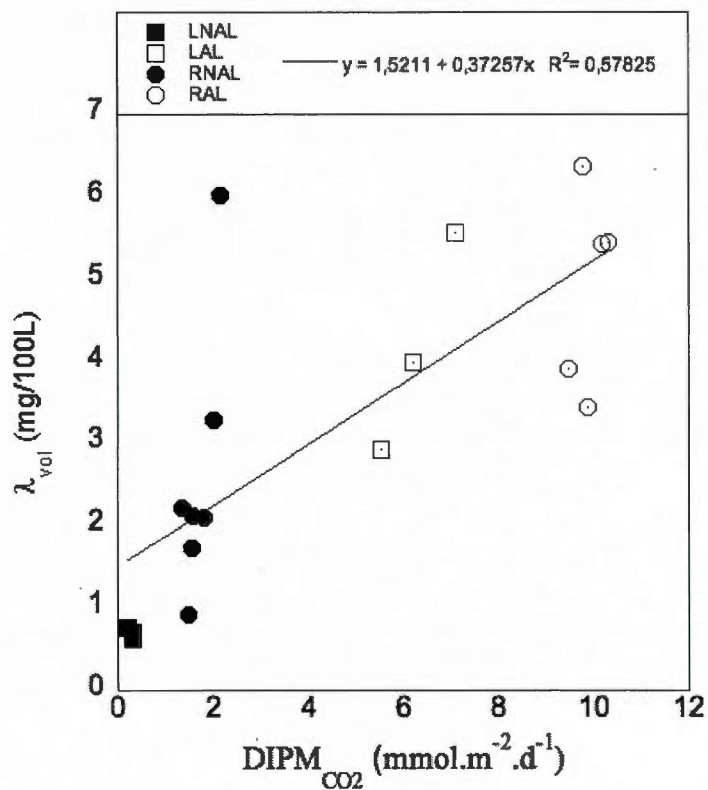
**Figure 3.10** Relationship between the concentration of the dissolved terrigenous matter ( $\lambda_{DOC}$ ) and the total concentration of DOC



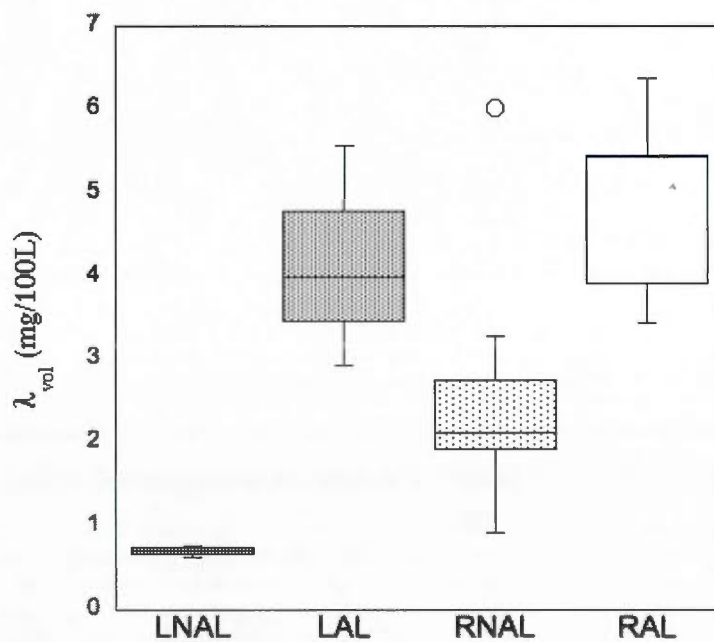
**Figure 3.11a**  $\lambda_{\text{DOC}}$  values obtained in the dissolved fraction in relationship with the  $\text{CO}_2$  production deriving from the photochemical mineralization



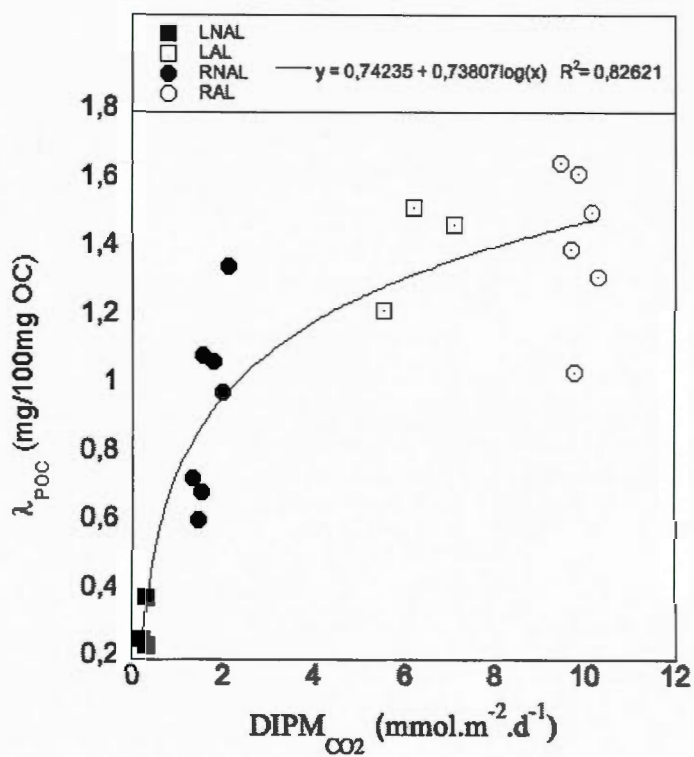
**Figure 3.11b**  $\lambda_{\text{DOC}}$  values obtained in the dissolved fraction according to the environmental conditions



**Figure 3.12a**  $\lambda_{vol}$  values obtained in the dissolved fraction in relationship with the  $CO_2$  production deriving from the photochemical mineralization



**Figure 3.12b**  $\lambda_{vol}$  values obtained in the dissolved fraction according to the environmental conditions



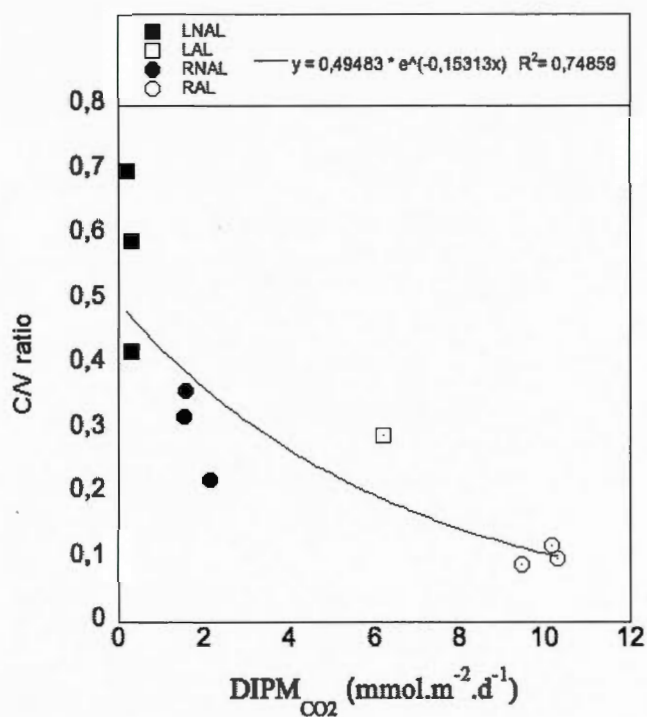


**Figure 3.14a** Values of the C/V ratio measured in the sedimentary matter in relationship with the total diffusive fluxes of CO<sub>2</sub> ( $f_{CO_2}$ )

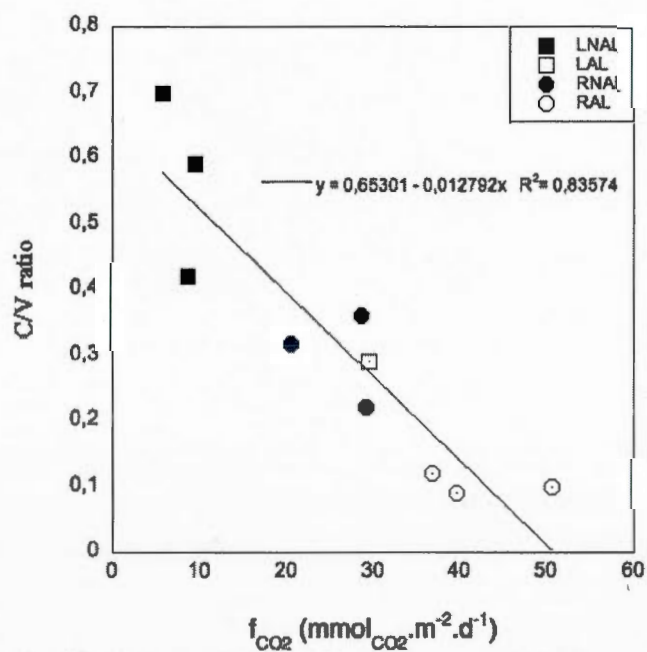


**Figure 3.14b** Values of the C/V ratio measured in the sedimentary matter in relationship with the daily production of CO<sub>2</sub> from photochemical mineralization over the entire water column ( $DIPM_{CO_2}$ )

## CONCLUSION GÉNÉRALE

Nous présentons, dans cette conclusion, une synthèse des résultats obtenus dans chacun des trois chapitres de cette thèse. Rappelons, tout d'abord, la structure générale de cette thèse. Le premier chapitre se concentre exclusivement sur le devenir du carbone en surface. On a ainsi observé, à l'instar d'autres études (Granéli et al. 1998; Lindell et al. 2000), une forte corrélation entre la production de  $\text{CO}_2$  par photominéralisation en surface ( $PM_{\text{CO}_2}(0)$ ) et la quantité de COD présente dans la colonne d'eau ( $R^2=0,81$ ;  $p<0,001$ ). De même, la production de  $\text{CO}_2$  par photominéralisation en surface est très liée au coefficient d'absorption spectrale de la matière organique dissoute colorée, mesurée à 305nm ( $\alpha_{\text{CDOM},305}$ ). En effet, la valeur  $\alpha_{\text{CDOM},305}$  des échantillons d'eau préalablement filtrés à  $0,2\mu\text{m}$ , puis incubés pendant 24h dans le milieu d'origine, est corrélée à la photoproduction en surface  $PM_{\text{CO}_2}(0)$  ( $R^2=0,78$ ;  $p<0,001$ ). Il apparaît également que la production de  $\text{CO}_2$  par photominéralisation en surface ( $PM_{\text{CO}_2}(0)$ ), fournit, comme attendue, une excellente corrélation avec la densité du flux de photons absorbée par le milieu aquatique dans premiers centimètres de la colonne d'eau ( $Q_{a,\lambda}$ ) ( $R^2=0,77$ ;  $p<0,001$ ). De plus, il a été constaté que la quantité de  $\text{CO}_2$ , produite en surface par photominéralisation, différait selon les situations environnementales étudiées. Ainsi, les milieux aquatiques qui n'avaient pas subi de perturbation par récolte forestière, LNAL pour les lacs, et RNAL pour le réservoir Cabonga, présentaient respectivement des valeurs  $PM_{\text{CO}_2}(0)$  estimées à  $1,41\pm 2,3 \mu\text{molCO}_2 \cdot \text{L}^{-1} \cdot \text{J}^{-1}$  et  $7,71\pm 2,62 \mu\text{molCO}_2 \cdot \text{L}^{-1} \cdot \text{J}^{-1}$ . De plus, la valeur

$PM_{CO_2}(0)$  s'est avérée plus élevée pour les réservoirs comparativement aux lacs, y compris lorsque l'écosystème avait été perturbé par une récolte forestière. Ainsi, les valeurs de  $CO_2$  produites par photominéralisation en surface pour les lacs perturbés par récolte forestière (LAL), estimées à  $19,29 \pm 9,13 \mu mol CO_2 \cdot l^{-1} \cdot j^{-1}$ , étaient légèrement inférieures à celles qui ont été mesurées à partir des sites d'échantillonnage du réservoir Decelles  $20,51 \pm 7,72 \mu mol CO_2 \cdot l^{-1} \cdot j^{-1}$ . De plus, les valeurs  $PM_{CO_2}(0)$  évaluée pour chaque station étudiée, normalisées selon la quantité de COD et standardisées selon le débit de flux de photons  $\left( \overline{PM_{CO_2}(0)} / DOC \right)$ , montrent que la quantité de  $CO_2$  produite quotidiennement dans la colonne d'eau varie entre 0,7 et 9,3%. De plus, l'indicateur  $\left( \overline{PM_{CO_2}(0)} / DOC \right)$  reste très bien corrélé à la concentration en fer dissous ( $[Fe]$ ) dans la colonne d'eau ( $R^2=0,59$  ;  $p<0,001$ ). Ce résultat tend à montrer que la quantité de carbone photodégradée dans les quatre premiers centimètres de la colonne d'eau et menant à la production de  $CO_2$  serait liée à un apport supplémentaire en matière organique terrigène (MOT) qui parviendrait aux écosystèmes aquatiques. Les résultats obtenus dans le premier chapitre de cette thèse permettent également de supposer que le  $CO_2$  produit par photodégradation pourrait contribuer substantiellement aux émissions totales de  $CO_2$  provenant des plans d'eau. Afin de vérifier cette hypothèse, nous avons évalué la production totale de  $CO_2$  issue de la photodégradation en basant nos efforts sur un calcul identique à celui proposé par Vähätalo et al. (2000). Ce calcul permet d'estimer, pour l'ensemble de la colonne d'eau, un flux de  $CO_2$  dérivé des processus de photodégradation  $\left( \overline{DIPM_{CO_2}} \right)$ . Conformément à nos hypothèses de travail, il est apparu que le rendement quantique de la minéralisation par photochimie était, globalement, lié au degré de perturbation de l'écosystème aquatique étudié. Ainsi, les stations du réservoir Decelles (regroupées sous l'acronyme RAL) présentent une valeur de production quotidienne de  $CO_2$  qui provient de la minéralisation photochimique sur

l'ensemble de la colonne d'eau ( $\overline{DIPM}_{CO_2}$ ), évaluée à  $9,38 \pm 2,59$  mmol.CO<sub>2</sub>.m<sup>-2</sup>.j<sup>-1</sup>.

Cette valeur moyenne est largement supérieure à celle de la production quotidienne de CO<sub>2</sub> par minéralisation photochimique estimée pour des lacs soumis à une récolte forestière récente (LAL). En effet, la valeur moyenne,  $\overline{DIPM}_{CO_2}$ , associée à cette situation environnementale, a été évaluée à  $5,16 \pm 2,30$  mmol.CO<sub>2</sub>.m<sup>-2</sup>.j<sup>-1</sup>. Selon notre calcul, les milieux aquatiques étudiés, qui ne sont pas perturbés par récolte forestière, minéralisent le carbone avec un rendement photochimique plus faible que celui des écosystèmes aquatiques soumis à une déforestation partielle de leur bassin versant. Ce flux quotidien de CO<sub>2</sub> provenant de la minéralisation du carbone par photochimie, bien qu'inférieur à celui des situations environnementales précédentes (RAL et RNAL), reste plus important pour les réservoirs (RNAL) avec  $2,51 \pm 0,49$  mmol.CO<sub>2</sub>.m<sup>-2</sup>.j<sup>-1</sup> tandis qu'il est estimé à  $0,24 \pm 0,16$  mmol.CO<sub>2</sub>.m<sup>-2</sup>.j<sup>-1</sup> pour les lacs (LNAL).

Dans ce second chapitre, la contribution relative du CO<sub>2</sub> produit par photodégradation par rapport à l'ensemble des flux des CO<sub>2</sub>, estimés selon une méthode d'échantillonnage dans la couche mince de surface, est estimée à  $24,77\% \pm 18,77\%$ . Par ailleurs, la production de CO<sub>2</sub> par photodégradation sur l'ensemble de la colonne d'eau est très bien corrélée aux flux diffusifs totaux de CO<sub>2</sub> émis vers l'atmosphère, indépendamment des plans d'eau à l'étude ( $R^2=0,81$ ;  $p<0,001$ ). Le système d'incubation, qui a permis la quantification des flux quotidiens de CO<sub>2</sub> produits par photodégradation sur l'ensemble de la colonne d'eau, a également été utilisé pour évaluer un flux quotidien de production de CO<sub>2</sub> résultant de la respiration bactérienne (noté  $DIBR_{CO_2}$ ). Ce dispositif d'incubation, grâce à l'utilisation de plusieurs filtrations de 1,2 µm et 210 µm, fournit également la possibilité d'estimer la quantité de CO<sub>2</sub> fixée quotidiennement par photosynthèse ( $DIPH_{CO_2}$ ). Nous proposons qu'il soit possible d'estimer un flux diffusif total de CO<sub>2</sub> (noté  $f_{CO_2}^*$ ) à partir des trois

principaux flux de carbone précédemment définis ( $\overline{DIPM}_{CO_2}$ ,  $DIBR_{CO_2}$  et  $DIPH_{CO_2}$ ). Par ailleurs, la corrélation entre cette estimation  $f_{CO_2}^*$  et la valeur de flux de CO<sub>2</sub> obtenue selon la méthode d'échantillonnage dans la couche mince de surface ( $f_{CO_2}$ ), est extrêmement forte ( $R^2=0.97$ ,  $p<0.001$ ). Cette corrélation entre  $f_{CO_2}^*$  et  $f_{CO_2}$  indique également une contribution importante du flux  $DIBR_{CO_2}$  dans les processus totaux d'émissions de CO<sub>2</sub> des écosystèmes aquatiques vers l'atmosphère. Bien que le flux quotidien de CO<sub>2</sub> provenant de la respiration bactérienne représente une proportion importante du flux total ( $f_{CO_2}$ ), les autres flux considérés ( $\overline{DIPM}_{CO_2}$  et  $DIPH_{CO_2}$ ) dépendent plus fortement des différentes situations environnementales. En effet, la valeur du flux de CO<sub>2</sub> associée au processus de photominéralisation ( $\overline{DIPM}_{CO_2}$ ) est d'autant plus élevée que la perturbation de l'écosystème est importante. De même, la valeur du flux de CO<sub>2</sub> associée au processus de photosynthèse ( $DIPH_{CO_2}$ ) est d'autant plus faible que la perturbation de l'écosystème est importante. En définitive, dans ce second chapitre, nous avons validé la bonne représentativité du dispositif expérimental utilisé. Les résultats obtenus laisse également pressentir qu'une partie non négligeable du carbone inorganique dissous, produit dans la colonne d'eau, ait comme origine une dégradation du carbone terrigène. De plus, la respiration bactérienne, qui contribue sensiblement aux émissions totales de CO<sub>2</sub> vers l'atmosphère ( $f_{CO_2}^*$ ), joint au fait que ( $f_{CO_2}^*$ ) soit très bien corrélé aux flux diffusifs totaux déterminés selon la méthode d'échantillonnage dans la couche mince de surface ( $f_{CO_2}$ ), permet d'envisager qu'une partie non négligeable du carbone photominéralisé conduise à la photoproduction de composés labile pour les bactéries.

Dans le troisième chapitre, la question à laquelle nous souhaitons répondre concerne l'origine autochtone ou allochtone des photoproduits évoqués précédemment. Pour répondre à cette question, nous avons considéré les biomarqueurs de la lignine. Ces

composés sont jugés comme étant de très bons indicateurs de caractérisation de la matière organique terrigène présente dans les écosystèmes aquatiques. Les résultats obtenus conduisent à une explication partielle. Tout d'abord, selon les situations environnementales à l'étude, plus l'écosystème aquatique a subi de perturbations et plus la quantité de MOT présente sous forme dissoute dans la colonne d'eau sera élevée. L'indicateur de quantité de matériel terrigène ( $\lambda_{\text{DOC}}$ ) témoigne d'une telle tendance avec une valeur  $\lambda_{\text{DOC}}$  estimée à  $0,29 \pm 0,07$  mg/100mgCO pour des lacs non perturbés (LNAL) alors que  $\lambda_{\text{DOC}}$  est évalué à  $0,93 \pm 0,26$  mg/100mgCO pour des réservoirs n'ayant pas été soumis à une récolte forestière récente (RNAL). Quant aux lacs et réservoirs assujettis à une récolte forestière, les quantités relatives de MOD d'origine terrigène semblent remarquablement similaires avec une mesure de  $\lambda_{\text{DOC}}$  estimée à  $1,40 \pm 0,16$  mg/100mgCO pour les lacs (scénario LAL) tandis qu'elle se situe à  $1,42 \pm 0,22$  mg/100mgCO pour les réservoirs (scénario RAL). La quantité totale de MOD d'origine terrigène suit une tendance similaire lorsque l'indicateur  $\lambda_{\text{vol}}$  est considéré. En effet, cet indicateur  $\lambda_{\text{vol}}$ , qui est caractéristique de la quantité de MOT présente sous forme dissoute dans l'épilimnion, a été mesuré à  $0,70 \pm 0,06$  mg/100L pour le scénario LNAL, et à  $2,63 \pm 1,64$  mg/100L pour le scénario RNAL. De plus, selon ce même indicateur, la quantité de MOD d'origine terrestre, estimée dans l'épilimnion, serait légèrement inférieure dans le cas de lacs perturbés par récolte forestière ( $4,16 \pm 1,33$  mg/100L) par rapport à celle estimée dans le cas d'un réservoir soumis à une récolte forestière récente. Dans ce cas en effet  $\lambda_{\text{vol}}$  est égal à  $4,91 \pm 1,21$  mg/100L (RAL). De plus les valeurs de  $\delta^{13}\text{C}$  indiquent que, pour ces mêmes plans d'eaux, le carbone organique dissous présente un fractionnement isotopique similaire à celui du sol (Ouellet 2010). Ainsi, conformément à la synthèse publiée récemment sur le COD présent dans la colonne d'eau (Prairie 2008), la majeure partie du carbone organique dissous serait, dans cette étude, d'origine terrestre. Par ailleurs, les valeurs des biomarqueurs ligneux  $\Sigma_8$  et  $\lambda_{\text{vol}}$  sont bien corrélés aux flux quotidiens de  $\text{CO}_2$  provenant de la photominéralisation du carbone

sur l'ensemble de la colonne d'eau ( $\overline{DIPM}_{CO_2}$ ). En effet, les valeurs des coefficients de corrélation des fonctions de régression linéaires évaluées pour les quantités  $\overline{DIPM}_{CO_2}$  et  $\lambda_{DOC}$  ou  $\overline{DIPM}_{CO_2}$  et  $\lambda_{vol}$  respectivement sont évaluées à  $R^2=0,60$  ( $p<0,001$ ) et  $R^2=0,57$  ( $p<0,001$ ). Il est donc probable que la photodégradation s'opère principalement sur la matière organique terrigène présente sous forme dissoute dans la colonne d'eau. D'autre part, les biomarqueurs de la lignine, évalués pour les différentes fractions (dissoutes, particulières et sédimentaires) montrent une extrême variabilité de la composition ligneuse selon les familles de composés phénolés ( $\Sigma_C, \Sigma_V, \Sigma_S, \Sigma_P$ ). Le changement le plus remarquable concerne la valeur des rapports C/V, qui est très faible dans la colonne d'eau en variant entre 0,02 mg/100mgCO et 0,16 mg/100mgCO pour la fraction dissoute et entre 0 et 0,07 mg/100mgCO pour la fraction particulaire. Dans le matériel sédimentaire, par contre, ce rapport s'étend entre 0,1 à 0,7 mg/100mgCO. De façon similaire, le rapport S/V varie considérablement selon les fractions pour lequel il est analysé. Ce constat permet de conclure que les rapports S/V et C/V estimés à partir du matériel sédimentaire, dont les valeurs sont caractéristiques de la morphologie et du couvert forestier du bassin versant (Teisserenc et al. 2010), ne peuvent être mesuré à partir de la fraction dissoute ou particulaire pour cette même caractérisation. Finalement le rapport C/V mesuré à partir du matériel sédimentaire, qui est un indicateur de la quantité de matériel boisé, est très fortement corrélé aux flux totaux de  $CO_2$  ( $f_{CO_2}$ ) émis des plans d'eau vers l'atmosphère ( $R^2=0,83$ ,  $p<0,001$ ). De plus, le rapport C/V mesuré à partir du matériel sédimentaire est fortement corrélé aux flux quotidiens de  $CO_2$  provenant de la photominéralisation du carbone sur l'ensemble de la colonne d'eau ( $\overline{DIPM}_{CO_2}$ ) ( $R^2=0,75$ ,  $p<0,001$ ). Alors que le rapport C/V n'est habituellement pas très utilisé, il est, dans le cadre de cette étude, représentatif d'un gradient de perturbation. Ce résultat provient du fait que la quantité relative de Cynamiles ( $\Sigma_C$ ) mesuré dans le matériel sédimentaire, diminue avec le niveau de perturbation tandis

que la quantité relative de Vanylilles ( $\Sigma_V$ ), également mesuré dans le matériel sédimentaire, augmente avec le niveau de perturbation. Le rapport C/V contribue donc à préserver la tendance observée pour les Cynamiles et constituerait donc un très bon indicateur de perturbation d'un système aquatique. Suite à la mise en eau d'un réservoir, le rapport C/V va fortement diminuer (Houel et al. 2006). De ce fait, il apparaît que de vieux réservoirs hydroélectriques puissent continuer à émettre une quantité importante de CO<sub>2</sub> vers l'atmosphère.

## Références

- Granéli, W., M. Lindell, B. M. De Faria, and F. De Assis Esteves. 1998. Photoproduction of dissolved inorganic carbon in temperate and tropical lakes – dependence on wavelength band and dissolved organic carbon concentration. *Biogeochemistry* **43**: 175-195.
- Hanson, P. C., A. I. Pollard, D. L. Bade, K. Predick, S. R. Carpenter, and J. A. Foley. 2004. A model of carbon evasion and sedimentation in temperate lakes. *Global Change Biology* **10**: 1285-1298.
- Houel, S., P. Louchouart, M. Lucotte, R. Canuel, and B. Ghaleb. 2006. Translocation of Soil Organic Matter Following Reservoir Impoundment in Boreal Systems: Implications for In situ Productivity. *Limnology and Oceanography* **51**: 1497-1513.
- Lindell, M. J., H. W. Granéli, and S. Bertilsson. 2000. Seasonal photoreactivity of dissolved organic matter from lakes with contrasting humic content. *Can J Fish Aquat Sci* **57**: 875-885.
- Ouellet, A. 2010. Assessing carbon dynamics in natural and human-perturbed boreal aquatic systems. Concordia University.
- Prairie, Y. 2008. Carbocentric limnology: looking back, looking forward. *Can J Fish Aquat Sci* **65**: 543-548.
- Teisserenc, R., M. Lucotte, S. Houel, and J. Carreau. 2010. Integrated transfers of terrigenous organic matter to lakes at their watershed level: A combined biomarker and GIS analysis. *Geochimica et Cosmochimica Acta* **74**: 6375-6386.
- Vähätalo, A. V., M. Salkinoja-Salonen, P. Taalas, and K. Salonen. 2000. Spectrum of the Quantum Yield for Photochemical Mineralization of Dissolved Organic Carbon in a Humic Lake. *Limnology and Oceanography* **45**: 664-676.